CHAPTER 1

Transparent Organic–Inorganic Nanocomposite Coatings

Shuxue Zhou and Limin Wu

Department of Materials Science and Advanced Coatings Research Center of Ministry of Education of China, Fudan University, Shanghai, P.R. China

1.1 INTRODUCTION

The combination of organic and inorganic ingredients is the most popular strategy to achieve coatings with optimal properties. The two components with different or even opposing intrinsic properties can be mixed at the microscale, nanoscale, and even molecular level. Composite coatings at the microscale actually are conventional pigmented coatings with an opaque appearance. Molecular hybrids were first reported in the 1980s and are an early form of organically modified ceramics (Ormocers) wherein the organic groups act as an inorganic network modifier or network former [1, 2]. These products were further developed in this century as organic phase-dominated materials with an unmatured inorganic phase especially as crystalline inorganics. Nanoscale hybrid coatings based on an organic matrix are actually organic–inorganic nanocomposite coatings (OINCs). The inorganic domain is a dispersed phase with at least one dimension on the nanometer size regime (1–100 nm). In the past 15 years, OINCs have attracted broad research interest both in academics and in industries. Many papers and patents have been published related to OINCs.

Based on Rayleigh scattering theory, the transmission (T) of light through the heterogeneous coatings like OINCs can be calculated according to the following equation:

$$T = \exp\left[-\frac{3\phi_p L r_p^3}{4\lambda^4}\left(\frac{n_p}{n_m} - 1\right)\right] \tag{1.1}$$

where L is the thickness of the coatings, r_p is the radius of the scattering element (namely, the inorganic phase), ϕ_p is the volume fraction of the inorganic phase, λ is

Functional Polymer Coatings: Principles, Methods, and Applications, First Edition.
Edited by Limin Wu and Jamil Baghdachi.

the wavelength of the incident light, and n_p and n_m are the refractive indices of the inorganic phase and the polymer matrix, respectively. It can be clearly seen from Equation (1.1) that the transparency of OINCs depends on the size of the dispersed phase, coating thickness, and the refractive index (RI) difference between the organic matrix and the inorganic phase. The OINCs have a high transparency because the size of the inorganic phase is significantly smaller than the wavelength of light. Normally, 40 nm is an upper limit for nanoparticle diameters to avoid intensity loss of transmitted light due to Rayleigh scattering and thus achieve highly transparent OINCs.

In addition to excellent transparency, OINCs can efficiently combine the advantages of rigidity, functionality (optic, electric, magnetic, etc), durability (to chemicals, heat, light) of the inorganic phase with the softness and processability of the organic phase. They can find wide applications in abrasion- and scratch-resistant coatings, optical coatings, barrier coatings, corrosion-resistant coatings, antibacterial coatings, electrically conductive coatings, self-cleaning coatings (superhydrophilic and superhydrophobic), heat-resistant coatings, flame-retardant coatings, etc. The OINCs are often the best solution especially for those cases that require high coating transparency.

The nanophase of the OINCs can be either simply introduced by blending with *ex situ* nanostructure materials or *in situ* by a sol–gel process or intercalation. The blending method is similar to the fabrication process of conventional organic coatings wherein the inorganic nanostructure materials rather than microparticles are used as the filler. As for the sol–gel method, the inorganic nanophase can be created in the formulating step or the drying step in bottom–up strategies. In most cases, the nanophases precursors are first prehydrolyzed and then blended with a binder. Normally, amorphous metal oxides and metal nanophases in OINCs can be fabricated with this method. The intercalation method is particularly suitable for layered inorganic fillers, for example, clay. In this method, the process is quite analogous to the blending method. However, the inorganic nanophase is *in situ* generated based on a top–down strategy.

In this chapter, the general fabrication principles and performance features of OINCs as well as partially transparent OINCs are presented. Primarily focus is on transparent OINCs with mechanically reinforced, high RI, ultraviolet (UV)-shielding, near-infrared (NIR) light-shielding, barrier, conductive coatings, etc. Because the pigmented OINCs even with the aforementioned performance are opaque, they are beyond the scope of this chapter and not discussed further.

1.2 FABRICATION STRATEGIES

1.2.1 Blending Method

Blending is frequently adopted for inclusion of *ex situ* nanostructure materials into organic coatings. These nanostructures include nanoparticles, nanofibers, nanorods, nanotubes, nanosheets, etc. Among them, nanoparticles are the most

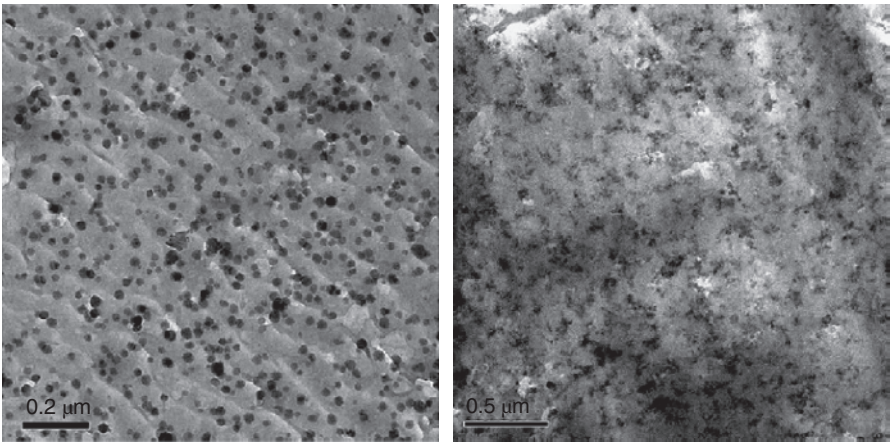

FIG. 1.1 TEM micrographs of nanocoatings filled with 10 wt.% nanoparticles: colloidal nanosilica (left) and pyrogenic nanosilica (right). Reprinted with permission from Ref. 3. © 2011 Elsevier.

common nanofiller for the fabrication of transparent OINCs. The particles can be nanopowders or colloidal. Figure 1.1 shows the typical morphology of colloidal silica and pyrogenic silica in coatings. Colloidal silica particles are spherical and individually dispersed in the organic matrix, whereas pyrogenic silica particles are irregular aggregates. Table 1.1 summarizes some typical nanostructure materials. All nanostructure materials could be possibly used to produce mechanically reinforced OINCs. Nevertheless, the functionality of nanostructure materials determines the functional performance of the resulting OINCs.

The nanoparticles in sols are already nanoscale. Thus, they can be directly mixed with other ingredients [4]. However, these metal oxide nanoparticles in commercial sols are generally amphorous, which is useless for the fabrication of functional OINCs. In recent years, colloidal sols using crystalline oxide nanoparticles from nonaqueous synthesis or controlled hydrolysis have been successfully acquired, opening a new route to obtain transparent functional OINCs.

The nanoparticles can be embedded into coatings during formulation. Sometimes, the incorporation of nanoparticles is moved forward to the stage of resin synthesis, that is, the so-called "*in situ* polymerization" method. This approach enhances the dispersion of nanoparticles and/or the interaction between nanoparticles and the polymer.

1.2.1.1 Deagglomeration of Nanopowder Nanoparticles in the powder state aggregate due to their large surface areas. The aggregates deteriorate the mechanical properties and transparency of OINCs [5]. Therefore, dispersing nanoparticles in resins or coatings is an extremely important task for the field. Various techniques have been developed for dispersing nanopowders into different liquids, including high shear rate mixing, sonication, milling (or grinding), and microfluidic techniques.

TABLE 1.1 The Physical Properties of Some Typical Nanostructure Materials

Type	Density, (g/cm^3)	Mohn's Hardness	Refractive Index	Functionality
SiO_2	2.2	7	1.42–1.46	Mechanical hardness
Al_2O_3	4.0	9	1.7–1.8	Mechanical hardness
ZrO_2	5.6–6.3	6.5	2.13–2.14	Mechanical hardness, high refractive index
TiO_2	3.9	6.0–6.5	2.7	UV absorption, photocatalytic activity, anti-bacterial property
ZnO	5.6	4.5	2.02	UV absorption, photocatalytic activity, anti-bacterial property
ITO	4.3–7.0	—	1.85–1.95	Electric conductivity, near infrared light-shielding
ATO	—	—	—	Electric conductivity, near infrared light-shielding
$CaCO_3$	2.9	3.0	1.6	Mechanical strength
Silver	10.5	2.5–4	0.13	Anti-bacterial property, optical
Boehmite	3.0–3.1	3.0–3.5	1.64–1.67	Anisotropic mechanics
Carbon nanotube	~1.3	25 GPa for single walled[a]	—	Electric conductivity, anisotropic mechanics
Graphene	—	—	—	Electric conductivity, anisotropic mechanics and barrier property

[a] Indentation hardness.

Figure 1.2 summarizes the possible routes for preparation of waterborne or solvent-based nanocomposite coatings from nanopowders. Ultrasonic and microfluidic techniques are usually used in the lab but are infeasible for industrial applications. High shear-rate mixing deagglomerates nanopowders somewhat, but not completely. Bead milling is the most efficient current technique.

The bead milling apparatus is composed of a bead mill, a circulation pump, and a mixing tank equipped with a stirrer. Besides size reduction, loss of crystallinity often occurs during the intensive grinding process. This crystalline change is undesired especially for crystalline nanoparticles application, for example, the use of titania (TiO_2) nanoparticles for photocatalytic self-cleaning applications. Here, the photocatalytic performance is directly related to crystallinity. Smaller bead size and the appropriate induced energy input better destroy nanoparticle aggregates and maintain crystallinity. Beads down to 15–30 μm can reduce TiO_2 nanopowders to a primary particle size of 15 nm [7, 8]. To separate the small beads, a centrifugation bead mill has been developed (Fig. 1.3). The slurry containing agglomerated particles is pumped into the dispersing section of the vessel, where it interacts with the violently agitated beads. Gradually, the slurry reaches the upper part of the dispersing region, where it is

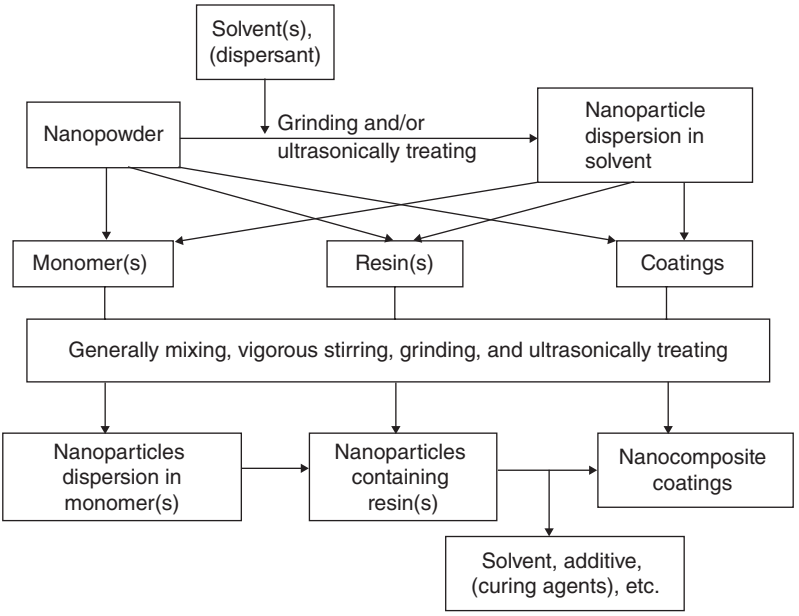

FIG. 1.2 The possible routes for preparation of nanocomposite coatings from nanopowders. Reprinted with permission from Ref. 6. © 2009 American Chemical Society.

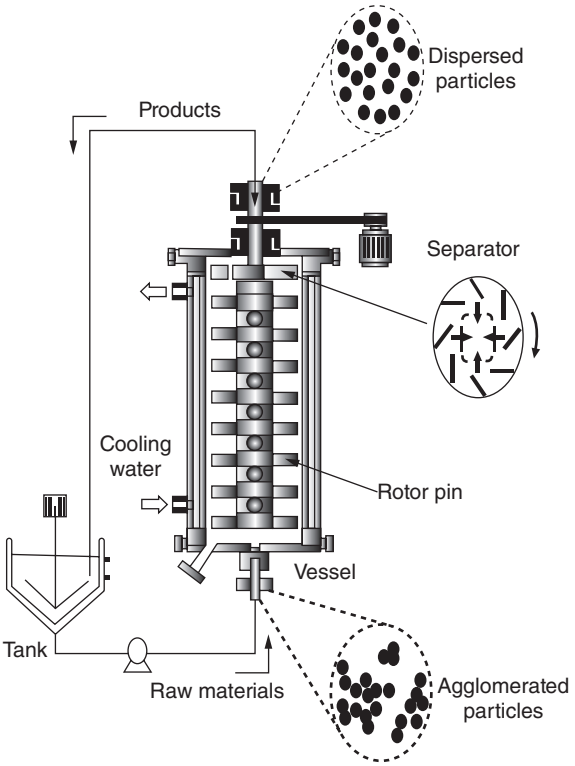

FIG. 1.3 Schematic of the bead mill with centrifugal bead separation. Reprinted with permission from Ref. 7. © 2006 Elsevier.

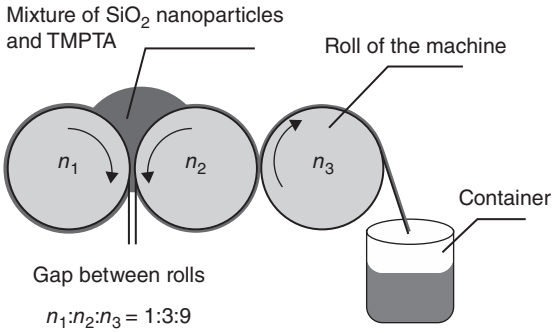

FIG. 1.4 The schematic of a three-roll mill for dispersing silica nanoparticles in TMPTA. The letters (n_1, n_2, and n_3) stand for the rotation speed of the rolls. Reprinted with permission from Ref. 3. © 2011 Elsevier.

separated from the beads by centrifugal force. As a result, the beads remain inside the mill, while the nanoparticle slurry is pumped out of the vessel. We also used a patent describing small beads with an average diameter of 10–70 μm [9]. A stable nanoparticle suspension ($D_{50} < 50$ nm) with a dry matter content of more than 10 wt.% and a crystallinity loss less than 10% was obtained by controlling the induced energy (E_{kin}) above the deaggregation energy ($E_{de\text{-}aggr}$) but less than the amorphization energy ($E_{amorphous}$), that is, $E_{amorphous} > E_{kin} > E_{de\text{-}aggr}$.

A three-roll mill machine is occasionally used to deagglomerate nanopowder (Fig. 1.4). The distance and the nip forces between the three rolls can be programmatically controlled. Reducing the gap distance and increasing the nip forces generate strong shear force that can break up the agglomerates effectively.

In addition, high pressure (>1 MPa) jet dispersion using at least one nozzle was reported for dispersing of SiO_2 nanopowder [10].

1.2.1.2 Surface Modification of Nanoparticles Surface modification of nanoparticles improves the dispersibility of nanoparticles and their compatibility with polymer matrix and/or solvent and makes them reactive with the coating binder. Both macromolecules and small molecules can be employed for surface modification in the physical/chemical bonding.

The commercial polymer dispersants that traditionally are used for the preparation of microparticle slurries also work well for nanoparticle slurries [11–13]. However, much more quantities of polymer dispersants have to be used because of the large specific surface area of nanoparticles. Polyelectrolytes such as polyacrylate sodium, polyallylamine hydrochloride, and poly(sodium 4-styrenesulonate) can also be employed as polymer modifiers for transferring nanoparticles from aqueous phase to nonpolar organic solvent or to hydrophobic polymer matrix without aggregation [14]. Some new macromolecules have also been designed to aid the dispersion of nanoparticles. For instance, a series of hybrid dendritic-linear copolymers (Fig. 1.5) with carboxy-, disulphide-, and phosphonic acid-terminated groups are reported [15]. These copolymers have been demonstrated to be highly efficient for dispersing

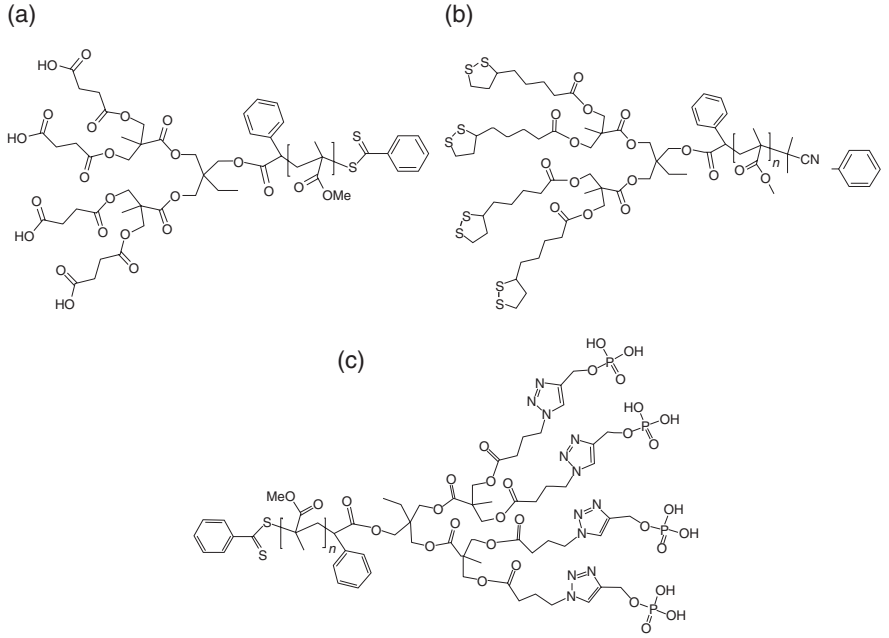

FIG. 1.5 The structures of (a) carboxy-terminated, (b) disulphide-terminated, and (c) phosphonic acid-terminated dendritic-linear block copolymers [15]. Ref. 15. © 2009 Wiley Periodicals, Inc.

TiO_2, Au, and CdSe nanoparticles and are superior to commercial dispersants. Poly(propylene glycol) phosphate ester was synthesized for functionalization of SiO_2 nanoparticles, which are particularly suitable for their application in polyurethane (PU) coatings [16].

The polymer chains chemically attach to nanoparticles through two strategies: "grafting to" and "grafting from." The polymers are directly bonded via the surface hydroxyl groups of nanoparticles in the "grafting to" method. In some cases, chemically reactive organic groups are first attached and then polymers are grafted to nanoparticles chemically. Amici *et al*. even grafted polymer onto magnetite nanoparticles by a "click" reaction between azido functionalized nanoparticles and acetylene end-functionalized poly(ε-caprolactone) or PEG [17]. In contrast, polymer directly propagates from the surface of nanoparticles in the "grafting from" route. In this strategy, an initiator is always attached to nanoparticles in advance. For example, Mesnage's group invented a "Graftfast™" process for functionalization of TiO_2 nanoparticles with poly(hydroxyethyl) methacrylate [18]. In that process, a diazonium salt initiator was first bonded to the surface of nanoparticles.

Besides polymers, organophiliation of nanoparticles with small molecules can be adopted. These short organic segments can attach to the surface of nanoparticles through versatile means. Figure 1.6 gives some possible bonding modes of the grafted organic chains on the nanoparticles. Functionalization of some organic

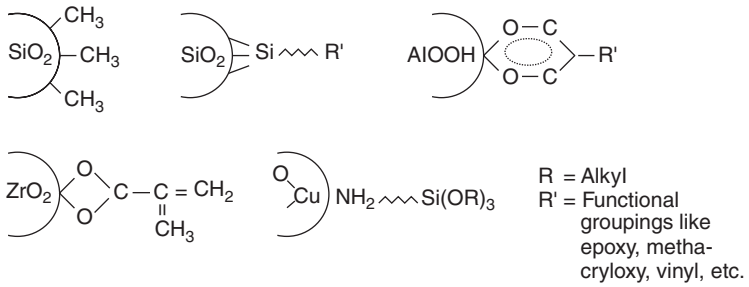

FIG. 1.6 Some principles for surface modification of nanoparticles. Reprinted with permission from Ref. 19. © 1998 Kluwer Academic Publishers.

groups, that is the methyl group, can be done during the nanoparticle synthesis, for example, methylation of pyrogenic silica.

Of the small molecular modifiers, silane coupling agents (SCAs) are the most frequently used. The alkoxyl groups of SCA molecule can react with the hydroxyl groups of nanoparticles while their organic chains have vinyl, epoxide, amine, isocyanate, and mercaptanol end groups that can provide chemical interaction and/or compatibility with organic matrix. The γ-methacryloxypropyltrimethoxysilane (MPS) is one of the most common SCAs for organophilation of nanoparticles because its methacrylate group makes the nanoparticles polymerizable in radical polymerization. The MPS-functionalized nanoparticles have been widely used in the fabrication of UV-curable nanocomposite coatings. Many reports show that MPS molecules bind to nanoparticles via either T^2 or T^3 mode [20, 21]. In most cases, the adsorbed MPS molecules form monolayers with perpendicular and parallel orientations in the absence of catalyst. The parallel orientation might be induced by hydrogen bonding between the MPS-carbonyl and a hydroxyl group of the oxide. With monolayer structure, the amount of MPS bonded could theoretically change in the range of 3.0–6.9 μmol/m^2 [22]. This deviation is due to incomplete coverage or multilayers. If an acidic or basic catalyst is employed during modification, a precondensed MPS structure would be attached to nanoparticles. For an example, a ladder-like arrangement of two linked siloxane chains forming connected eight-membered rings (Fig. 1.7) was demonstrated by Bauer *et al*. [23]. This group used nanosilica (nano-SiO_2) or nanoalumina (nano-Al_2O_3) particles modified with MPS under maleic acid catalyst in acetone. The ladder-like structure was expected to build up a short range of interpenetrating networks with polyacrylate chains during UV or EB curing [24].

To date, many oxide nanoparticles such as SiO_2 [25], TiO_2 [26], ZrO_2 [27], antimony-doped tin oxide (ATO) [28], etc. have been functionalized with MPS. However, MPS-functionalized nanoparticles do not always provide good dispersion in organic solvents, monomers, and oligomers. Modification of highly-dispersible ZrO_2 nanoparticles and deagglomeration of TiO_2 nanopowder with MPS indicate that MPS-functionalized nanoparticles are soluble in THF and butyl acetate [26, 29]. Nevertheless, there is a critical MPS-functionalized nanoparticle load. Above this loading level, phase separation occurs during dispersion in tripropyleneglycol

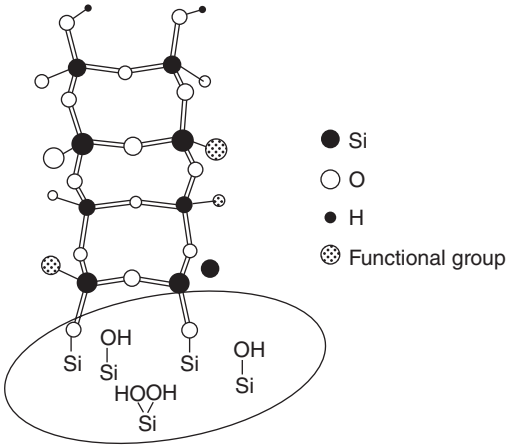

FIG. 1.7 Ladder-like structure of silicon atoms in polysiloxanes grafted on the silica surface [23]. Ref. 23. © 2003 Wiley-VCH Verlag GmbH & Co. KGaA.

diacrylate (TPGDA), 1,6-hexanediol diacrylate (HDDA), trimethylolpropane triacrylate (TMPTA), polyurethane acrylate oligomer, and their mixtures [26, 30–32]. Moreover, as more MPS is attached or higher fraction of PU oligomer in UV-curable coatings is adopted, lower critical MPS-functionalized ZrO_2 load is revealed. This suggests that MPS-functionalized nanoparticles are partially compatible with conventional UV-curable monomers, but poorly compatible with PU oligomer. Therefore, modifying nanoparticles with MPS for UV-curable coatings should be done carefully.

The γ-glycidoxypropylmethoxytriethoxysilane (GPS) and γ-aminopropyltrimethoxysilane (APS) are the other two SCAs for functionalization of nanoparticles [33, 34]. They endow nanoparticles with epoxy and amino groups, respectively, and hence chemical reactivity with the organic binder. The GPS-modified nanoparticles can be readily embedded into epoxy coatings [35], and GPS-based polysiloxane coatings are part of the cross-linking network [36, 37]. More interestingly, the prehydrolyzed GPS is amphiphilic and can modify the aqueous nanoparticle sol [38]. The silylated colloidal particles thus have improved cross-linking ability with themselves or with other polymer binders via the grafted epoxy and/or silanol groups. The APS-modified nanoparticles can be applied to epoxy coatings [39] and PU coatings [40]. It should be noted that nanoparticles grafted with excess APS are unstable in organic solvents due to the high polarity of the amino groups. On the contrary, a high quantity of bonding APS favors the dispersion of nanoparticles in acidic or alkaline water [33]. Therefore, unlike MPS, both GPS and APS can be used to modify nanoparticles for applications not only in solventborne coatings but also in waterborne coatings.

Other SCAs reported for functionalization of nanoparticles include vinyltrimethoxysilane (VTS) [23], *n*-propyltrimethoxysilane (PTS) [23], hexadecyltriethoxysilane (HDTS) [41], *N*-aminoethyl-*N*-aminopropyltriethoxysilane (AEAPS) [42], and even mixtures of SCAs (decyltrimethoxysilane/APS [43]). The VTS has a C=C bond similar

to MPS. However, the C=C bond is much less active because of its relatively high rigidity on the nanoparticle surface. The PTS and HDTS are inert SCAs without any terminated groups, and are therefore mainly used for improving the dispersion of nanoparticles in nonpolar solvents [41]. The AEAPS has higher polarity than APS and is an ideal ligand for the fabrication of aqueous nanoparticle dispersions [42]. Mixed SCAs offer more control of the surface wettability to facilitate dispersion of modified nanoparticles in versatile solvents.

Besides SCAs, other small molecule modifiers include acrylic acid [29, 44], 2-acetoacetoxyethyl methacrylate [45], hydroxyethyl methacrylate [46], and cathediol group-containing ligands [29]. Details of their utility with nanoparticles are in the literature.

1.2.2 Sol–Gel Process

The sol–gel process combines inorganic and organic units at the molecular and nanosized level. In a typical sol–gel process the precursors, that is, metal alkoxides, metal salts, etc., are prehydrolyzed/condensed to form an inorganic sol in the presence of acid or base catalyst. The as-synthesized inorganic sol is then cast on a substrate for further condensation under drying. Baking at a high temperature results in the formation of inorganic coatings, which is very thin (several hundred nanometers) and brittle. To reduce the brittleness, organic-group tethered precursors are always introduced. An inorganic–organic (I/O) hybrid coating (Ormocer) is thus formed at a drying temperature below the decomposition temperature of the organic groups. Besides the inorganic network modifier, some organic groups can react to aid the film formation. If the organic network dominates the film formation, the dried coatings actually transform into organic–inorganic (O/I) hybrid coatings wherein the organic component constitutes the continuous phase [47]. The O/I hybrid coatings can also be prepared by introducing prehydrolyzed inorganic sol into conventional polymer coatings. Nevertheless, it is hard to quantitatively judge the boundary between I/O and O/I hybrid coatings.

The O/I hybrid coatings mixed at the nanosize have distinguished inorganic phases (amphorous or crystalline). Therefore, they are best described as OINCs. The O/I hybrid coatings are generally limited to those sol–gel derived coatings without distinguished inorganic phase. These "hybrid nanocomposites" are often seen in publications [39, 48, 49] and actually represent one important source of OINCs—nanocomposite coatings prepared from a sol–gel process.

Tetraethoxysilane (TEOS) and tetramethoxysilane (TMOS) are the most popular precursors in sol–gel-derived coatings because of their mild hydrolysis and condensation reactions. In most cases, organotrialkoxysilane such as MPS, GPS, APS, and VTS are added to tetraalkoxysilane to endow the inorganic silica sol with reactivity and compatibility with the organic phase. Besides silica precursors, other precursors include titanium *n*-butoxide, titanium tetraisopropoxide (TTIP), aluminum isopropoxide, aluminum *sec*-butoxide, zirconium butoxide, and zirconium tetrapropoxide. These metal alkoxides are highly active in hydrolysis/condensation reactions. To decrease their reactivity, ligands such as ethylene glycol, acetic acid, ethyl acetoacetate, acetylacetone, and their derivates are usually coordinated with them.

Controlling phase separation is very important to achieve sol–gel derived OINCs. Both insufficient and serious phase separations are undesirable. Generally, chemical reactions between an inorganic sol and an organic component are designed to control phase separation. The polymer chains with pendant carboxylic acid groups or triethoxysilyl groups can chemically interact with the inorganic sol to hinder serious phase separation. The growth of the inorganic phase can also be controlled by a limited supply of water. In addition, the hydrolysis/condensation of precursors in dried coatings—aided with moisture from air—is another ideal way to generate OINCs because of the limited space for the growth of inorganic domains.

In comparison with the blending methods, the sol–gel process is an easier route to transparent OINCs. Therefore, transparent sol–gel-derived OINCs are promising as optical (high RI, UV-shielding) coatings and scratch-resistant clearcoats. They are also widely used as corrosion-resistant coatings for metals, in which high transparency is not necessary.

1.2.3 Intercalation Method

The intercalation method is utilized for the fabrication of nanocomposite coatings based on clays or other layered inorganic fillers. These special fillers are incorporated into coatings via high-speed mixing, ball milling, bead milling, and three roll milling similar to nanopowders. However, the nanophases are *in situ* generated through intercalation. Table 1.2 gives the commercial name and suppliers of some layered silicates. Transparent nanocomposite coatings can be readily obtained because the RI of clay (bentonite clay = 1.54) closely matches that of most organic coatings, and at most cases, the clay loading in coatings is very small (usually <5%).

TABLE 1.2 The Type and Supplier of Layered Silicate

Commercial Name	Ingredient	Supplier
Cloisite® Na^+	A natural unmodified montmorillonite clay (cation exchange capacity, 92 mEq/100 g)	Southern clay products (Gonzales, TX)
Cloisite 30B	Organic layered silicate, montmorillonite treated with methyl tallow bis-(2-hydroxyethyl) quaternary ammonium	Southern clay products (Gonzales, TX)
Laponite RD	Synthetic layered silicate, $Na^+_{0.7}[(Si_8 Mg_{5.5}Li_{0.3}) O_{20}(OH)_4]^{0.7}$	Rockwood Additives Ltd. (Cheshire, UK)
Cloisite 20A	Dimethyl dehydrogenated tallow quaternary ammonium modified	Rockwood specialties
Cloisite 20B	—	Rockwood specialties
I.30P	Primary octadecylamine modified	Nanocor Inc.
I.30E	An onium ion surface modified montmorillonite	Nanocor Inc.
Saponite clay	$Ca_{0.25}(Mg,Fe)_3((Si,Al)_4O_{10})(OH)_2 \cdot n(H_2O)$	Kunimine Ind. Co. Ltd., Japan

Quaternary alkylammonium salts or quaternary alkylphosphonium salts are often employed as an intercalating agent. One special ammonium salt, [2-(methacyloyloxy)ethyl] trimethylammonium methyl sulfate, was adopted to modify clay when the clay was used in UV-curable coatings [50]. The clays or related products are first treated with the intercalating agent to cause organophilation of the filler and enlarge the interlayer distance. Sometimes, commercial clays have been already treated with organic groups (see Table 1.2). After that, the organophiliated clay is incorporated into a polymer solution and stirred at a controlled temperature. The polymer chains gradually diffuse into the interlayer of the filler to further increase the interlayer distance and even cause exfoliation. This process is the "solution dispersion" technique [51]. The organically modified clay can also be introduced via "*in situ* polymerization" route in which treated clay is mixed with monomer and then polymerized. The interlayer distance enlarges during the propagation of polymer chains.

The intercalation and exploitation depend on the intercalation degree and are revealed for clay-containing nanocomposites. Actually, the morphology of clay-containing OINCs is also strongly related to the deagglomeration technique due to the initial powder state of clay. Figure 1.8 presents the typical dispersion state of clay in

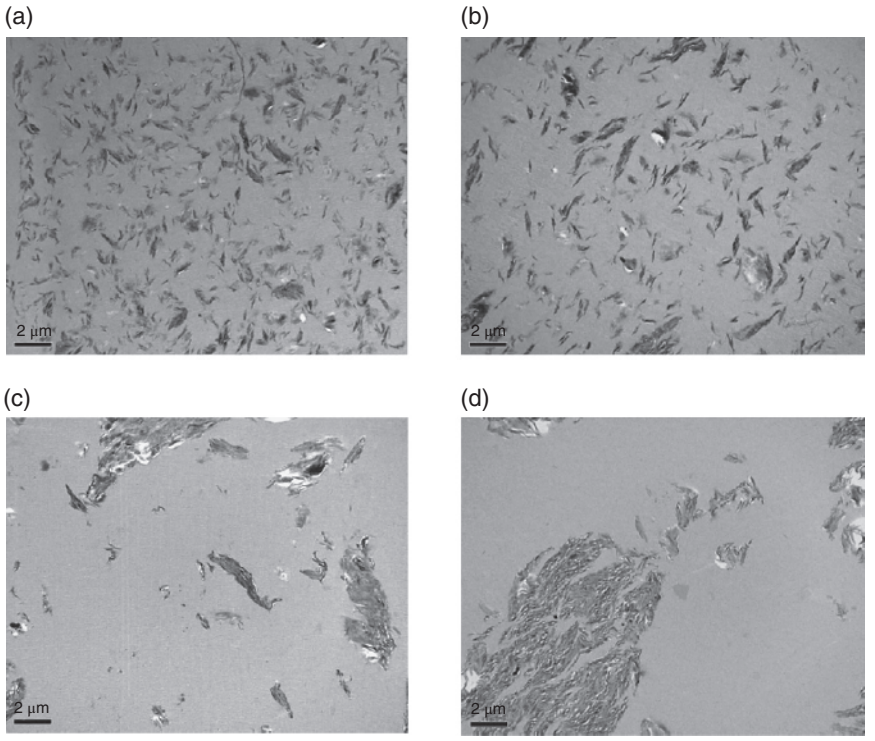

FIG. 1.8 TEM images of the UV-curable clay-containing coatings prepared with 10% clay by (a) three-roll milling, (b) bead milling, (c) ball milling, and (d) high speed mixing. Reprinted with permission from Ref. 52. © 2008 Elsevier.

UV-curable coatings prepared with various mixing techniques. The best dispersion is achieved with a three-roll mill and bead mill. For the ball milling and the high-speed mixing dispersion, large aggregates are observed. This deagglomeration behavior is quite similar to that observed in the deagglomeration of nanopowder.

Clay can improve the hardness, scratch resistance [53], and viscoelastic properties of coatings. Importantly, it can provide corrosion resistance and barrier properties superior to spherical particle fillers [54]. Enhancing corrosion resistance and barrier properties of H_2O and O_2 by clay was observed for different polymer matrices such as polyaniline, poly(*o*-ethoxyaniline), poly(methyl methacrylate) (PMMA), poly(styrene-*co*-acrylonitrile), etc. even at low loading levels (0.5–3%). This excellent barrier performance of polymer-clay nanocomposites is a result of the increased tortuosity of the diffusion pathway for oxygen and water. However, clay does not improve organic coatings with originally excellent mechanical and/or corrosion-resistant properties [53, 54].

Besides mechanical, barrier, and corrosion resistant applications, some clay-containing nanocomposite coatings have been reported in special applications. For example, Majumdar *et al*. developed an aqueous transparent nanocomposite coating consisting of laponite/polyvinylpyrrolidone (PVP)/poly(ethylene oxide) (weight ratio 35:15:50) as a fast drying, high-quality, image-receiving layer for inkjet printing on a variety of substrates such as polyester, polyethylene-coated, or polypropylene-laminated photo paper, GP paper, etc. [55]. Ranade *et al*. prepared a mixed exfoliated and intercalated polyamide–imide nanocomposite with montmorillonite (MMT) as magnetic wire coatings with reduced specific heat and improved Vicker hardness [56].

1.3 MECHANICALLY ENHANCED NANOCOMPOSITE CLEARCOATS

Clearcoats are generally used as topcoats in automobile, wood flooring, wood furniture, and optical plastic applications. High mechanical strength and excellent transparency are two essential properties of these coatings. Traditionally, the mechanical properties of clearcoats are determined by their macromolecular structure and cross-linking density especially for thermoset coatings. Nevertheless, the addition of inorganic nanoparticles provides a new way to improve the mechanical properties of clearcoats [57]. The nanoparticle-embedded coatings can retain the origin transparency of clearcoats because of the small size of the nanoparticle. The rigidity of clearcoats would be naturally enhanced due to the high hardness of inorganic nanoparticles because all inorganic materials have a higher hardness relative to the organic materials. Considering the economic cost and enhanced efficiency, only some inorganic nanofillers—nano-SiO_2, nano-Al_2O_3, nano-ZrO_2 particles, boehmite, and layered silicate—are feasible for the mechanical improvement of clearcoats.

The enhanced mechanical properties can be revealed from the change of the hardness (pencil hardness, pendulum hardness, and micro-indentation hardness) of the coatings upon inclusion of nanofillers. According to the "mixing rule," the hardness (H) of composite coatings could be approximately predicted to be:

$$H = H_p\phi_p + H_m(1-\phi_p) \tag{1.2}$$

where H_p and H_m represent the hardness of organic matrix and inorganic filler, respectively. However, two other aspects are not negligible for nanocomposite coatings. One is the interfacial phase between the organic matrix and the inorganic nanophase. The other is the change in the condensation state of the organic matrix initiated by the embedded nanophase. The volume fraction of the interfacial phase could be high because of the large specific surface area of nanoparticles. Consequently, the properties of the nanocomposite coatings are determined from the organic matrix, nanoparticle filler, and interfacial phase. Equation (1.2) thus becomes

$$H = H_p\phi_p + H_m(1 - \phi_p - \phi_i) + H_i\phi_i \tag{1.3}$$

where H_i and ϕ_i are the hardness and volume fraction of interfacial phase.

Besides the specific surface area of nanoparticles, the volume fraction of the interfacial phase is related to the interaction distance of the nanoparticle impacting the matrix, the volume fraction, and the dispersion state of the nanofiller. The interfacial phase may be harder or softer than the organic matrix depending on the interfacial bonding mode between the organic chains and inorganic nanophase. Generally, chemical bonding leads to a hard interfacial phase while weak interactions such as Van der Waal force and hydrogen bonding (low number of anchoring points) produce a soft interfacial phase. Unfortunately, both the volume fraction and the mechanical properties of the interfacial phase are difficult to measure, and thus the mechanical properties of the nanocomposite coatings are difficult to theoretically predict. Nevertheless, Equation (1.3) can theoretically explain the complexity of the mechanical change in nanocomposite coatings or vice versa probe the properties of the interfacial phase.

For cross-linked clearcoats, the addition of nanoparticles will possibly impact the cross-linking density of the matrix. Actually, inorganic nanoparticles can be regarded as cross-linking points if strong interfacial bonding occurs. That is why the solvent resistance of thermoplastic coatings is enhanced via the addition of nanoparticles. On the other side, strong interfacial interactions will hinder the motion of organic chains and deteriorate the cross-linking behavior of the organic matrix. The double-face of the nanoparticle during cross-linking causes a diverse cross-linking structure of matrix. In addition, if the nanophase materials are introduced into a crystalline polymer matrix, the nanoparticles will influence the original crystallinity of the polymer. As a result, the mechanical properties of nanocomposite coatings is possibly dependent on the crystallinity rather than on the nanoparticle material itself. Consequently, variation in the mechanical properties of clearcoats via incorporation of nanoparticles is more complicated than that of microparticles. It must be determined empirically.

To date, many polymer clearcoats have been combined with inorganic nanophases to achieve mechanically-improved clearcoats. These clearcoats include solventborne two-component (2K) PU coatings, waterborne clearcoats, UV-curable coatings, etc. Thereafter, the mechanical improvement of the clearcoats due to the nanophase is introduced based on the type of clearcoats.

1.3.1 Solventborne Polyurethane Nanocomposite Coatings

Nano-SiO_2 particles are most frequently adopted to modify the mechanical properties of 2K PU coatings because they are affordable and available. Nano-SiO_2 particles could more efficiently increase the macro hardness, scratch resistance, elastic modulus of acrylic-based PU coatings than micro-silica particles [58]. They also enhance the microhardness and abrasion resistance of polyester-based PU coatings [59].

Fumed silica (10–40 nm) is one of the nano-SiO_2 particles that was first used in these coatings. These silica nanoparticles are a rheological additive for coatings. Because of the existence of hydroxyl groups in polyol resins, both hydrophilic and hydrophobic fumed silica are quite compatible with polyol resins. Thus, they are easily incorporated into the polyol resins or its solution.

Different groups have reported different results. Zhou *et al*. found that both hydrophilic and hydrophobic fumed silica (Wacker N-20 and Aerosil R972) have the same dispersion in acrylic-based PU coatings with very similar influences on the tribological properties (microindentation hardness, elastic modulus, and the critical force for crack) of acrylic-based PU coatings [60]. Jalili *et al*. also compared the addition effect of hydrophilic Aerosil TT600 and hydrophobic R972 on the 2K PU clearcoat from acrylic polyol (commercial name: Uracrone CY433)/Desmodure N75 [61]. They concluded that the incorporation of 4–8 wt.% of R972 in the 2K PU clearcoat gave optimal rheological, mechanical, and optical properties of the final nanocomposite coatings.

Barna *et al*. produced silica nanoparticles with an average particle size below 100 nm by flame synthesis [62]. These nanoparticles were treated with trimethylchlorosilane (TMCS), dimethyloctylchlorosilane (DMOCS), or APS. The treated or untreated silica nanoparticles were then blended with acrylic polyol (Setalux C-1184 SS-51)/Desmodur N 3300 to form PU nanocomposite coatings. They found that the lacquers containing untreated silica showed the best transmission results. This suggests that the treated silica nanoparticles have poor compatibility with the lacquer. These different results differ in the use of different organic solvents in the acrylic polyol solutions. When fumed silica was added to the polymer solution, the organic solvent imposes considerably on the dispersion of silica nanoparticles besides acrylic polyol. The dispersion of the treated nanoparticles is inferior to the untreated nanoparticles in Barna's case [62] and is because of the extreme nonpolarity (TMCS- or DMOCS-treated SiO_2) or the extreme polarity of silica nanoparticles. Consequently, adequate surface polarity of fumed silica would be desired for their combination with acrylic polyol.

The transparency of PU nanocomposite coatings with fumed silica deteriorates because of nano-SiO_2 aggregates. Completely transparent PU nanocomposite coatings are prepared preferentially using colloidal silica, another type of nanosilica particles. Colloidal silica particles are generated from two ways: ion-exchange of polysilicate and Stöber method with TEOS. The commercial silica sols or alcosols are usually manufactured with the ion-exchange route. Due to the large quantity of hydroxyl groups on the surface of the particles, colloidal silica particles are poorly compatible with the organic solvents that are contained in acrylic polyol solution (butyl acetate, xylene, etc.).

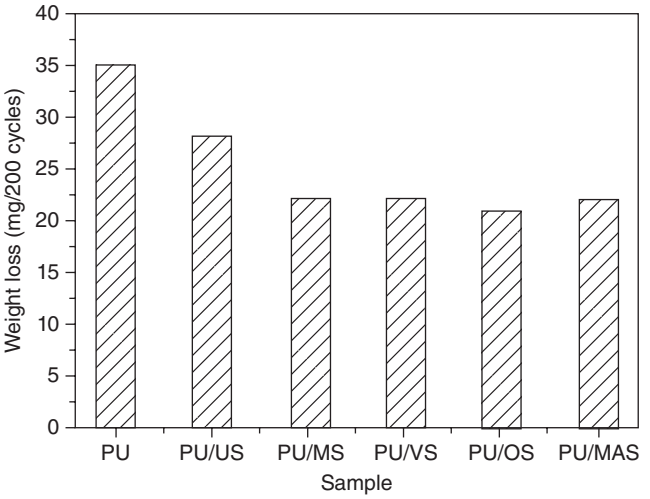

FIG. 1.9 Abrasion resistance of PU/silica composite films. Reprinted with permission from Ref. 63. © 2005 Elsevier. (200 cycles under 1000 g load, US, MS, VS, OS, and MAS represent unmodified, MTES-, VTS-, OTES-, and MPS-modified silica nanoparticles, respectively.)

In addition, the water and/or alcohol in the silica sol are not desired in the curing of polyol with isocyanate. Hence, the silica sol is not allowed to directly mix with acrylic polyol solution. A more complicated process has to be adopted such as the colloidal silica particles should be surface-modified, centrifuged from the sol, and then redispersed in monomers or acrylic polyol solution [63, 64]. Alternatively, the silica nanoparticles are modified in the sol state and then alcohol is substituted with butyl acetate through distillation [65]. Experiments indicate that MPS and octyltriethoxysilane (OTES) are better than methyltriethoxysilane (MTES) and VTS for the redispersion of the functionalized silica nanoparticles in acrylic polyol. The modified silica nanoparticles are superior to unmodified ones in improving the abrasion resistance of acrylic-based PU coatings. However, the type of surface modifier does not obviously influence the abrasion resistance of PU nanocomposite coatings (Fig. 1.9).

Unlike acrylic polyol, silica sol can be directly blended with polyester polyol (blending method) or with dicarboxylic acid and diol monomers and subsequent condensation polymerization [66]. The water and/or alcohol introduced by the silica sol can be removed through evaporation at elevated temperature. The latter *in situ* polymerization caused more polyester segments to chemically bond onto the surfaces of the silica particles than the blending method. This lowers the viscosity of the nanocomposite resins and increases the critical silica load for sharp increases in viscosity [67]. Better abrasion resistance is achieved by polyester-based PU nanocomposite coatings via *in situ* polymerization regardless of silica content and diameter (Fig. 1.10) [68].

Some other nanofillers improve the mechanical properties of solventborne PU coatings. Ahmadi *et al*. studied the effect of nanolayered silicates (Sud Chemie) on the properties of an automotive refinish clear coat based on 2K PU [69]. They found

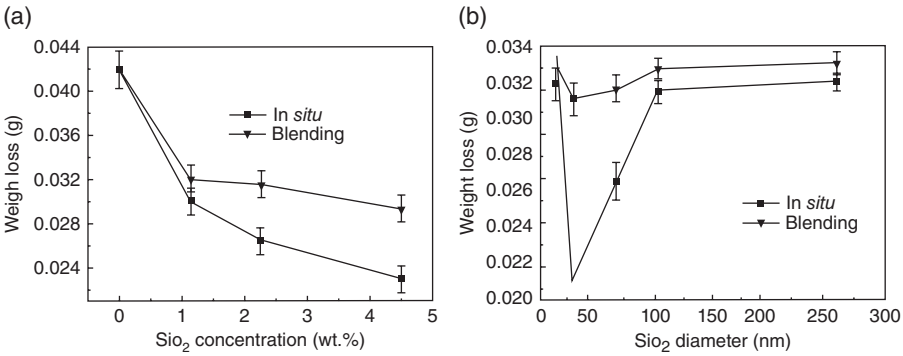

FIG. 1.10 Change of weight loss of PU/nano-SiO_2 composites as a function of (a) silica concentration (silica particle size 66 nm) and (b) silica diameter (silica content 2.25 wt.%) [68]. Ref. 68. © 2005 Wiley Periodicals, Inc.)

a significant improvement in scratch and mar resistance. Meanwhile, there was no gloss reduction due to nanofiller. On the contrary, gloss retention was increased by about 10% in the presence of only 3 wt.% nanofiller. Sabzi *et al*. embedded APS-modified TiO_2 nanoparticles into 2K PU coatings. The nanoparticles increase the mechanical strength and UV protection of PU coatings [70]. However, the transparency of the coatings is unavoidably decreased. Colloidal silica nanoparticles are the best candidate for mechanical improvements in solventborne PU coatings without scarifying its original transparency.

1.3.2 Waterborne Nanocomposite Clearcoats

Waterborne clearcoats are increasingly popular because they are environmentally friendly. However, they are usually weaker in mechanical performance and water resistance versus with their solventborne counterparts. In recent years, the addition of nanofillers was demonstrated to compensate their weakness, which promotes the development of waterborne coatings.

Because of the intrinsic hydrophilicity of inorganic nanofiller, they are very compatible with water and can be directly incorporated into waterborne resins, that is, polymer latex and aqueous polymer dispersion. However, when the aqueous nanocomposite resins are dried, the compatibility between the polymer chains and the inorganic nanofiller dominates the dispersion state of the nanofillers. Poor compatibility generally leads to aggregates of nanofillers during drying. It is fortunate that waterborne resins generally have a hydroxyl or carboxyl groups on their chains. These groups can interact with nanofiller via hydrogen bonding and providing compatibility of nanofillers with polymer matrix. Nevertheless, serious aggregation of nanofillers still exists at high nanofiller load because polymer chains cannot encapsulate the nanofiller during drying.

Prior encapsulation of nanofiller within polymer latex is another way to achieve waterborne nanocomposite coatings [71]. In this strategy, the preparation of a

TABLE 1.3 Properties of P(St-BA-AA)/Silica Nanocomposite Films With Various Nanosilica Contents[a]

	Run 15	Run 6	Run 7	Run 8	Run 9	Run 10
Nanosilica content[b] (wt.%)	0	9.1	16.7	23.1	28.6	33.3
Pencil hardness	2B	H	2H	2H	3H	4H
Pendulum hardness (s)	41	78	95	120	108	66
Flexibility (mm)	0	0	0	0	1	2
Impact strength (kg·cm)	40	50	50	50	40	40
Gel[c] (%)	0	35(28.5)	43(31.6)	56(42.8)	64(49.6)	77(65.6)

[a] Reprinted with permission from Ref. 75. © 2009 Society of Chemical Industry.

[b] Based on the total weight of nanocomposite film.

[c] The data in parentheses represent the weight fraction of insoluble polymer, which is calculated on the assumption that the weight loss after immersion in acetone results entirely from dissolution of the polymer chains.

polymer/nanofiller composite latex is crucial. To date, there are many reports on this topic. The methods include emulsion polymerization using a cationic initiator, 2,2′-azobis(2-methylpropionamide) dihydrochloride [72], seed emulsion polymerization [73], miniemulsion polymerization [74], etc. These will not be described in detail for space limitations. The nanocomposite latex can be used as the new filler for waterborne coatings or can directly form a film. Because the nanofillers in the composite particles generally have a strong interaction with the polymer matrix, aggregation does not happen during drying.

Silica sol is frequently used to improve the performance of polymer latex coatings. Table 1.3 gives the typical influence of colloidal silica nanoparticles on the mechanical properties of poly(butyl acrylate-*co*-styrene-*co*-acrylic acid) [P(BA-St-AA)] latex film. The pencil hardness of latex film increases from 2B to 4H when 33.3% silica nanoparticles are incorporated. Interestingly, the solvent resistance of the polymer latex is also improved [75].

Silica sols can be introduced into waterborne coatings via blending. However, it should be noted that the same surface charge of the silica nanoparticle with polymer latex is essential to avoid destabilization of the nanocomposite latex. The morphology of the polymer/silica nanocomposite latex film is rather complex depending on the size and volume fraction of the colloidal silica nanoparticles, the size ratio of polymer latex/silica, and the T_g of polymer latex [76]. Generally, transparent nanocomposite film can be achieved at low silica load. Because of the enrichment of inorganic nanoparticles at the interfaces, high silica content leads to silica frameworks or silica aggregates and thus may yield an opaque film [75]. Nevertheless, the silica framework can aid the formation of structure color films if monodispersed polymer latex is used.

Although transparent crack-free films can be prepared at silica loads as high as 70 wt.% based on 14 nm silica particles [76], the film thickness is limited to several micrometers due to its brittleness. This does not match the film thickness of the traditional latex paint. Silica nanopowders can also be blended with polymer latex by bead milling [77], but do not usually meet the optical transparency requirements for a clearcoat.

Beside nanosilica, nano-$CaCO_3$ is introduced into the waterborne coatings. Yao *et al*. incorporated nano-$CaCO_3$ into water-soluble PU resin via an *in situ* biomineralization process using CaO solution and CO_2 [78]. A transparent PU nanocomposite film was obtained at 2 wt.%. The storage modulus increased from 441 MPa of neat PU matrix to 1034 MPa of the nanocomposite film. In addition, the same nanocomposite films displayed a significant improvement in its water resistance. However, the transparency of the film beyond 2 wt.% remarkably declined. Gumfekar *et al*. synthesized nanocomposite latex of P(MMA–BA)/nano-$CaCO_3$ (53 nm) by *in situ* emulsion polymerization [79]. The nanocomposite latex was then added to a water-based coating. Superior coating with pencil hardness of 2H and gloss of 18 was obtained at MMA:BA (1:1), 4 wt.% nano-$CaCO_3$, and 50 wt.% alkyd emulsion. The control sample without nano-$CaCO_3$ had a pencil hardness of 3B and a gloss of 9. The impact strength decreases from 20 to 10 cm.

Needle-shaped boehmite, disc-shaped laponite, and MMT platelets were used to improve the one-component (1K) self-crosslinkable acrylic dispersion. Hydrophilic nanoparticles at the interfaces of the polymer droplets and hydrophobic nanoparticles completely or partially located inside the polymer droplets dramatically increased the cured film stiffness [80]. Nevertheless, the dependence of rheological behavior on the dispersion and location of nanoparticles has not been considered. Nitric acid–treated multiwalled carbon nanotubes (A-MWCNT) were added to a water-soluble PU resin (WBPU) [81]. The initial tensile moduli and tensile strengths of the nanocomposite film with 1.5 wt.% loading of A-MWCNT were enhanced by about 19 and 12%, respectively, compared to the corresponding values for the original WBPU film.

1.3.3 UV-Curable Nanocomposite Coatings

UV-curable nanocomposite coatings can be prepared via three routes: (1) Nanoparticles are *ex situ* modified (see Section 1.2.1.2) and then dispersed into the coatings (the *ex situ* method); (2) nanoparticles and surface modifier are added to the coating formulation and the modification of nanoparticles is finished during fabrication (the *in situ* method); and (3) commercial nanoparticle dispersions in monomer (Table 1.4) are used as additives for UV-curable coatings. In comparison with Route 1, Routes 2 and 3 are easier for industrialization of UV-curable nanocomposite coatings.

Much attention has been given to the curing behavior of UV-curable nanocomposite coatings because the curing behavior strongly determines their mechanical properties. Many studies suggest a decline in the photopolymerization rate and final carbon–carbon

TABLE 1.4 Some Commercial Nanoparticle Dispersions in Monomers

Commercial Name	Composition	Supplier
Highlink OG 100	A 50 nm SiO_2 in HEMA at 30 wt.%	Clariant
Highlink NanO G 103-53	A 50 nm SiO_2 in HDDA at 50 wt.%	Clariant
Highlink NanO G 107-53	A 50 nm SiO_2 in DPGDA at 50 wt.%	Clariant
Nanocryl C 145	A 15 nm SiO_2 in TPGDA at 50 wt.%	Hanse Chemie
Nanobyk 3602	A 45 nm Al_2O_3 in HDDA at 30 wt.%	Byk-Chemie
Nanobyk 3601	A 40 nmAl_2O_3 in TPGDA at 32 wt.%	Byk-Chemie
C150	50 wt.% sol–gel-formed silica nanoparticles and 50 wt.% TMPTA	Nanoresins AG, Germany

double bond conversion after addition of nanoparticles. This alleviates the reinforced efficiency of nanofiller in UV-curable coatings. The negative effects of nanofillers on curing behavior may result from three aspects: First, nanoparticles (from nanopowder) cannot deagglomerate very well in UV-curable coatings. These aggregates will scatter the light resulting in a reduced UV-irradiation intensity. Because light scattering is strongly related to the RI of nanoparticles, better curing is seen in nanocomposite formulations with relatively low-refractive-index nanofillers. For example, Landry *et al*. found that a formulation prepared with alumina nanoparticles (from nanopowder, size: 13 nm) via a *in situ* preparation presented higher levels of curing and a higher rate of reaction [82]. On the contrary, zirconia decreased the conversion and the rate of curing. This may be because of the increase in light scattering caused by the high RI of zirconia, around 2.14. This is quite high compared to alumina and acrylate resin. In another case, UV waterborne nanocomposite coatings containing nano-Al_2O_3 or MPS-functionalized nano-SiO_2 (concentration: 1, 3, and 5 wt.%), differential scanning calorimetry (DSC)-exothermic curves showed that the photopolymerization was less efficient when nanoparticles were introduced, but the UV-curing of coatings based on functionalized nano-SiO_2 were better than those containing nano-Al_2O_3 [83]. Second, increased viscosity of nanocomposite coatings restricts the mobility of acryl radicals [52]. Third, compared with the UV-curable coatings without nanofiller, vitrification occurs early for the UV-curable coatings because these polymerization-active nanoparticles act as multifunctional monomers. Usually, a higher functionality of monomer results in earlier vitrification due to the higher cross-linking efficiency. For example, due to a vitrification effect, decreased photopolymerization rate and epoxy-group conversion are observed for photopolymerization of epoxy resin/GPS-modified Fe_2O_3 nanocomposite coatings with increasing amount of iron oxide in the photocurable formulations [84].

Fast curing rates and a high final conversion are generally seen at low nanoparticle content or for those completely transparent nanocomposite coatings. For instance, a remarkable increase in the UV curing rate and final conversion is seen only for coatings prepared at 1 wt.% clay using bead milling (Fig. 1.11) [52]. Unchanged or deteriorated curing behaviors are demonstrated for other samples due to poor dispersion of clay and high viscosity. For the coatings based on methyltrimethoxysilane (MTMS)/MPS comodified colloidal silica nanoparticles and acrylic resin, the

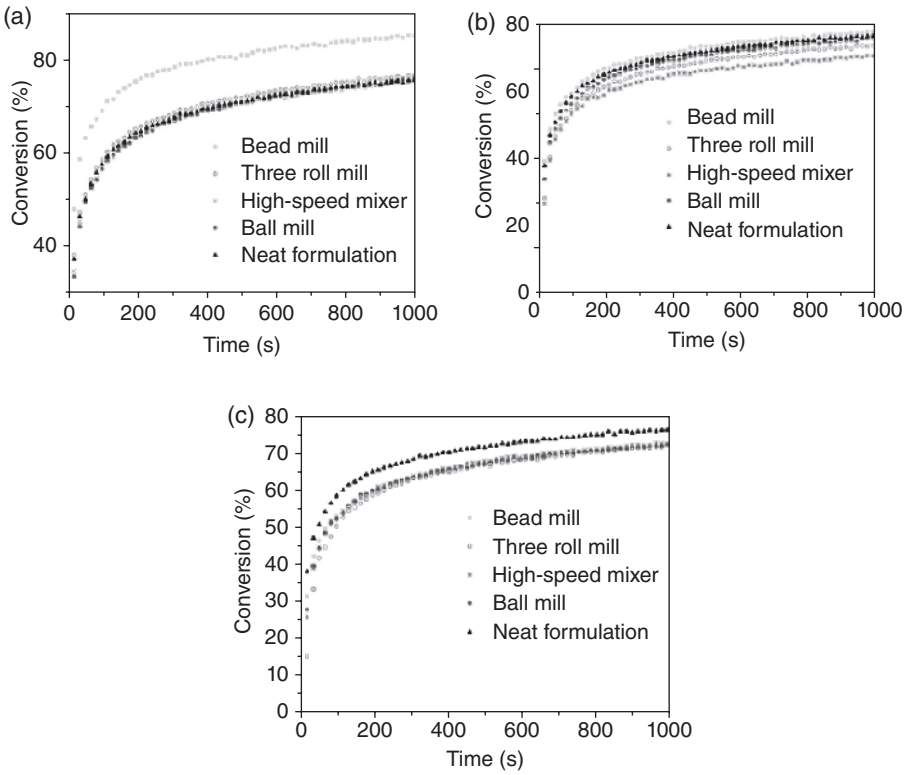

FIG. 1.11 Percent conversion versus time plots of formulations prepared with 1, 3, and 10 wt.% of clay with the roll mill, the ball mill, the bead mill, and the high-speed mixer. Reprinted with permission from Ref. 52. © 2008 Elsevier.

conversion degree of the C=C bond increased up to 85–88% at composition ranges of 0–40 wt.%. However, the conversion degree decreased to 50% at 80 wt.% colloidal silica nanoparticles because of the screen effect of nanoparticles on the polymerization of the acryl or methacryl radicals [85]. In the nanocomposite coatings based on nonaqueous synthesized ZrO_2 nanocrystal (3.8 nm), the final conversion steadily increases from 80.5 to 91.3% as the ZrO_2 content increases from 0 to 20 wt.%. It declines to 68.0% at 25 wt.% of ZrO_2 because of phase separation (Fig. 1.12) [31]. The increased limited conversion of UV-curable nanocomposite coatings may be caused by the reduced oxygen inhibition because inorganic nanoparticles can enhance the barrier property of the coating.

Mechanical improvement of nanoparticles has been widely demonstrated for UV-curable coatings. Bauer *et al*. [86] showed that fumed silica can improve the abrasion and scratch resistance of UV-curable coatings. Soloukhin *et al*. found that nanocolloidal silica particles could enhance the elastic modulus and hardness of acrylic-based UV-curable coatings on a polycarbonate (PC) substrate [87]. Even for those cases with negative effects of nanofiller on UV curing, the addition of

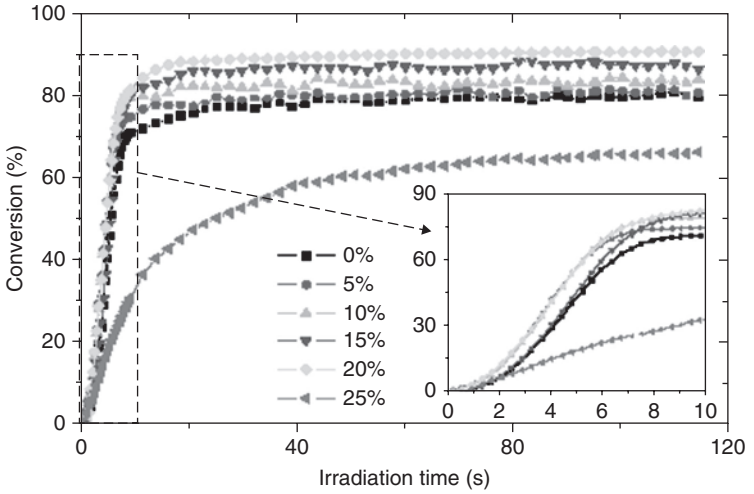

FIG. 1.12 Photopolymerization profiles of PUA/ZrO_2 nanocomposite coatings with different MPS-ZrO_2 loads (10 mW/cm^2, air, 5 wt.% Iragure 184 based on the weight of PUA coating). Reprinted with permission from Ref. 31. © 2009 Springer Science + Business Media, LLC.

nanofiller still results in a rise of cross-linking density and hence an enhanced rigidity of coatings. Kang *et al*. embedded MPS-modified colloidal silica particles (20 nm) into acrylic resin (SK CYTEC, UP 053) [85]. The coating keeps the same transparency as the neat material even with silica loads as high as 80 wt.%. The nanoindentation hardness steadily increases from 0.41 to 0.59 GPa when the silica load increases from 0 to 80 wt.%. Kim *et al*. found that when 10 wt.% MPS-modified ZnO nanoparticles were added, the hardness and elastic modulus of UV-cured PU coating increased from 0.03 to 0.056 GPa and from 2.75 to 3.55 GPa, respectively [88]. However, the reinforced efficiency of nanoparticles in UV-curable coatings strongly depends on the type of nanoparticle, the surface modifier, as well as the polymer matrix [89]. Leder *et al*. incorporated 5–15% treated pyrogenic silica into Laromer PO 43 F oligoether acrylate [90]. An improvement in the mar resistance of 10–35% was seen. This refers to remaining gloss after scrubbing. Meanwhile, the viscosity of the liquid coatings was more stable. Zhang *et al*. mixed C150 sol with a urethane-acrylate oligomer to get a UV-curable nanocomposite coating [91]. They saw a 20% decrease in the coefficient of friction of a coating filled with 40 wt.% nanosilica particles relative to unfilled coating. Under the same fretting test conditions, the wear rate in terms of wear volume of the hybrid coating containing 40 wt.% nanoparticles was about 70 times lower than that of the neat coating, confirming the wear-reduction capability of the nanoparticles. In the UV-waterborne PU-acrylate nanocomposite coatings, the addition of nanoalumina and nanosilica decreases the hardness because of nanoparticle aggregation. Versus the neat coating, the scratch resistance (gloss retention after scratch) of the nanocomposite coatings was significantly improved. Other

TABLE 1.5 Haze and Diamond Microscratch Hardness of Pure SR494/HDDA (1:1) Polyacrylate Film and Nanocomposite Coatings (9 wt.% SiO_2)[a]

	SR494/HDDA	Unmodified Pyrogenic Silica	MPS-Coated Silica	Colloidal Silica
Haze (%)	85	45–65	25–35	50–65
Hardness (N)	1.0	3.0	2.5	1.5

[a] From Ref. 96. © 2002 WILEY-VCH Verlag GmbH & Co. KGaA.

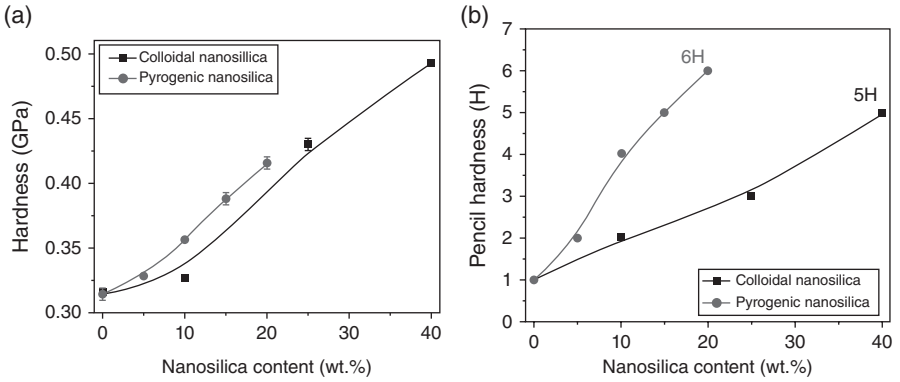

FIG. 1.13 Nanoindentation hardness (a) and pencil hardness (b) of the coatings samples as a function of the silica nanoparticle content. Reprinted with permission from Ref. 3. © 2011 Elsevier.

nanofillers, such as clay [92, 93], boehmite [94], nanotitania [95], have also been employed to enhance the hardness and scratch resistance of UV-curable coatings.

Similar to solventborne or waterborne nanocomposite coatings, pyrogenic silica and colloidal silica are frequently adopted and compared in terms of efficiency and mechanical improvement. In Bauer's report, a distinct improvement in the mechanical properties of a UV-curable SR494/HDDA coating was seen for surface-modified pyrogenic silica compared with colloidal SiO_2, as seen in Table 1.5 [96]. It is assumed that the higher density and hardness of the fumed nanoparticles give better abrasive resistance at the same filler content. Zhang *et al*. also compared the influence of colloidal and pyrogenic silica on the properties of PU coatings [3]. The results are presented in Fig. 1.13. In comparison with colloidal nanosilica-filled coatings, the pyrogenic nanosilica-filled ones had a higher modulus, hardness, wear resistance (in terms of pencil hardness and fretting resistance) as well as slightly lower optical transmittance, gloss, and higher haze. Bautista *et al*. found that nanoalumina did not influence wear resistance [89]. However, nanosilica did modify the elastic and plastic deformation in different ways depending on the polymer matrix and improve the wear resistance of the coating. These different behaviors of nanosilica and nanoalumina in the wear resistance may be due to the chemical nature of the particles or to the surface treatment of the particles to obtain stable commercial suspensions.

TABLE 1.6 Abrasion, Haze, and Diamond Microscratch Hardness of Pure SR494 Polyacrylate and Nanocomposite Coatings (ca. 25 wt.% SiO_2, Modified by Different Silanes)[a]

	Unmodified	Modified With MPS-Coated Silica	Modified With VTS-Coated Silica	Modified With PTS-Coated Silica
Abrasion (mg)	53.1	21.1	16.4	19.8
Haze (%)	85	14.4	3.2	8.5
Hardness (N)	1.0	1.5	2.5	1.7

[a] From Ref. 96. © 2002 WILEY-VCH Verlag GmbH & Co. KGaA.

Nevertheless, enhancement of scratch resistance is independent of the intrinsic hardness of inorganic domains for the UV-curable nanocomposite coatings from a sol–gel process [97].

Nanoparticles modified with polymerization-active silanes such as MPS and VTS form cross-links within UV and EB curable acrylate/nanoparticle systems. This changes the viscoelastic data of the copolymerized composites. However, as seen in Table 1.6, even the simple organophilation of nanosized pyrogenic silica by the polymerization-inactive PTS results in transparent polyacrylate nanocomposite films with improved scratch and abrasion resistance [96]. Various MPS coverage on the surface of nanoparticles also impacts the performance of nanocomposite coatings. In a MPS-modified SiO_2/HDDA/acrylate resin, it was shown that as the MPS/SiO_2 weight ratio increased from 0.2 to 0.6, the dispersion, compatibility, and cross-linking density between the MPS-modified SiO_2 particles and acrylate resin were improved, leading to an increase in pencil hardness from 4H to 6H as well as increased abrasion resistance [98, 99]. Interesting mechanical results were also found in the UV-curable nanocomposite systems using sol–gel derived titania nanoparticles modified with a isopropyl tri(dioctyl)pyrophosphato titanate coupling agent. Both the hardness and flexibility of the photocured nanocomposite films were improved simultaneously, in contrast to neat organic UV-curable formulations [95].

Some studies clearly show that the mechanical increase in nanocomposite coatings is related to the type of polymer matrix. Table 1.7 gives the parameters obtained in wear tests and scratch tests for the nanocomposite coatings based on acrylated polyester resin (A series), acrylated epoxy resin (B series), and acrylated urethane resin (C series) [89]. Improvement in the specific rate of wear was seen for all three coatings, but the increased critical load of scratch start (L_{C1}) with increasing nanosilica load was only seen for the softest polyester coating and hardest epoxy coatings. Figure 1.14 shows the pendulum hardness (Koenig hardness) of the nanocomposites coatings as a function of ZrO_2 content [32]. The efficiency (namely, the slope) for enhancing the hardness of the coating is independent of the inherent hardness of the organic matrix but is strongly related to the amount of PU oligomer in the UV-curable formulation. Lower slopes are seen at higher amounts of PU oligomer because of the low compatibility of PU oligomer with MPS-modified ZrO_2 nanoparticles.

TABLE 1.7 Wear and Scratch Parameters for the Nanocomposite Coatings[a]

		Wear test		Scratch test			
Sample	Nanosilica g/100 g polymer	Specific rate (kg/mN × 10^9)	Total penetration depth[b] (μm)	Elastic recovery[b] (%)	Residual depth[b] (μm)	L_{C1}[c] (mN) ± 100	L_{C3}[c] (mN) ± 100
AH1	0	7.6	22.2	98.6	0.31	590	—
AH2	5	6.4	17.2	98.6	0.24	640	—
AH3	20	4.7	14.3	98.9	0.16	960	1690
BH1	0	11.0	3.8	77.6	0.85	530	—
BH2	5	9.1	3.3	74.7	0.84	550	—
BH3	20	4.3	5.1	912	0.45	530	—
CHI	0	9.1	7.2	99.0	0.07	400	1620
CH2	5	7.3	10.3	96.9	0.32	400	1540
CH3	20	8.5	9.7	97.9	0.20	210	1670

A, polyester matrix; B, epoxy matrix; C, urethane matrix.

[a] Reprinted with permission from Ref. 89. © 2011 Elsevier.

[b] Determined at 1570 mN.

[c] L_{C1}, critical load of scratch start and L_{C3}, critical load of layer breaking.

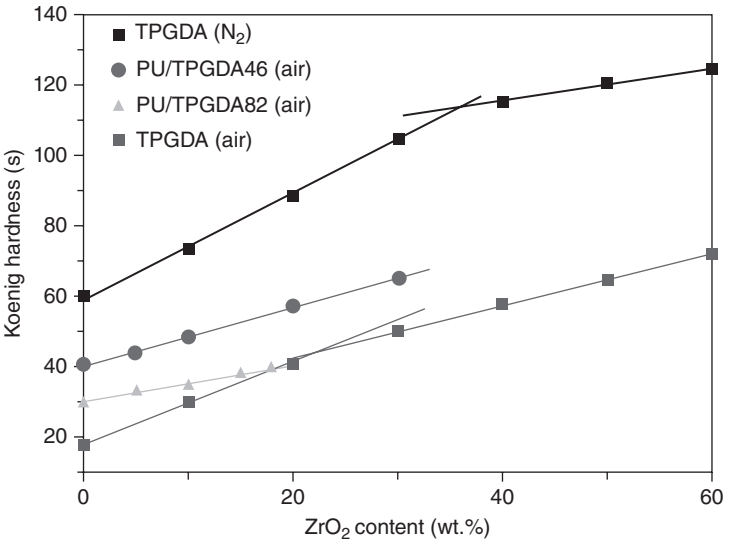

FIG. 1.14 The pendulum hardness of the samples with different ZrO_2 contents. Reprinted with permission from Ref. 32. © 2010 Elsevier. Symbol, the determined value; solid line, linear fitting curve.

1.3.4 Other Mechanically Strong Nanocomposite Coatings

Protection coatings against scratch are critical for transparent plastics such as PC and PMMA. One of the routes for fabrication of these coatings is to mix nanofillers with organoalkoxylsilane-containing hybrid binder. With this route, nanofillers work as dense hard phase, cross-links, and may even serve as the catalyst.

GPS-based hard nanocomposite coatings have been frequently reported since the 1990s. Schmidt *et al*. fabricated a ultrahard coating from acetic acid-modified boehmite powder (8–17 nm) and an I/O hybrid binder that was composed of GPS, aluminum alkoxide, and TEOS [19, 100]. The coatings cast on a PC substrate showed prominent scratch resistance in a modified Vickers test (Fig. 1.15). A scratch resistance below 2% haze was also obtained in 1000 cycles of the Taber abrading test—this is comparable with that of floatglass (1.5% haze after 1000 cycles). The boehmite particles served as the cross-linking catalyst for epoxides in this example also.

Daniels and Francis reported GPS-modified colloidal silica coatings based on the addition of GPS to a commercial acidic silica sol [101]. The GPS/silica weight ratio is crucial to both the critical cracking thickness and the abrasion resistance. The critical cracking thickness of the coatings increased dramatically when the weight ratio of GPS/silica surpassed 0.4. Better abrasion resistance was obtained at a GPS/silica weight ratio of 0.5. Excess GPS content deteriorated the abrasion resistance of the coatings. Mosher *et al*. reported the synthesis of three particles (SiO_2, ZrO_2/CeO_2, CeO_2) that reinforced water-based nanocomposite coatings. The films are sol–gel derived using a nonionic surfactant, aluminum perchlorate [$Al(ClO_4)_3$] catalyst, nanoparticle colloids, and GPS [102]. The silica colloid

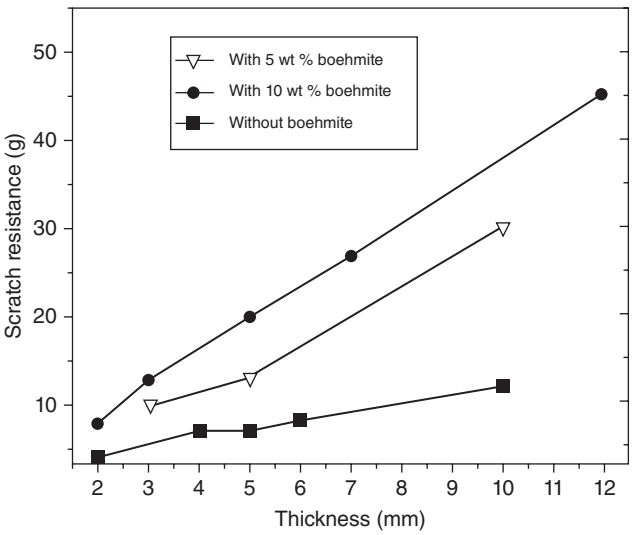

FIG. 1.15 Results of the scratch tests (modified Vickers test) on composite coatings with different amounts of boehmite particles [100].

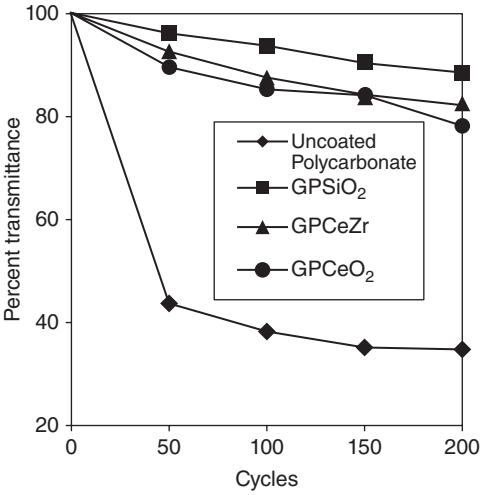

FIG. 1.16 Light transmittance in wear track as a function of wear cycles. Reprinted with permission from Ref. 102. © 2006 Elsevier.

composites ($GPSiO_2$) provide the best mechanical properties without decreasing the unique optical properties of inorganic materials (Fig. 1.16).

Chen *et al*. fabricated transparent GPS composite coatings filled with up to 40 wt.% boehmite nanoparticles and nanorods [103]. The hardness and modulus of the boehmite nanorod filled coatings were slightly lower than those of the same coating filled with boehmite nanoparticles. However, nanorods with an aspect ratio around 20 significantly improve the crack toughness of the GPS composite coating. The authors attributed this observation to the formation of cross-ply structures and the orientation of nanorods in the coatings.

Ultrahard nanocomposite coatings can also be prepared based on MPS and MTMS precursors. For example, nanoscaled AlOOH particles were added to MPS and hydrolyzed in deionized water. The mixture was then diluted with 1-butanol and blended with the UV initiator BYK 306 to produce UV-curable hard coatings. The coatings can be sprayed on plastic substrates (PC, PMMA) to form a transparent film with a thickness of several micrometers. The transparent coatings show excellent adhesion on PMMA and PC (GT/TT = 0/0, DIN 53151) even in the absence of primers. Their abrasion resistance after the Taber test was haze values of 10% after 1000 cycles (CS 10F rolls, 5.4 N, DIN 52347) [104]. In another case, scratch-resistant hard coatings were successfully prepared by mixing a basic colloidal silica sol with hydrolyzed MTMS using the sol–gel method. Nanocomposite coatings were applied to PMMA substrates by dip coating and cured in a thermal oven. The presence of SiO_2 nanoparticles in this siloxane-based coating at optimal quantities—40, 50, and 60 wt.% of SiO_2—enabled highly transparent coating films with good hardness and scratch resistance [105].

Besides organoalkoxylsilane-based ultrahard nanocomposite coatings, mechanical protection coatings can also be prepared by mixing nanofillers with polymer. For

instance, silica nanoparticles from the hydrolysis and condensation of TEOS were surface modified with MPS and subsequently dispersed into dissolved PMMA solution. The coating with 10 wt.% silica content had good transparency (>90%) and high pencil hardness grade (>5H) [106]. Hard (4H), scratch resistant, and flexible nanocomposite coatings can also be achieved through the introduction of 3 wt.% unmodified nanoclay (Na^+MMT) into a polymer resin based on a hyperbranched polyester Boltorn H30 [107]. Nevertheless, the organoclay prepared by cation exchange between sodium ion MMTs and octadecyl ammonium increases the hardness of alkyd clear coatings much more dramatically. This may be due to the formation of exfoliated structures resulting from the high compatibility of long-chain hydrocarbons of octadecyl ammonium salts with the long-chain hydrocarbons of the fatty acids in the alkyd resin [108].

1.4 OPTICAL NANOCOMPOSITE COATINGS

Because nanocomposite coatings are transparent in visible range, they have high potential as optical coatings including UV-shielding coatings [109], RI-adjustable coatings, NIR-shielding coatings, nonlinear optical coatings [110], etc.

1.4.1 Transparent UV-Shielding Nanocomposite Coatings

Traditionally, choices for protecting coatings from the sun include organic UV absorbers as hindered amine light stabilizers. Organic UV absorbers are colorless or nearly colorless compounds having high absorption coefficients in the UV region. They protect coatings against photoinduced damages by absorbing the harmful solar radiation. The addition of organic UV absorbers protects the substrate, but the effect is not permanent and such stabilizers tend to migrate or decompose during exposure. An alternative is inorganic metal oxide nanoparticles. These do not migrate from the matrix and exhibit excellent photo- and thermostability. Hot topics in inorganic nanoparticles for UV-shielding coatings include nano-TiO_2, nano-ZnO, and nano-CeO_2.

TiO_2 nanoparticles have two main crystalline forms: rutile and anatase. The rutile nano-TiO_2 with high UV opacity and lower photoactivity is an effective UV protector in coatings [111]. Figure 1.17 compares the UV–vis spectra of the cured alkyd films containing organic UV absorber, rutile nano-TiO_2, and anatase nano-TiO_2. The films with organic benzophenone or benzotriazole are excellent at UV-blocking and highly transparent in the visible range regardless of film thickness (0.32 or 0.85 mm). The UV blocking of these films with nano-TiO_2 is incomplete at 300–400 nm because of their inherent wide band gaps. UV-shielding performance can be enhanced by increasing the film thickness. Nevertheless, the visible transmission of thick films via nano-TiO_2 considerably declined. In other words, better UV blocking with TiO_2 nanoparticles usually leads to poorer transparency of the coating [112].

Low transparencies or glosses of UV-block nanocomposite coatings were also demonstrated for APS-modified TiO_2 nanopowder in poly(vinyl alcohol) [113], GPS-modified TiO_2 nanoparticles in polyacrylic clearcoats [114], and heptaisobutyltrisilanol

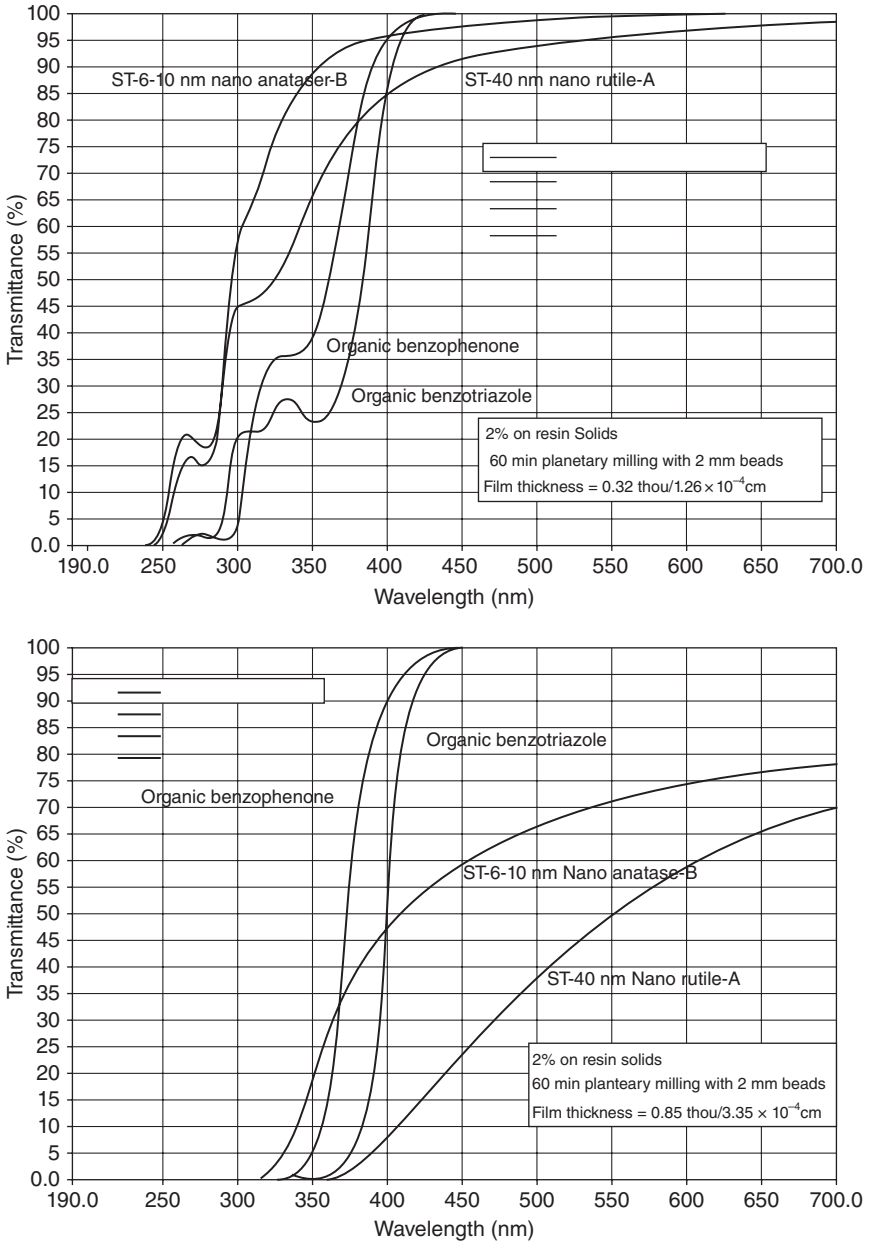

FIG. 1.17 Transmission spectra of Lowilite 24 and Lowilite 26 compared with nanoparticles of anatase-B and rutile-A in a cured alkyd resin film at 2% w/w on resin solids. Reprinted with permission from Ref. 111. © 2002 Elsevier. Film thickness: a, 0.32 mm; b, 0.85 mm.

polyhedral oligomeric silsesquioxanes (POSS)-modified TiO_2 nanoparticles in waterborne coatings [115]. Light scattering by the nano-TiO_2 aggregates is due to the opacity of the coatings. The high RI of the nano-TiO_2 in particular further consolidates the light scattering. In addition, the photocatalytic activity of nano-TiO_2 can degrade most polymer matrices and shorten the durability of the UV-shielding coatings. These two shortcomings seriously restrict the use of TiO_2 nanoparticles as UV absorbers in coatings.

To depress the photocatalytic activity of TiO_2 nanoparticles, they can be encapsulated with SiO_2 or Al_2O_3 to form core/shell composite particles [114, 116] or create rattle-type TiO_2@void@SiO_2 particles [117]. The use of a polymer matrix, that is, polysiloxane that can tolerate photocatalytic degradation, is another solution for fabricating UV-shielding coatings [118]. The opacity of TiO_2-based coatings can be solved using a commercially available colloidal TiO_2 sol. Hwang *et al*. [119] treated HIT-30 M TiO_2 sol (Nissan Chemicals, Japan) with GPS and then performed hydrolysis and condensation reactions with dimethyldimethoxysilane and MTMS to produce UV protective coatings for PC. The coating can completely block the UV light below 350 nm with high visible transmission (>85% at 550 nm).

Transparent TiO_2-based, UV blocking coatings can also be prepared by combining TiO_2 nanophase *in situ* via a sol–gel process using polymer or hybrids. Chen *et al*. employed trialkoxysilane-capped PMMA and titanium(IV) *n*-butoxide to prepare titania-based hybrid optical coatings via an *in situ* sol–gel process combining spin coating and multistep baking [120]. The prepared hybrid films show very high optical transparency in the visible region. The shift in the absorption maximum of the prepared hybrid thin films correlates with the titania content. Sangermano *et al*. introduced TiO_2 nanophase into the cationic UV-curable formulations using nanoparticles *ex situ* or *in situ* from a sol–gel process [118]. The UV-shielding effect of *in situ* TiO_2 is comparable to that of *ex situ* TiO_2. Moreover, the *in situ* TiO_2 offered transparent coatings without interfering with the photopolymerization process or compromising the UV-cured film properties. Mazzocchetti *et al*. reported the synthesis of new polymer-titania hybrids, where the organic phase contains polyesters such as poly(ε-caprolactone), poly(D,L-lactic acid), and poly(L-lactic acid) [121]. Hybrids coated on transparent substrates have their intrinsic optical transparency and the ability to completely block UVB and UV-A2.

When textiles are coated with hybrids, they become radiopaque thus offering new personal protective clothing and equipment. Que and Hu prepared I/O hybrid films using GPS, MTES, and tetrapropylorthotitanate as precursors [122]. The absorption band red shifts as the titanium content in the coatings increases (Fig. 1.18). Complete blocking of UV light below 350 nm was realized when the titanium molar content reached 0.4 M. Xiang *et al*. prepared hybrid materials *via* an aqueous sol–gel technique from tetra-*n*-butyl titanate as the precursor of titania in the presence of MQ silicone resin [123]. The hybrid nanocomposites were colorless and highly transparent in visible light region. It absorbed light below 320 nm.

Although the coatings generated *in situ* with TiO_2 nanophase are highly transparent, they are usually yellow especially those with wide band blocking performance. The colorful appearance will restrict their applications. To avoid phase separation,

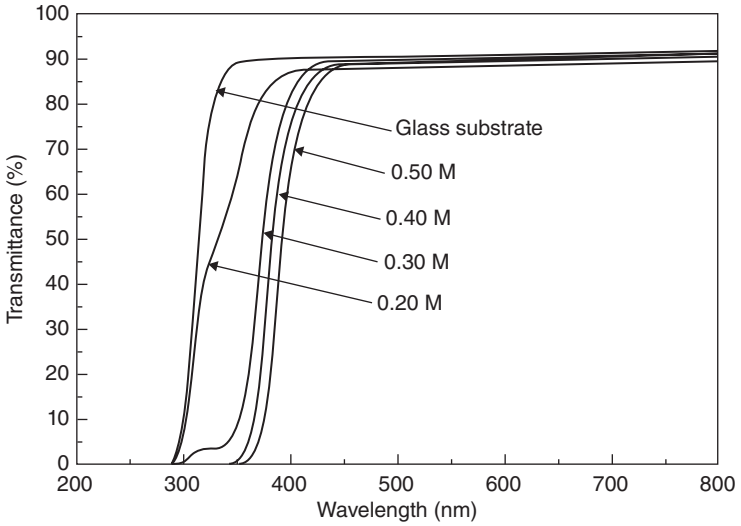

FIG. 1.18 Dependence of the optical transmittance of the films heated at 100°C on titanium content. Reprinted with permission from Ref. 122. © 2013 IOP Publishing Ltd.

chemical bonding between the TiO_2 nanophase and the polymer or hybrid matrix is usually designed in the sol–gel-derived TiO_2-based UV blocking coatings. This chemical bonding design suggests that the coatings have to be 2K coatings—one component for prehydrolyzed TiO_2 sol (or TiO_2 precursor) and the other for the binder (polymer or hybrid). The pot life of coatings thus limits their utility. The sol–gel-derived TiO_2 nanophase in the coatings is usually amphorous. Its photocatalytic activity would be low however, and may not be negligible for long-term service. Unfortunately, the effect of the photocatalytic activity of amphorous TiO_2 on the durability of UV-block coatings is seldom reported and unclear. Nevertheless, similar to coatings based on TiO_2 nanoparticles, the polysiloxane or sol–gel-derived silica hybrids would be a better choice as the binder of UV blocking coatings with TiO_2 nanophase generated *in situ*.

ZnO nanoparticles are a semiconductor with a band gap of 3.37 eV and have been widely used as UV absorbers in sunscreens [124], textile fibers [125], transparent packing materials for UV-light based white light–emitting diodes [126], and especially coatings. For example, Li *et al*. indicated that nanosized ZnO particle could be an UV absorbent for I/O hybrid coatings derived from TEOS and GPS on a PMMA substrate [127]. Khrenov *et al*. incorporated ZnO nanoparticles prepared by inverse emulsion polymerization into a solution of poly(2-ethylhexyl methacrylate), PMMA, and PS [128]. These nanocomposite films demonstrated good UV absorption. Weichelt *et al*. introduced various kinds of commercial ZnO nanoparticles into a UV-curable wood lacquer [129]. Spruce wood coated with the ZnO-based nanocomposites showed comparable brightness change (ΔL^*) but decreased yellowing factor (Δb^*) versus those in the conventional HALS/UVA system (Fig. 1.19). Even better protection can be realized using a combination of lignin protecting impregnation and nano-ZnO in

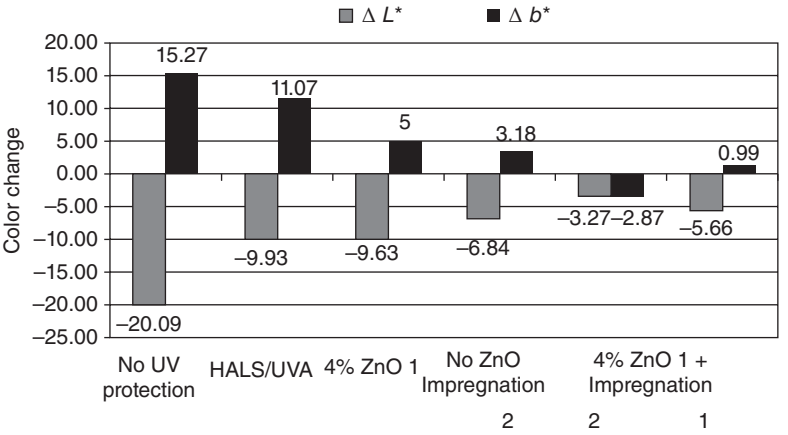

FIG. 1.19 Change of brightness (ΔL^*) and b^* value (Δb^*) of spruce wood samples coated with nanocomposite UV lacquer as UV protectant [129]. (Weathering time 1500 h, ZnO 1: 20 nm, Impregnation 1: an aqueous wood impregnation H5100 containing 2 wt.% of a solid lignin protecting agent 1; Impregnation 2: containing 5% of water-based lignin protecting formulation 2.) Ref. 129. © 2010 WILEY-VCH Verlag GmbH & Co. KGaA.

the top coat. Kim *et al*. found that UV light below 450 nm can be efficiently absorbed by incorporating ZnO nanoparticles into a UV-curable PU matrix [88]. However, because of their intense scattering of visible light, the pigmentary grades of ZnO nanoparticles usually produce opaque systems when they are embedded into polymer matrices [88, 129]. This seriously restricts their applications in highly transparent materials.

ZnO quantum dots (ZnO QDs) produce highly transparent ZnO-based UV-shielding coatings. They have very small size (usually <10 nm) and retain the excellent UV absorption capability making them good inorganic UV absorbers. Some UV-shielding polymer-based nanocomposites, such as PMMA/ZnO nanocomposites [130], PS/ZnO thin films [131], and poly(butyl methacrylate) (PBMA)/ZnO nanohybrid films [132] have been reported. Figure 1.20 shows the UV–vis absorbance and transmittance spectra of PBMA/ZnO nanocomposite films prepared by bulk polymerization [132]. The nanocomposite films can completely block the UV light below 350 nm while maintaining the same transparency as pure PBMA film with greater than 90% visible light transmittance regardless of the nanophase content. Nevertheless, Jeeju *et al*. found that the absorption window shifts toward a shorter wavelength as the size of the ZnO nanocrystals decreases [133]. This implies that the UVA and even part of UVB may not be blocked by nanocomposite coatings containing ZnO QDs. The remarkable photocatalytic activity of ZnO QDs is even higher than that of TiO_2 nanoparticles (P25) [134] and is another disadvantage of ZnO QDs as a UV absorber. Bare ZnO QDs cannot fabricate long-term durable UV-shielding coatings. However, encapsulation of ZnO QDs with inert silica shells can efficiently insulate their photocatalytic activity depressing the ZnO QD–induced decomposition of polymer matrices [135].

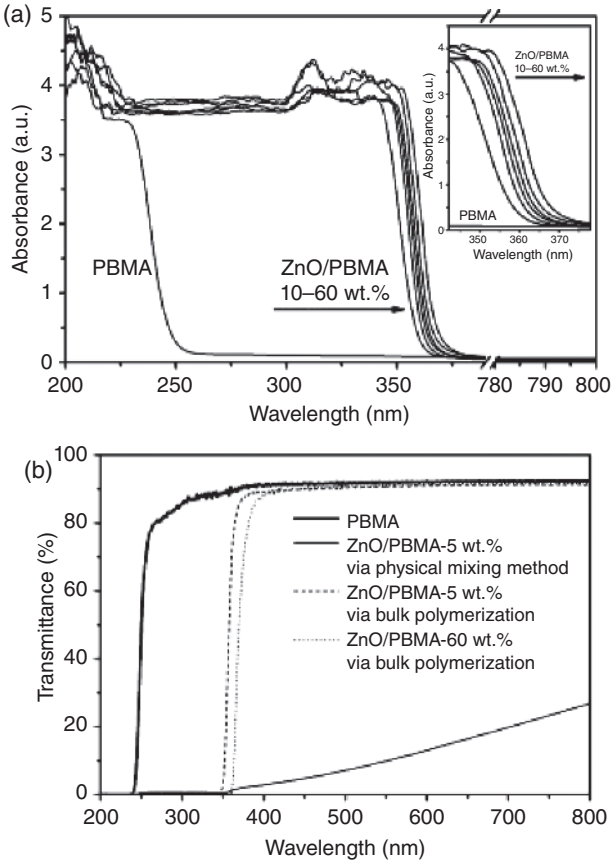

FIG. 1.20 (a) The UV–vis absorbance spectra of pure PBMA film and ZnO/PBMA nanohybrid films synthesized by bulk polymerization containing ZnO NPs from 10 to 60 wt.% in 10 wt.% increments. (b) The UV–vis transmittance spectra of pure PBMA film and ZnO/PBMA nanohybrid films prepared by bulk polymerization and physical mixing method. The thickness of each film was about $100 \pm 5\,\mu m$. Reprinted with permission from Ref. 132. © 2012 American Chemical Society.

Compared to nano-TiO_2 and nano-ZnO, CeO_2 nanoparticles have minimal photocatalysis. Their disadvantage is oxidation catalytic activity. It can be significantly reduced by doping with metal oxide. CaO-doped cerium dioxide had excellent UV absorption and transparency in the visible ray region even better than undoped cerium dioxide [136]. Figure 1.21 shows the absorption spectra of water-based coatings containing various colloidal particles. The coating with colloidal CeO_2 displays strong UV absorption. In contrast, UV absorption is not present for the coating with colloidal SiO_2 [102]. Protection of organic coatings by UV-induced degradation from CeO_2 nanoparticles was also demonstrated in a water-based PU clearcoat [137].

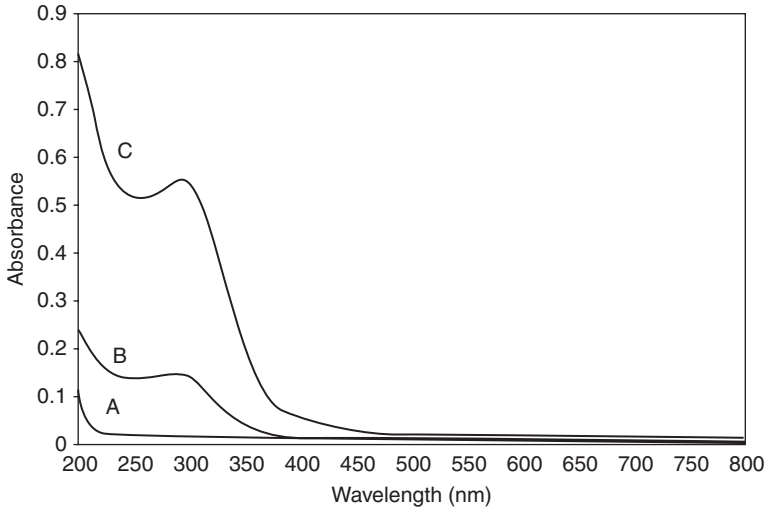

FIG. 1.21 Absorption spectra of coatings sols diluted 10,000 times in H_2O. Coating with (A) colloidal silica, (B) colloidal ceria and zirconia, and (C) colloidal ceria. Reprinted with permission from Ref. 102. © 2006 Elsevier.

Recently, cerium phosphate ($CePO_4$) nanoparticles with low photocatalytic activity and high absorption in the UV region were developed [138]. This provides new route to formulate transparent, UV-shielding OINCs.

1.4.2 High Refractive Index Nanocomposite Coatings

High RI coatings are used as optical coatings of lens, optical fiber coatings, and antireflective coatings. Unfortunately, the refractive indices of conventional organic coatings such as polyacrylate, PU, alkyd, and polysiloxane are lower than 1.50. The introduction of sulfur, bromine, heavy metals, or phenyl and alicylic groups into the polymer chains is one strategy to increase the RI of the polymer. Nevertheless, with development of nanomaterials, embedding the nanofillers with high RI into organic coatings has been increasingly employed to acquire high RI coatings.

The RI (n) of nanocomposite coatings can be approximately calculated by the following equation:

$$n = \phi_p n_p + (1 - \phi_p) n_m \tag{1.4}$$

If the weight fraction of the inclusion nanoparticles is adopted, Equation (1.4) can be changed as follows,

$$n = \frac{\rho_p n_m - w_p(\rho_p n_m - \rho_m n_p)}{\rho_p - w_p(\rho_p - \rho_m)} \tag{1.5}$$

where ρ_p and ρ_m are the densities of nanoparticle and host matrix, respectively, and w_p is the weight fraction of nanoparticles.

The RI of nanocomposite coatings can also be theoretically calculated with an equation deduced from the Maxwell–Garnett approximation,

$$n = n_m \sqrt{1 + \frac{3\phi_p \beta}{1 - \phi_p \beta}} \tag{1.6}$$

$$\beta = \frac{m^2 - 1}{m^2 + 2} \tag{1.7}$$

where β is a coefficien, and m is the relative RI, namely, n_p/n_m. If the inherent RI of the host matrix is not impacted by the nanoparticles, then the calculated value from Equation (1.6) will equal that from Equation (1.4).

Equation (1.4) clearly shows that high RI and high volume fraction of nanoparticles both favor high RI OINCs and thus a wide modulation range of the RI. To date, the inorganic nanoparticles with high RI, that is, metal sulfides (PbS, ZnS) and metal oxides (TiO_2, ZrO_2, ZnO), have been employed to fabricate high RI nanocomposite coatings.

PbS nanoparticles exhibit an RI on the order of 4 across a wide wavelength range. They were ever combined with gelatin to produce nanocomposite films through aqueous solution mixing and subsequent spinning [139]. Figure 1.22 shows the RI of the obtained films as a function of weight fraction of PbS. The weight fraction of PbS is up to 86.4 wt.%, and RI values as high as 2.5 were achieved. ZnS nanoparticles with RI of 2.36 in the visible range are also used to tune the RI of coatings. Antonello *et al*. synthesized ZnS nanoparticles with a mean diameter of 4.8 nm from Na_2S and

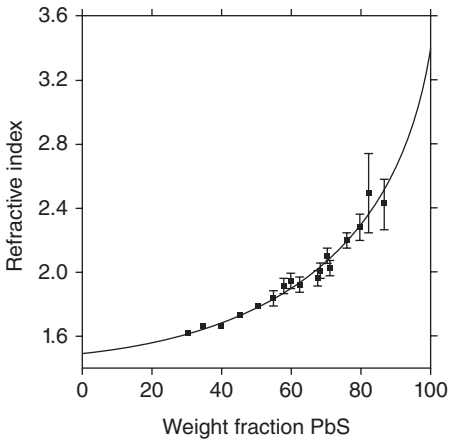

FIG. 1.22 The refractive index of PbS-gelatin nanocomposites as a function of weight fraction of PbS. The solid line represents best-fitting of Equation (1.5). Reprinted with permission from Ref. 139. © 1993 Materials Research Society.

$ZnSO_4$ in the presence of mercapto-group containing capping agents [140]. Then, the nanoparticles were blended in the sol–gel hybrid GZ and DGZ films that were correspondingly synthesized using molar ratios of GPS/zirconium tetraisopropoxide (ZrOPr) = 75:25 and diphenyldymethoxysilane/GPS/ZrOPr = 50:25:25. The RI was adjusted from 1.50 to 1.56 for the GZ film and 1.53 to 1.59 for the DGZ film when the volume fraction of ZnS increased to 0.077%. However, the toxic character of PbS and the photocatalytic activity of ZnS are important considerations.

Among the metal oxides, TiO_2 has the highest RI at 2.7. Thus, high RI nanocomposite coatings commonly use TiO_2 nanophase. The routes to attain high RI TiO_2-based nanocomposite coatings are analogous to those for UV-shielding TiO_2-based nanocomposite coatings. Nevertheless, in order to assure absolute optical transparency, high RI TiO_2-based coatings are mainly fabricated through a sol–gel process. The sol–gel-derived TiO_2-based coatings have two typical morphologies—distinguished TiO_2 nanophase (or nanocrystal) and tianium-oxo network structure. These depend on the sol–gel process. The former morphology is acquired by mixing the TiO_2 nanoparticles, premade from the hydrolysis/condensation of titania precursor, with binder. The TiO_2 content could be high and the TiO_2 nanophase is relatively dense resulting in a high RI of the coatings. The latter is formed by mixing titania precursor with binder and then carrying out a sol–gel process. It is difficult to achieve high Ti loading levels because of the use of a crosslinkable chelating agent (i.e., methylacrylic acid (MAA), 2-(methacryloyloxy) ethyl acetoacetone [141]) and incomplete removal of organic species of the titania precursor. This leads to a narrow range of RI modulation of coatings (generally 1.5–1.6 [122, 141]). Hence, the sol–gel process for high RI TiO_2-based nanocomposite coatings mostly uses advanced synthesis of TiO_2 nanoparticles.

For example, Chau *et al*. synthesized highly dispersed TiO_2 nanoparticles via HCl-catalyzed hydrolysis/condensation reactions in absolute ethanol with TTIP precursor [142]. When these nanoparticles were incorporated into epoxy coatings, an RI of 1.668 was obtained at 30 wt.% TiO_2. Although higher RI values can be obtained by increasing the content of the TiO_2 nanoparticles, cracks appear beyond 50 wt.% TiO_2. Antonello *et al*. prepared TiO_2 nanocrystals with a similar HCl-catalyzed sol–gel process but in a methanol/water mixture [143]. The TiO_2 nanocrystal was mixed with an O/Ihybrid via the cohydrolysis/condensation of GPS/TTIP. The RI values of the coatings are tunable between 1.51 and 1.89. Figure 1.23 shows the RI evolution of the coatings with TiO_2 content (both in volume fraction and in weight fraction).

Chang *et al*. prepared a TiO_2 sol via HCl-catalyzed hydrolysis of tetrabutyl orthotitanate (TBOT) in 1-butanol [144]. The TiO_2 nanoparticles are subsequently coated with MAA or MPS and mixed with dipentaerythritol hexacrylate and photoinitator to yield UV-curable nanocomposite coatings with RI of 1.64–1.77. Liu *et al*. premade TiO_2 nanoparticles by hydrolysis/condensation of TIPP in water, dissociation of gel with nitric acid, and low-temperature (80°C) treatment [145]. After a washing step, the wet TiO_2 nanoparticles were redispersed in a mixture of *N,N*-dimethylacetamide and butanol (1:1, w/w). The TBOT and epoxy resin were then added to the nanoparticle dispersion. As the composition of TBOT/epoxy/TiO_2 film

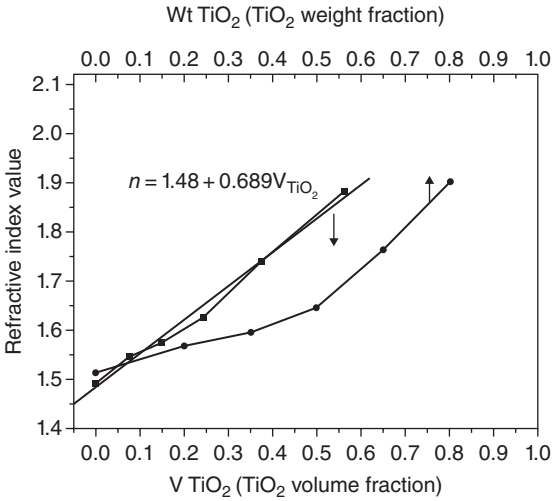

FIG. 1.23 Refractive index values at 630 nm plotted versus TiO_2 volume fraction and weight fraction. Reprinted with permission from Ref. 143. © 2010 Springer Science+Business Media B.V.

TABLE 1.8 Compositions and Properties of TBOT/epoxy/TiO_2 Hybrid Films[a]

Codes	TiO_2 Nanoparticles (wt.%)	TBOT(TiO_2[b]) (wt.%)	Epoxy Resin (wt.%)	Residue[c] (wt.%)	Refractive Index[d]
TE75	75	35.2(8.4)	16.6	55.3	1.908
TE79	79	37.2(8.8)	12.2	65.9	1.965
TE84	84	39.5(9.4)	6.6	68.5	1.972
TE87	87	40.9(9.7)	3.3	72.7	1.917
TE88	88	41.4(9.8)	2.2	79.4	1.873

[a] Reprinted with permission from Ref. 145. © 2011 Elsevier.
[b] Calculated based on the conversion of 1 g of TBOT into 0.2347 g of TiO_2.
[c] Determined through TGA at 500°C.
[d] Measured at 633 nm.

changed, the RI became as high as 1.972 (Table 1.8)—close to that of a pure anatase titania thin film fabricated at high temperature.

Besides the sol–gel process, bead milling of TiO_2 nanopowder was adopted to prepare high RI nanocomposite films. In a typical example [146], TiO_2 nanopowder, which has a primary diameter of 15 nm and a needle-like rutile crystal structure, was milled using 50 μm zirconia beads in disperse media, that is, two monomers (either neopentyl glycol dimethacrylate or divinylbenzene) and butylacetate. The TiO_2-dispersed monomers after addition of benzoyl peroxide were polymerized under heating to form the dried film. The TiO_2 content in the film can be adjusted via addition of TiO_2/butylacetate slurry. Figure 1.24 shows the RI value

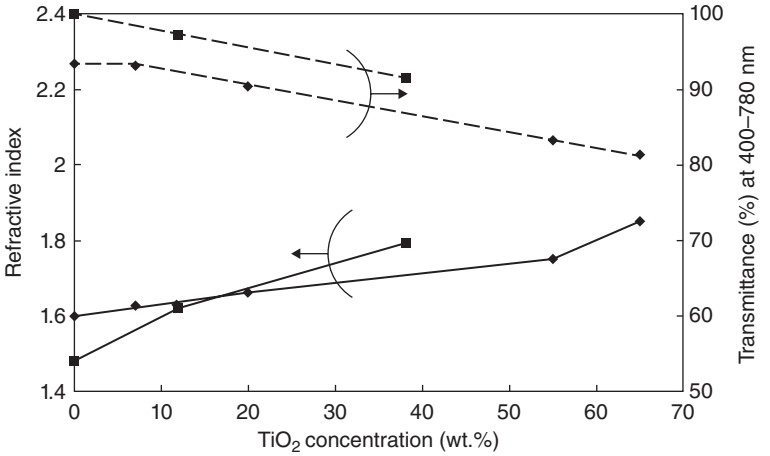

FIG. 1.24 Refractive index and average transmittance of TiO_2-dispersed polymer films fabricated via the bead milling method (◆, neopentyl glycol dimethacrylate; ■, divinylbenzene; straight line, refractive index; dotted line, transmittance (400–780 nm) at film thickness of 5 μm). Reprinted with permission from Ref. 146. © 2008 The Society of Polymer Science, Japan.

of the nanocomposite film as a function of TiO_2 content. The highest concentration achieved was 65 wt.% TiO_2 and gave a nanocomposite film with a RI of 1.85 and transmittance of 81.5% (thickness: 5 μm).

The combination of TiO_2 nanophase with a high RI polymer is another way to obtain high RI nanocomposite coatings at relatively low TiO_2 content. Nakayama and Hayashi synthesized TiO_2 nanoparticles from titanium oxychloride and further treated the TiO_2 surface with ZrO_2 to depress its photocatalytic activity [147]. The resulting TiO_2-ZrO_2 nanoparticles were modified with acrylic acid and then added into a mixture of 2-mercapatoethylsulfide diacrylate (MES-DA) and urethane acrylate (UA-306I) along with photoinitiator to formulate UV-curable high RI coatings. The RI value of the cured coatings can be readily tuned from 1.59 to 1.81 with increasing TiO_2-ZrO_2 content from 0 to 80 wt.%.

Nakayama and Hayashi further blended the TiO_2-ZrO_2 nanoparticles with mercaptoethylsulfide-thiourethane methacrylate (MES-TUMA) or isophorone diisocyanate-mercaptoethylsulfide-thiourethane methacrylate (IPDI-MES-TUMA) [148]. This UV-curable nanocomposite coating is suitable for hard coating of high RI lens substrates (polythiourethane and PC). Chang *et al*. prepared high RI polyimide/titania nanocomposite thin films from a soluble polyimide, a coupling agent (APS), and TTIP [149]. Transparent hybrid thin films can be obtained at TiO_2 content as high as 40 wt.%. The refractive indices at 633 nm of the prepared hybrid thin films increase linearly from 1.66 to 1.82 with increasing TiO_2 content. Photosensitive polyimide–nanocrystalline titania optical thin films were synthesized in Chen's research group using TBOT, and the soluble polyimide with residual carboxyl acid groups and pendant methacrylate groups [150]. The carboxylic acid groups provided bound to titania while methacrylate groups offered photosensitivity. The prepared hybrid films

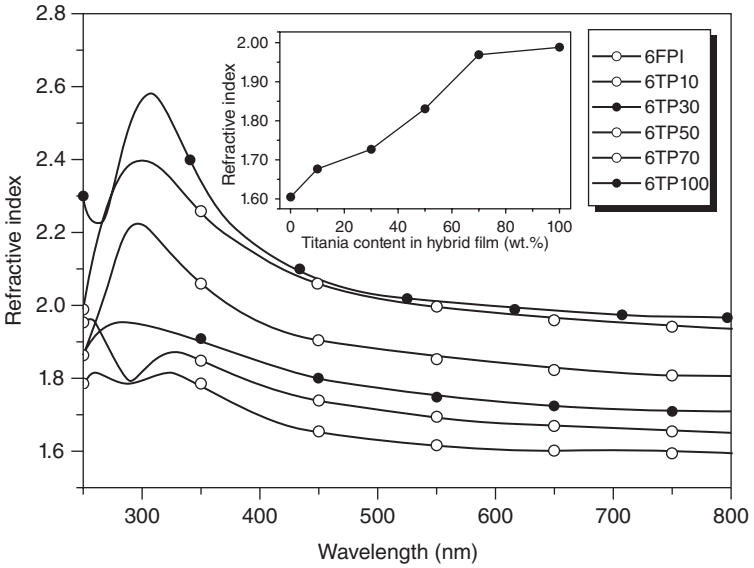

FIG. 1.25 Variation of the refractive index of the 6FPI/TiO_2 nanocomposites with wavelength. The inset shows the variation of refractive index at 633 nm with titania content. Reprinted with permission from Ref. 151. © 2009 The Royal Society of Chemistry.

had tunable and high RI (n = 1.58–2.03), surface planarity, excellent thermal properties, and good transparency in the visible range. Crystalline anatase titania domains in the hybrid films were around 4–7 nm.

Chen's group also employed 6F-poly(p-hydroxy-imide) (6FPI) to fabricate polyimide/TiO_2 nanocomposite films [151]. The bulky CF_3 in the polyimide backbones enhanced both the solubility and optical transparency while the attached hydroxyl groups provided the O/I bonding. Figure 1.25 shows the RI of the films at 300–800 nm and the inset is the variation of RI at 633 nm as a function of titania content. These nanocomposite films can be utilized to fabricate a three-layer antireflection coating that revealed a reflectance of less than 0.7% in the visible range (Fig. 1.26).

ZrO_2 nanophase materials are good candidates for the fabrication of high RI coatings because of their chemical inertance, high hardness, and non-photocatalytic activity. ZrO_2 has a RI value (~2.1) lower than TiO_2. Nonaqueous synthesized ZrO_2 nanocrystals with high dispersibility synthesized from a solvothermal reaction of zirconium (IV) isopropoxide isopropyl alcohol complex in benzyl alcohol were even adopted to prepare UV-curable ZrO_2-based nanocomposite coatings [30–32]. Prior to addition to the coatings, the ZrO_2 nanocrystal was treated with MPS. The upper limit of ZrO_2 content for completely transparent nanocomposite coatings changed with the composition of the coatings as well as the amount of MPS attached to ZrO_2 nanoparticles. The highest ZrO_2 content was 60 wt.% when the MPS-modified ZrO_2 nanoparticles were mixed with TPGDA. The cured coatings had a RI value of as high as 1.78 [32].

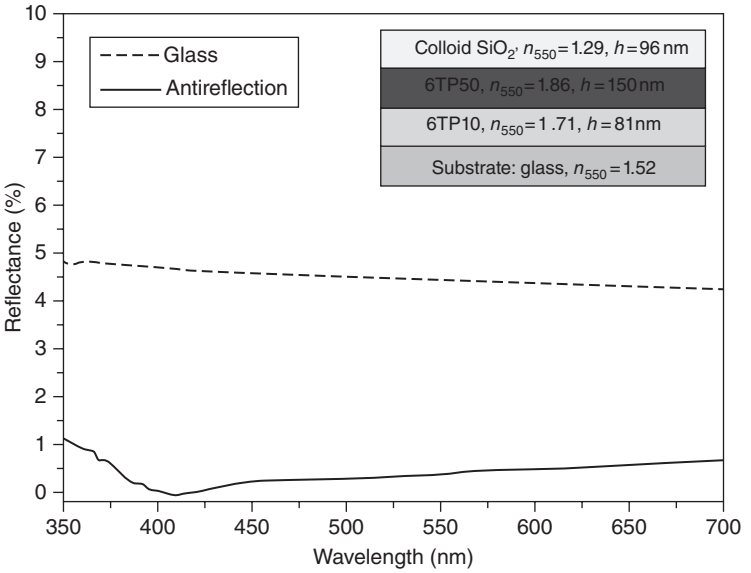

FIG. 1.26 Variation of the reflectance with wavelength: BK7 optical glass and the three-layer anti-reflection coating. The inset shows the structure of the three-layer anti-reflection coating. Reprinted with permission from Ref. 151. © 2009 The Royal Society of Chemistry.

Nonaqueous synthesized ZrO_2 nanocrystals were functionalized with AEAPS and dispersed in water under basic condition (pH 13–14) [42]. The aqueous ZrO_2 nanoparticle dispersion together with the cross-linker 1,4-butanediol digylcidyl ether was formulated as a water-based scratch resistant and high RI coating for PC substrates. Figure 1.27 presents the refractive indices of ZrO_2 nanoparticle films. The absolute refractive indices at 632 nm are 1.70, 1.73, and 1.77 for films prepared at AEAPS-to-ZrO_2 molar ratios of 0.25, 0.18 and 0.12, respectively. Commercial ZrO_2 nanoparticle dispersions in toluene were ever used to prepare high RI nanocomposites with polydimethylsiloxane (PDMS) matrix [152]. The obtained ZrO_2–PDMS nanocomposite had a transparency of 93.3% across the entire visible range via ligand molecule engineering. The RI of the ZrO_2–PDMS nanocomposite could be varied from 1.39 to 1.65 simply by increasing the ZrO_2 content from 0 to 20.8 vol.%.

ZnO nanoparticles are seldom used in the fabrication of high RI coatings due to their low RI value (2.02) and photocatalytic activity. Tsuzuki dispersed ZnO nanoparticles prepared by mechanochemical processing and coated with poly(methylsilsesquioxane) into caprylic capric triglyceride using poly(hydroxystearic acid) in a bead mill at 60 wt.% [153]. The product was 20 μm thick with a RI of 1.44–1.55 and high visible transparency.

Other high RI inorganic nanofillers include Si (n=3.91 at 620 nm, crystalline), Ge (n=5.59 at 620 nm), GaP (n=3.33 at 620 nm), Ta_2O_5 (n=2.1 at 550 nm), indium-doped tin oxide (ITO, n=2.0 at 550 nm), Nb_2O_5 (n=2.3 at 550 nm), $Bi_4Ti_3O_{12}$ (n=2.3 at 520 nm), etc. The details can be found in a prior review [154].

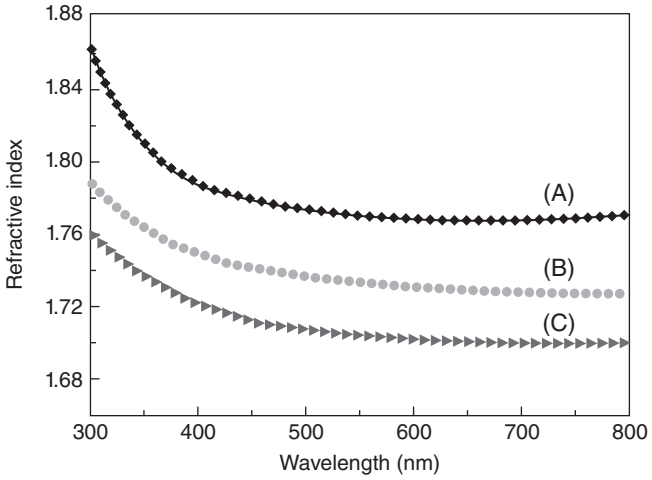

FIG. 1.27 Refractive indices of ZrO_2 nanoparticle films prepared at AEAPS-to-ZrO_2 molar ratio of (A) 0.12, (B) 0.18, and (C) 0.25. Reprinted with permission from Ref. 42. © 2010 Elsevier.

1.4.3 Transparent NIR-Shielding Nanocomposite Coatings

Transparent NIR (700–2600 nm)-shielding coatings are strongly desired for solar control of windows in automotive and architectural applications to provide internal comfort as well as reduce energy consumption. Transparent NIR-shielding coatings can be either in the form of inorganic coatings or as OINCs. Due to low cost and easy *in situ* application to windows, NIR-shielding OINCs are especially developed via inclusion of functional inorganic nanoparticles into the polymer or hybrid matrix. The character (type, size) and introduction method of the nanoparticles are crucial to the performance of the coatings. For practical applications, a stronger and wider-band NIR with high visible light transmittance is required for the inorganic NIR absorbent.

As one of the most common transparent conductive oxides, ITO nanoparticles absorb NIR light by activating surface plasmon polaritons of the free electrons. Thus, they are often used as the functional nanofiller of transparent NIR-shielding nanocomposite coatings. The ITO nanoparticles can be in the form of commercial nanopowders. With this source, adequate deagglomeration of the nanopowder is a key step to achieve nanocomposite coatings with the desired transparency. Chemical synthesis of ITO nanoparticles from ITO precursors under mild conditions is usually reported.

As examples, ITO nanoparticles were prepared by a solvothermal synthesis at 300°C using octadecene as the solvent, indium acetate and tin acetate as precursors, and oleic acid and oleylamine as the capping agents [155]. The ITO nanoparticles were also synthesized at 220°C for 8 h using *N*-methyl-pyrrolidone as both the reaction solvent and surface modifier and indium acetylacetonate and tin bis(acetylacetonate) dichloride as the precursors [156]. The former ITO nanoparticles were grafted with

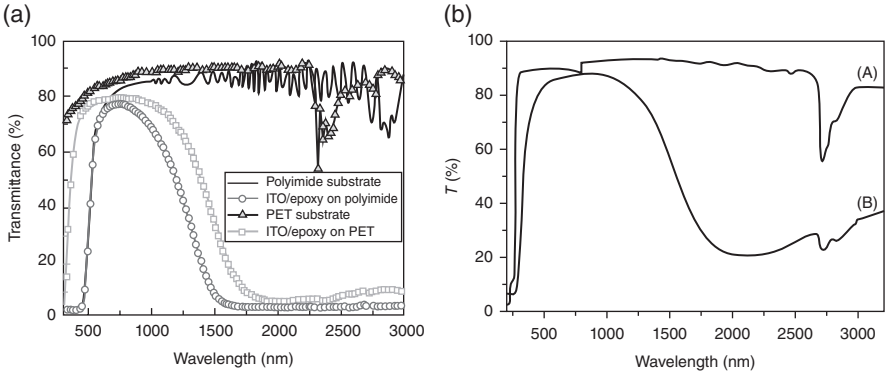

FIG. 1.28 (a) UV–vis–NIR transmittance spectra of epoxy/ITO coating (with thickness of 5 μm) with 35 wt.% ITO on plastic substrates. Reprinted with permission from Ref. 155. © 2010 American Chemical Society. (b) UV–vis–NIR transmittance spectra of (A) pure PUA and (B) PUA/ITO nanocomposite films at 5 wt.%. Reprinted with permission from Ref. 156. © 2010 Elsevier.

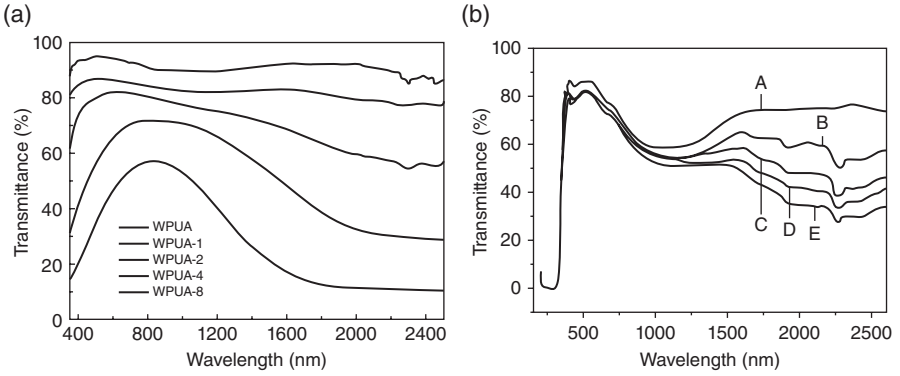

FIG. 1.29 UV–vis–NIR spectra of (a) waterborne UV-cured PUA/ITO coatings (WPUA, WPUA-1, WPUA-2, WPUA-4, and WPUA-8 correspond to the nanocomposite coatings containing 0, 1, 2, 4, 8 wt.% ATO). Reprinted with permission from Ref. 158. © 2010 Elsevier. and (b) poly(MMA-BA)/ATO nanocomposite films with different ATO amounts: (B) 3%, (C) 5%, (D) 7%, and (E) 10%. Reprinted with permission from Ref. 159. © 2011 Springer.

poly(glycidyl methacrylate) and added to epoxy coatings while the latter ones were added to acrylic polyurethane varnish. Figure 1.28 presents the UV–Vis–NIR spectra of the nanocomposites. Both ITO nanoparticles offer similar NIR shielding in organic coatings. The absorption band is wide, yet is limited to above 1200 nm. One limitation is that ITO nanoparticles are relatively expensive despite their commercial availability and routine synthesis.

Alternatives include ATO nanoparticles. Unlike ITO nanoparticles, ATO nanoparticles are mostly from a commercial product [157–159]. Figure 1.29 shows the UV–vis–NIR spectra of waterborne UV-cured PUA/ATO coatings and poly(MMA-BA)/ATO films. The IR shielding performance of ATO nanoparticles is not as good as that

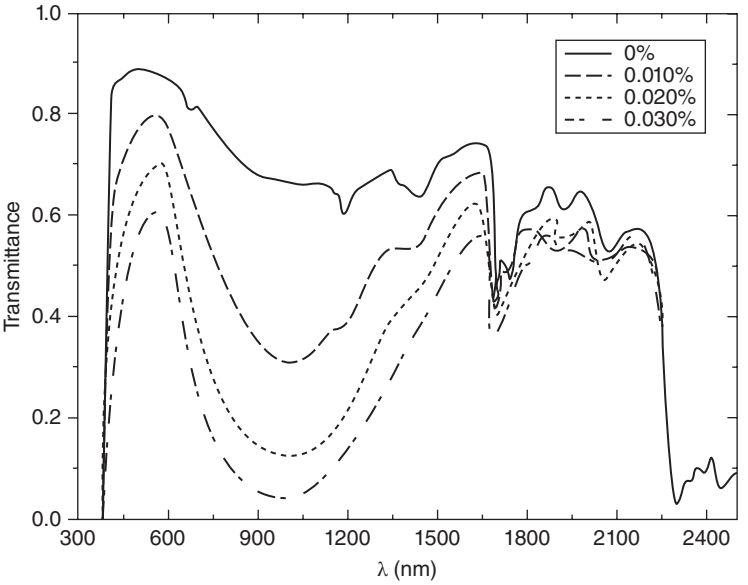

FIG. 1.30 Normal incidence transmission of polyvinyl butyral/LaB_6 nanocomposite laminate sheets for different weight percent of LaB_6 nanoparticles. Reprinted with permission from Ref. 161. © 2003 American Institute of Physics.

of ITO nanoparticles. Therefore, other efficient NIR absorbents have to be added in addition to ATO to enhance the NIR-shielding performance. Furthermore, Al-doped ZnO (AZO)/epoxy composite was fabricated as thermal insulation coating for glass [160]. Compared to ITO- or ATO-based nanocomposite coatings, the AZO-based coating is suboptimal for NIR shielding.

Highly conducting metals and black compounds can also behave as a tinted NIR absorber when dispersed at nanosized dimensions. Metals and black compounds reported include silver, gold, ruthenium dioxides, rhenium trioxides, and lanthanum hexaborides (LaB_6) [161]. The LaB_6 nanoparticles have a characteristic absorption around 1000 nm and a shorter NIR wavelength in contrast to ITO/ATO. Figure 1.30 shows the UV–vis–NIR spectrum of polyvinyl butyral/LaB_6 nanocomposite sheet with a thickness of 0.8 mm. The NIR shielding efficiency of LaB_6 is quite high. Even at 0.030% LaB_6, transmittance at the NIR absorption peak of the nanocomposite approaches zero. Meanwhile, the transmittance in the visible region remains 0.6. However, the tail of the NIR absorption peak extends to the visible range and deteriorates the transparency of the nanocomposite.

Size effect of LaB_6 on the optical properties of LaB_6-based composites was reported by Yuan *et al*. [162]. They found that PMMA/LaB_6 composites prepared via *in situ* polymerization with 70 nm LaB_6 particles had the best performance in the NIR and visible absorption of particle sizes ranging from 50 to 400 nm. To date, preparation of LaB_6-based OINCs is rarely found in publications. Because LaB_6 nanoparticles are prepared via a solid state reaction at high temperature, a stirred bead milling process is necessary to achieve transparent LaB_6-based OINCs.

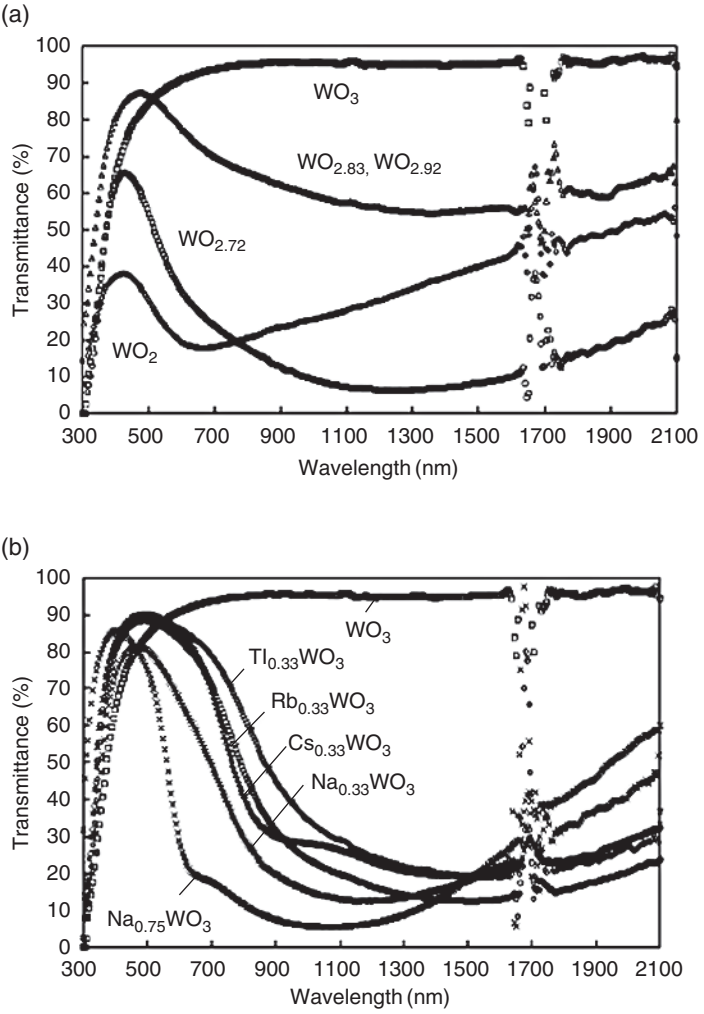

FIG. 1.31 Transmittance spectra of (a) tungsten oxide nanoparticles and (b) tungsten bronze nanoparticles dispersed by 0.01 wt.% in toluene. The disturbance at wavelengths between 1620 and 1790 nm is due to absorption by toluene. Reprinted with permission from Ref. 163. © 2007 The American Ceramic Society.

Tungsten trioxide (WO_3) has a wide band gap of 2.62 eV and is transparent to visible and NIR light. However, a metallic conductivity and a strong NIR absorption can be induced when free electrons are introduced into crystals by either decreasing the oxygen content or by adding ternary elements. Figure 1.31 is the transmittance spectra of tungsten oxide and tungsten bronze nanoparticles dispersed in toluene [163]. The pattern of the spectra strongly depends on the W/O atom ratio as well as the dopant. A remarkable NIR absorption effect was found in $WO_{2.72}$, $Na_{0.75}WO_3$, and $M_{0.33}WO_3$ (M = Na, Cs, Tl, Rb). Particularly, the $M_{0.33}WO_3$ with a hexagonal tungsten

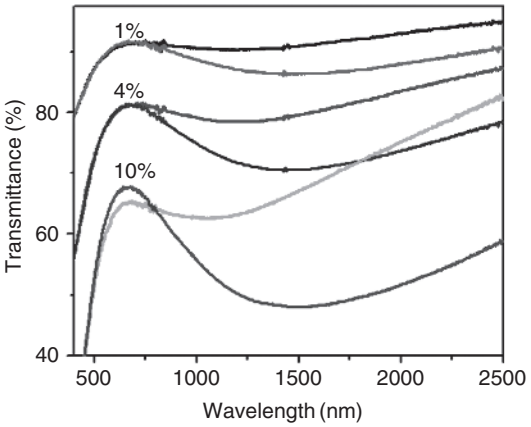

FIG. 1.32 Vis–NIR transmittance spectra of polysiloxane/VO_2(W) nanocomposite coatings with 1, 4, and 10 wt.% VO_2(W) content. Reprinted with permission from Ref. 164. © 2013 Elsevier. (Molar ratio of W:V = 0.15:100; film thickness: ~20 μm; the solid and dashed lines are for the films at 20 and 60°C, respectively.)

bronze structure is highly attractive in solar filter applications because the absorption in the visible range is small enough that their dispersion can yield a lower solar heat gain coefficient than that by ITO nanoparticle dispersion. Therefore, tungsten bronze nanoparticles will be very promising in the preparation of NIR-shielding OINCs.

Vanadium dioxide (VO_2) has a relatively low transition temperature (T_c) at 68°C for the change from a distorted to an undistorted rutile structure. Thus, VO_2 exhibits temperature-dependant reflective properties. At room temperature, VO_2 is almost transparent to NIR light but changes to reflective above the T_c. More interestingly, the transition temperature can be adjusted to near room temperature through doping with W, Mo, etc., demonstrating its positional application as a smart-window coating. Currently, most thermochromic coatings are inorganic VO_2 coatings. Thermochromic OINCs were prepared by blending the deagglomerated (W)VO_2 (T_c = 36°C) nanoparticles with the moisture-curable polysiloxane coatings [164]. Figure 1.32 gives the Vis–NIR transmittance spectra of the corresponding coatings. Luminous transmittance at 550 nm of about 60% and solar modulation at 2500 nm of 23% were achieved at 10% (W)VO_2 load. Nevertheless, VO_2-based OINCs are difficult to envision because W-doped VO_2 nanoparticles are not commercially available and have a reduced crystallinity and thus thermochromic property after deagglomeration process, for example, bead milling. They are also easily oxidized.

1.5 TRANSPARENT BARRIER NANOCOMPOSITE COATINGS

A coating layer is usually cast on a package to enhance the barrier properties or to improve the printability. Traditional barrier layers include vacuum-deposited aluminium or glass-like SiO_x films [165]. Currently, there is a trend toward chilled and possibly

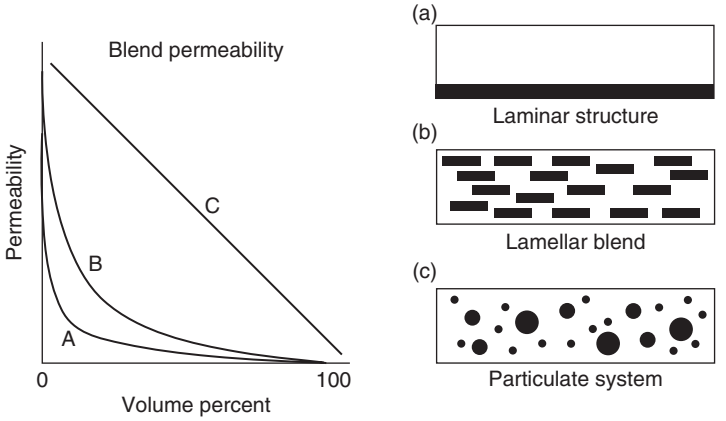

FIG. 1.33 Schematic illustration of the permeability of a blend of a high-barrier material in a low-barrier matrix as a function of the morphology: (a) laminar structure, (b) lamellar blend, and (c) particulate system [165]. Ref. 165. © 2003 John Wiley & Sons, Ltd.

modified atmosphere packaging. Consumers also demand high product visibility, as in food packaging. This requires a coating layer with good and sometimes selective barrier properties in combination with high transparency, good print quality, etc. Unfortunately, an aluminim layer is opaque and unsuitable for microwave heating. It also requires high energy during production. The SiO_x films are transparent, retortable, and microwaveable, but have limited flex and crack resistance. Nevertheless, organic barrier coatings are transparent and flexible. Epoxy-amine coating has been employed to improve the oxygen barrier of PET by a factor of 2 or more. However, the barrier performance of other conventional organic coatings such as PU and polyacrylate coatings is moderate. These coatings have been modified to include barrier inorganic nanofillers in the organic coatings to yield the so-called barrier nanocomposite coating. Besides packaging, barrier nanocomposite coatings are also useful in the anti-corrosion field.

Different modeling approaches have shown that significant barrier improvement factors of the order of 50 or higher can be achieved with high aspect ratio nanofiller particles [166, 167]. Figure 1.33 schematically illustrates the barrier properties of a blend as a function of the morphology. Lamellar, filler-based composites have a barrier performance close to the fully laminar layer, whereas particulate filler is not as efficient at improving the barrier. Using a model with a multiscale hierarchical approach, Xiao *et al*. proposed an empirical equation to predict the barrier properties of polymer nanocomposite coatings [168], as follows:

$$\frac{K_e}{K_m} = \exp\left(-\left(\frac{\alpha\phi_p^n}{1.33}\right)^{0.68} \times \left(\frac{\varepsilon^{pn*}}{1.72}\right)^{0.08}\right) \tag{1.8}$$

where ε^{pn*} and α denote the polymer–nanoparticle interaction strength and nanoparticle aspect ratio, respectively. The K_e and K_m correspond to the permeabilities of the

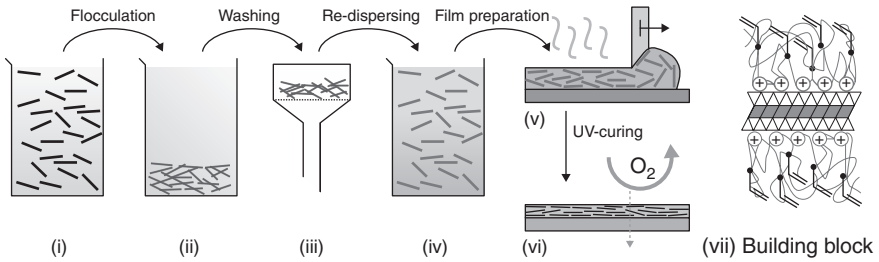

FIG. 1.34 Process steps to obtain UV-curable barrier coatings. Aqueous dispersions of clays (i) are flocculated via the addition of cationic, UV-curable polyurethane (ccPU)-dispersion (ii). Loose aggregates of obtained clay hybrids are washed (iii) and redispersed in THF (iv). Doctor-blading of the clay hybrid dispersions (v) allows a final UV-curing step (vi) to get the homogeneous composite films. An idealized O-HEC hybrid-platelet consisting of a clay lamella with ccPU adsorbed on both sides is shown in (vii) [172]. Ref. 172. © 2012 WILEY-VCH Verlag GmbH & Co. KGaA.

nanocomposite coatings and organic matrix. The equation can guide experimentalists in the rational design of nanocomposite coatings by offering quick screening of candidate formulations, identification of the most promising design spaces, and ideal experimental strategies. It also theoretically demonstrates why higher aspect ratio nanofillers offer better barrier performance.

Clay is currently the most common and most affordable high aspect ratio filler. Different clays have been reported in the fabrication of barrier nanocomposite coatings. The key factor lies in the type of clay as well as the dispersion state (i.e., intercalation and exfoliation) of the matrix filler. In a waterborne polymer latex/clay nanocomposite coating, the samples containing cetyltrimethylammonium bromide (CTAB)-modified saponite clay (Sap-CTAB) outperformed Cloisite 30B due to the much increased surface area of the Sap-CTAB after chemical modification [169]. When clay was incorporated into SILRES BS 1701, a polysiloxane emulsion sealant for concrete structure, reduced water permeability was observed [170]. Moreover, the moisture barrier performance was better for the nanocomposites containing Cloisite 20A clay than those with I.30P clay or the neat silane coating.

In an unsaturated polyester-based UV-curable coating, Choiste 30B is better in barrier performance for water but poorer in optical transparency versus CTAB-modified clay at the same load [171]. Recently, Möller *et al*. demonstrated that high charge, coarse-grained Li-hectorites obtained by melt synthesis delaminate spontaneously to yield platelets with aspect ratios typically larger than 1000 [172]. The synthetic hectorite was embedded into UV-curable coatings via a smart preparation process (Fig. 1.34). With respect to oxygen barriers, the hectorite-based hybrids outperform corresponding materials made from MMT by more than an order of magnitude while showing superb optical properties.

Influence of the preparation process on the barrier properties of nanocomposite coatings was also reported. Heidarian *et al*. prepared 3 wt.% PU/organically modified MMT (OMMT) composites by dispersing Cloisite 30B in castor oil polyol

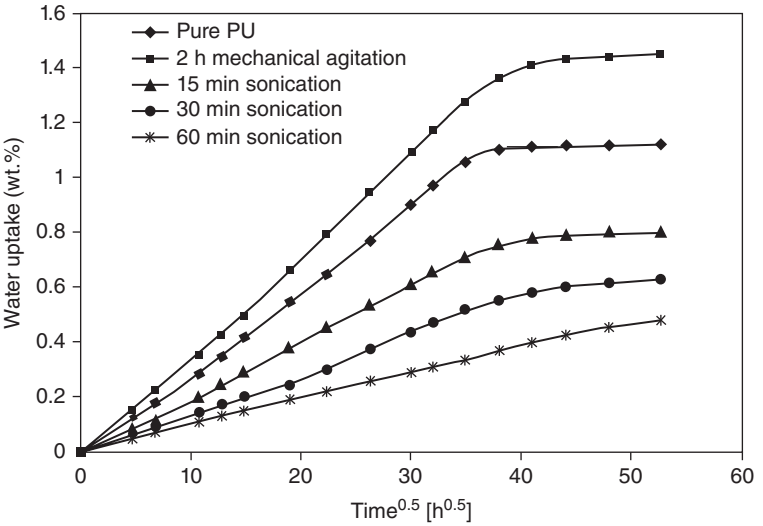

FIG. 1.35 Water absorption curves for pure PU and nanocomposite films after certain time intervals. Reprinted with permission from Ref. 173. © 2010 Springer.

resin through an ultrasonication-assisted technique [173]. Figure 1.35 shows the water uptake profiles of pure PU and 3 wt.% PU/OMMT composites after 2 h of mechanical agitation and 15, 30, and 60 min of sonication. For the composite film prepared by 2 h of mechanical agitation, the maximum water uptake (1.45 wt.%) and diffusivity coefficient (3.09×10^{-7} mm^2/s) were increased compared to that of pure PU (1.12 wt.% and 2.98×10^{-7} mm^2/s). However, the maximum water uptake and diffusivity coefficient is decreased to 0.49 wt.% and 2.23×10^{-7} mm^2/s, respectively, via 60 min sonication.

Pavlacky *et al*. reported UV-curable nanocomposite barrier coatings by dispersion of clay in monomers and then *in situ* polymerization or a sonication technique that synthesized unsaturated polyester and a dispersion of clay in the resin [171]. All the nanocomposite coatings demonstrate reduced water vapor permeability (WVP) and water vapor transmission (WVT), but no concrete changes to oxygen gas permeability. In contrast to those nanocomposite coatings prepared by sonication, the *in situ* nanocomposite coatings have lower WVP and WVT due to the better dispersion in the *in situ* process.

Actually, an ideal clay-based nanocomposite coating should have a fully exfoliated morphology with parallel orientation to the substrate. For conventional techniques (spraying, rolling, dipping, etc.), control of the orientation of the exfoliated clay is a rather difficult task because of the viscous binders. Priolo *et al*. employed a layer-by-layer assembly technique to create a super-gas barrier film where the cationic polyethylenimine (PEI) and anionic MMT clay and poly(acrylic acid) (PAA) are deposited in the sequence of PEI/PAA/PEI/MMT [174]. All the individual clay platelets lie parallel to the substrate to construct an open nano brick wall structure as illustrated in the TEM cross-sectional image (Fig. 1.36).

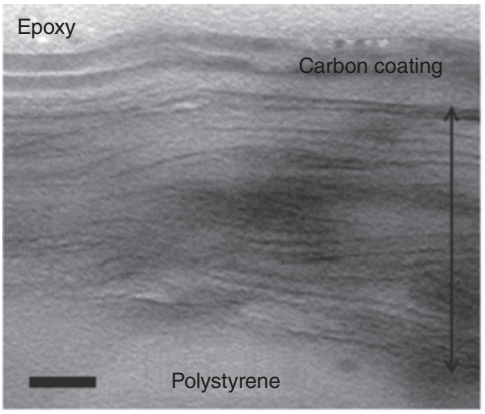

FIG. 1.36 TEM cross-section of a five QL thin film deposited on 250 μm polystyrene. The scale bar is 20 nm, and the double arrow spans the film's 80 nm thickness. Reprinted with permission from Ref. 174. © 2010 American Chemical Society.

At only 51 nm of thickness, these nanocomposite thin films exhibit an oxygen permeability of $\leq 5 \times 10^{-22}\,\mathrm{cm^3(STP)\cdot cm/(cm^2\cdot s\cdot Pa)}$. This is lower than that of SiO_x ($8.3 \times 10^{-20}\,\mathrm{cm^3(STP)\cdot cm/(cm^2\cdot s\cdot Pa)}$). This product combines high flexibility, transparency, and barrier protection and is thus a good candidate for a variety packaging applications.

1.6 TRANSPARENT CONDUCTING NANOCOMPOSITE COATINGS

Transparent conductive coatings are essential components in numerous applications that require high transmission and high electrical conductivity. Such coatings are therefore used as electrodes in photoelectronic devices, as an IR-reflecting or heatable layer, for electromagnetic shielding, for dissipating static, etc. The most common transparent conducting coatings are inorganic ITO, ATO, and AZO. However, these inorganic coatings are unadapted to applications as flexible plastic substrates or as big objects because of their inherent brittleness and limitations in fabrication techniques (high cost and small scale of physical and chemical vapor deposition, high temperature treatment during the sol–gel process, etc.).

An alternative is to utilize conducting OINCs that are mainly composed of conducting nanofillers and adequate organic (or hybrid) binders. The use of nanofillers leads to low light scattering and high transparency. Because the crystallization step of the conducting material in the OINC was separated from film formation, conducting OINCs can be cured either by a low temperature thermal treatment or by UV light irradiation using polymerizable organic additives. Therefore, the major advantages of OINC are large-scale fabrication, low cost, and adaptation to many different substrates. However, in contrast to inorganic conducting coatings, the conductivity of OINCs is relatively low.

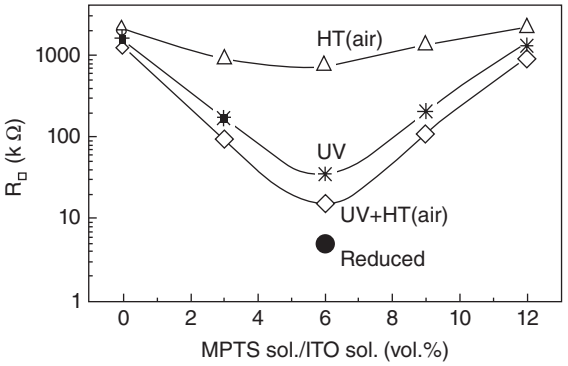

FIG. 1.37 Sheet resistance of 500 nm thick MPS/ITO coatings versus sol composition. Reprinted with permission from Ref. 176. © 2001 Elsevier. UV, UV irradiation 105 mW/cm^2, 110 s; HT (air), heat treatment in air: 130°C, 15 h.

Transparent conducting OINCs were first developed by Aegerter and coworkers [175]. The crystalline ITO or ATO nanoparticles, synthesized via a wet chemical method in the presence of the surface modifying agent β-alanine and subsequent calcination, were redispersed in ethanol or water. Organofunctionalized silanes such as MPS (together with photoinitiator) and GPS were used as the binder. Figure 1.37 shows the effect of annealing on the evolution of the sheet resistance ($R_\square$) with MPS/ITO coatings deposited on PC having sol composition [176]. Similar overall behavior was obtained with GPS/ITO coatings. Regardless of the treatment, the $R_\square$ for pure ITO is high (1 MΩ), and the coating adhesion is poor. Cured MPS/ITO coatings have a minimal sheet resistance for a composition volume ratio of 6%. At or above this ratio, they do not exhibit abrasion damage and only slight scattering. The lowest stable sheet resistances are $R_\square = 5\,\text{k}\Omega$ for MPS/ITO coatings and $R_\square = 15\,\text{k}\Omega$ for GPS/ITO coatings. This used a 110 s UV irradiation and a 15 h heat treatment at 130°C with further annealing in air. If annealing was conducted in a reducing atmosphere (N_2/H_2), the sheet resistance can be further reduced to as low as 800 Ω, and the transparency in the visible range is higher than 85% for 600 nm thick single layers [177].

Besides organoalkoxysilanes, PVP was also reported to be a binder in ITO nanoparticle coatings. Figure 1.38 presents the specific resistance of PVP/ITO nanocomposite coatings as a function of the volume fraction of PVP [178]. The lowest specific resistance was measured to be 6 Ω·cm at PVP contents of 33–40 vol.%. This further decreased to 0.5 Ω·cm after annealing at 200°C. The decrease in the specific resistance with increasing PVP content can be attributed to a densification of the ITO nanoparticle network due to shrinkage of PVP resulting from solvent evaporation. Unfortunately, the densification of the ITO nanoparticle network caused a transmission of just 50% at 550 nm for a layer thickness of 4 μm at a volume fraction of 40%. For PVP contents above 40 vol.%, the specific resistance increases as a result of the disturbed formation of ITO nanoparticle network.

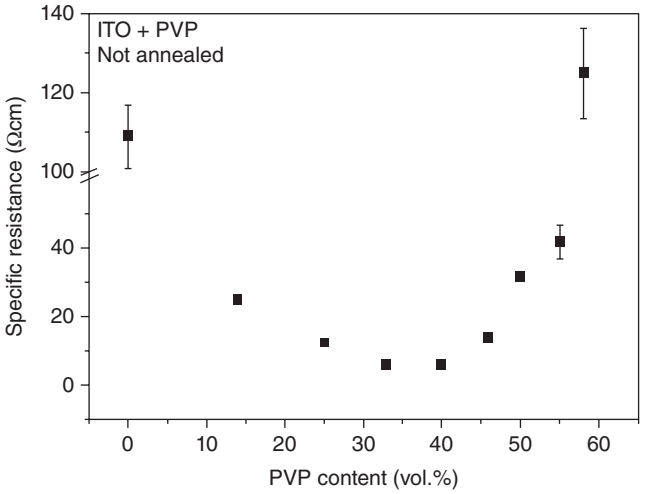

FIG. 1.38 Specific resistance of ITO/PVP nanocomposites as a function of the PVP content. Reprinted with permission from Ref. 178. © 2009 Springer Science + Business Media, LLC.

Maksimenko *et al*. introduced a binder from combination of PVP and MPS [179]. Table 1.9 compares the transparency and specific conductivity of ITO-MPS, ITO–PVP, and ITO–MPS–PVP coatings. In contrast to the ITO–PVP films, the optical properties were not dependent on the solvent even for the ITO–MPTS–PVP coatings. Compared to best pure ITO layers (3.1 Ω^{-1}/cm), the ITO–MPTS–PVP nanocomposite coatings have a conductance of 9.8 Ω^{-1}/cm. Stable sheet resistances of 750 $\Omega_{\square}$ at a coexistent transmittance of 86% at 550 nm for a layer thickness of about 1.3 μm were achieved. The combination effect of MPS and PVP on the conductance enhancement may be due to the filling of smaller cavities that cannot be completely filled with PVP because of the gyration radius (13.8 nm for commercial PVP K-15).

The above conducting OINCs involve the conducting behavior of the coatings with high volume fraction of nanofiller. Their conductivities are dominated by the densification degree of the conducting nanoparticle network. Actually, the conductivity of most composites containing fillers in an insulating matrix can be described by classic percolation theory:

$$\sigma = \sigma_0 \left(V - V_c\right)^t \tag{1.9}$$

where σ is the direct-current conductivity, σ_0 is the proportionality constant, V is the conductive filler volume fraction, V_c is the percolation threshold, and t is the critical conductivity exponent. Another prediction of conductivity is based on the effective medium approximation (EMA) theory and general effective media theory. A modified EMA model, which takes into consideration different types of contacts between the adjacent particles in a particle network, was proposed by Soloukhin *et al*. [180]. However, the modified EMA equation is much more complicated versus the percolation equation.

TABLE 1.9 Compositions and properties of fabricated ITO nanocomposite layers (thickness: 1–1.3 μm) deposited on glass substrates[a]

Coatings		Composition (wt.%)	T^b (550 nm), %	$\sigma_{\text{after treatment}}$, Ω^{-1}/cm	$\sigma_{\text{after reducing}}$, Ω^{-1}/cm
Pure ITO	Eth.	→got from Evonik 35.5 ITO, 64.5 EtOH	86	0.6 ± 0.02	3.1 ± 0.04
	Acac.	30.7 ITO, 69.3 Acac	86	0.6 ± 0.02	3.1 ± 0.04
ITO-PVP	Eth.	33.4 ITO, 6 PVP, 60.6 EtOH	43	0.9 ± 0.06	—
	Acac.	33.4 ITO, 5 PVP, 5.2 EtOH, 62.2 Acac	85	1.2 ± 0.02	—
ITO-MPS	Eth.	32.7 ITO, 3.3 MPS, 4.7 HCPK[c], 59.3 EtOH	88	1.5 ± 0.07	4.2 ± 0.15
	Acac.	27.1 ITO, 2.7 MPS, 3.9 HCPK, 5.1 EtOH, 61.2 Acac	88	1.9 ± 0.03	5.3 ± 0.09
OTP-MPS-PVP	Eth.	30.9 ITO, 3.1 MPS, 4.4 HCPK, 5.6 PVP, 56 EtOH	86	4.3 ± 0.17	9.8 ± 0.41
	Acac.	25.9 ITO, 2.6 MPS, 3.7 HCPK, 4.7 PVP, 4.9 EtOH, 58.2 Acac	86	3.7 ± 0.07	8.7 ± 0.34

[a] Reprinted with permission from Ref. 179. © 2010 Elsevier.
[b] $T_{max} = 92\%$ due to Fresnel reflection losses at the glass air interfaces.
[c] The photoinitiator, 1-hydroxycyclohexylphenylketone.

The percolation power-law equation was followed in the conductive composite coatings that were fabricated from poly(vinyl acetate-acrylic) (PVAc-*co*-acrylic) copolymer latices (50–600 nm) and nanosized ATO particles (15 nm) with V_c between 0.05 and 0.075 volume fractions of ATO and t ranging from 1.34 to 2.32 [181]. Compared to the PVAc-*co*-acrylic coating, the nanocomposite coatings had lower transparency because of the Rayleigh scattering. However, the transparency of the composite coatings can be improved by a reduction in the coating thickness. The best transparency for the coatings with a direct current conductivity of approximately 10^{-2} S/cm was around 85% at 600 nm. Interestingly, a low percolation threshold was exhibited at 1–2 vol% of ATO volume fraction for the UV-curable ATO-acrylate nanocomposite coatings using an acrylic prepolymer mixture (Ebecryl 745) as the binder and low amount of MPS grafted to the ATO nanoparticles [180]. Figure 1.39 gives the conductivity of the nanocomposite coatings as a function of ATO volume fraction and their modified EMA fitting curves.

Carbon nanotubes (CNTs) with properties ranging from semiconductor to metallic conductivity are the other candidates for fabrication of transparent conducting coatings. Because of the high aspect ratio, the conductivity of the nanocomposite coatings can be remarkably enhanced even at low loading levels. As shown in Figure 1.40, waterborne PU/CNT nanocomposite coatings containing 1.5 wt.% of

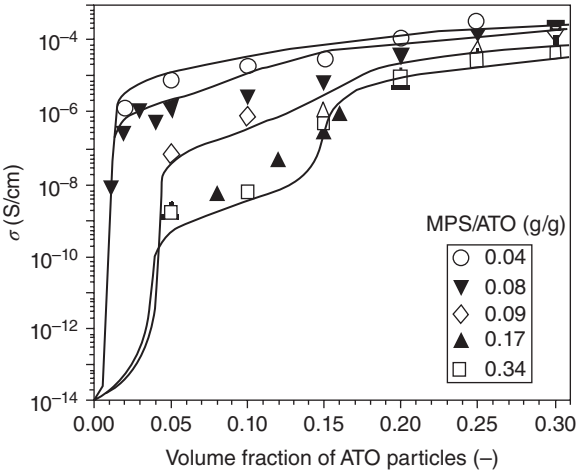

FIG. 1.39 The experimentally determined σ values for each volume faction of ATO for different MPS/ATO ratios (symbols) fitted with the modified EMA model (solid lines) [180]. Ref. 180. © 2007 Wiley Periodicals, Inc.

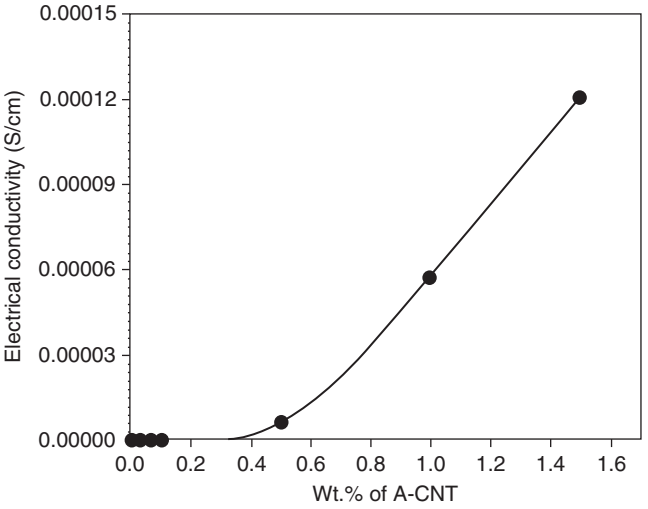

FIG. 1.40 Effect of nitric acid–treated MWCNT (A-MWCNT) content on the electrical conductivity of the WBPU/A-MWCNT nanocomposite films [81]. Ref. 81. © 2005 Wiley Periodicals, Inc.

A-MWCNTs exhibited a conductivity of 1.2×10^{-4} S/cm, which was nearly eight orders of magnitude higher than that of the pure PU film (2.5×10^{-12} S/cm) [81].

In another example, PU/MWCNT nanocomposite coatings were prepared based on a *para*-phenylenediamine-grafted MWCNT and toluene diisocyanate prepolymer with NCO functional groups as well as 4,4′-methylenebis(*o*-chloroaniline). The electrical

resistivity decreased from $10^{13}\,\Omega\cdot$cm (pure PU) to $10^{8}\,\Omega\cdot$cm at 0.5 wt.% MWCNTs and $10^{7}\,\Omega\cdot$cm at 3.0 wt.% MWCNTs [182]. Thus, MWCNT-based nanocomposite coatings easily meet the required level of resistivity necessary for antistatic application (volume resistivity: 10^{5}–$10^{10}\,\Omega\cdot$cm). Moreover, the MWCNT load in these antistatic coatings is usually lower than 1.0 wt.%, which gives the coatings reasonable transmission in the visible range.

To meet minimum industry standards, a material whose conductivity is invariant under flexing must have a sheet resistance of $R_s \leq 100\ \Omega_{\square}$ coupled with an optical transparency of $T \geq 90\%$ (550 nm). For thin conducting films, R_s and T are linked through

$$T(\lambda) = \left(1 + \frac{188.5}{R_s}\frac{\sigma_{Op}(\lambda)}{\sigma_{DC}}\right)^{-2} \tag{1.10}$$

where σ_{Op} and σ_{DC} are the optical (generally quoted at 550 nm) and direct current (DC) conductivities of the materials, respectively.

The single wall CNT (SWCNT) films typically have $\sim 1.5 \times 10^{4}$ S/m. Thus, to achieve the standard, σ_{DC} requires $\geq 5.3 \times 10^{5}$ S/m, which is a great challenge [183]. Academic efforts including the use of SWCNTs and a conductive polymer matrix have been made to tackle this challenge. Examples include metallic SWCNTs with a high conductivity that were separated from the arc discharge SWCNTs via 1-docosyloxymethyl pyrene and embedded into poly(3,4-ethylene dioxythiophene): poly(styrene sulfonate) (PEDOT:PSS) matrix [184]. Figure 1.41 demonstrates clearly the enhanced electrical conductivity of the separated metallic SWCNTs in the transparent conductive films. Meanwhile, the optical transparency of PEDOT:PSS is not sacrificed and make the composite films competitive to ITO coatings for transparent electrodes and other applications. Similar (PEDOT:PSS)/SWCNT nanocomposite films were prepared by De *et al*. [183]. DC conductivities of $>10^{5}$ S/m for mass fractions >50 wt.% were obtained. For an 80 nm thick composite filled with 60 wt.% arc discharge nanotubes, the conductivity ratio was maximized at $\sigma_{DC}/\sigma_{Op} = 15$. This translates into a transmittance (550 nm) and sheet resistance of 75% and $80\,\Omega_{\square}$, respectively, which are better than the data shown in Fig. 1.41. These composites were electromechanically very stable with <1% resistance change over 130 bend cycles.

1.7 OTHER FUNCTIONAL NANOCOMPOSITE COATINGS

Other functional OINCs have superhydrophilic, superhydrophobic, antibacterial, corrosion-resistant performance. When these functional coatings are used as clearcoats, high optical clarity is essential. Transparent superhydrophilic and superhydrophobic coatings are highly desired for self-cleaning and anti-frosting applications on windows or when the original surface appearance must not be impacted.

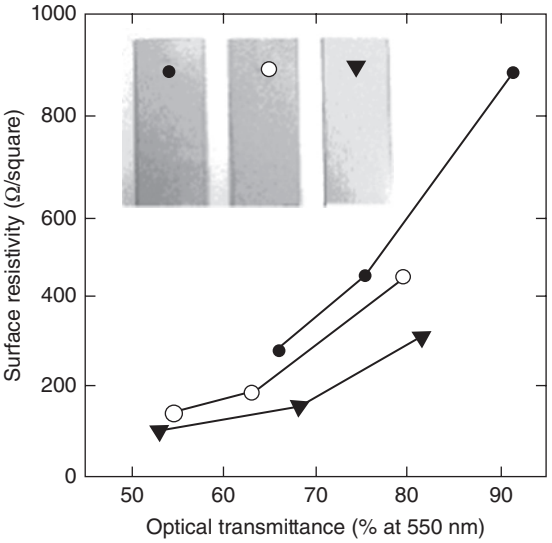

FIG. 1.41 Surface resistivity results of PEDOT:PSS/SWCNT films on glass substrate with the same 10 wt.% nanotube content but different film thickness and optical transmittance at 550 nm (○, preseparation purified sample; ▼, separated metallic SWCNTs, for comparison; ●, blank PEDOT:PSS without nanotubes) Inset shows representative films photographed with tiger paw print as background. Reprinted with permission from Ref. 184. © 2008 Elsevier.

These transparent superhydrophilic nanocomposite coatings are usually fabricated based on photocatalytic TiO_2 nanoparticles. Because of the high photodegradation of TiO_2 nanoparticles, hybrid or inorganic binders, not pure polymer, are generally used for the nanocomposite coatings. These binders are typically synthesized from a sol–gel process of TEOS [185] or TIPP [186]. Copolymer is sometimes added to avoid cracking during film formation [186]. This yields a porous structure via calcination [185] or nano-TiO_2-induced photodegradation [187] or both, for example, the role of *n*-octylamine in TiO_2-SiO_2 self-cleaning coatings for stones [188].

A typical morphology of TiO_2 nanoparticles dispersed in a mesoporous silica matrix is presented in Figure 1.42. The porous structure remarkably enhances the photocatalytic self-cleaning performance of the coatings but also deteriorates the optical transparency due to scattering [187]. Therefore, not only the dispersed size of the TiO_2 nanoparticles but also the pore size and distribution are crucial to successfully achieve transparent superhydrophilic coatings.

Superhydrophilic nanocomposite coatings are also developed using a simple mixture of polymers containing reactive TMOS groups, including quaternized poly(2-(dimethylamino) ethyl methacrylate and poly(MPS), and silica nanoparticles [189]. Superhydrophilic behavior is achieved with a high weight ratio of fumed silica nanoparticles or polymer/fumed silica nanoparticle bilayer coatings.

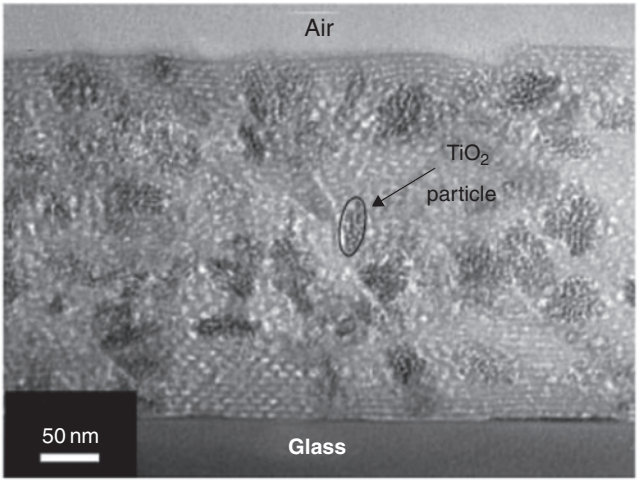

FIG. 1.42 Cross-sectional TEM image of a TiO_2/mesoporous silica film obtained with Ti/(Ti + Si) = 0.2 [185]. Ref. 185. © 2007 WILEY-VCH Verlag GmbH & Co. KGaA.

It is well known that a rough surface structure and low surface free energy are essential to acquire a superhydrophobic surface. The preparation of transparent superhydrophobic coatings is difficult because the rough surface can scatter light. The surface roughness and the aggregate size of nanoparticles have to be carefully controlled at the nanoscale level. Thus far, transparent superhydrophobic coatings are seldom reported. Hwang *et al*. did prepare a coating of 50 nm colloidal silica particles and a hybrid binder from a sol–gel process of GPS/TMOS [190]. The coating was deposited on glass or silicon wafer to form a 40 nm thick film. Thereafter, the film was covered in a layer of prehydrolyzed isobutyltrimethoxysilane (IBTMS). The highest water contact angle of 130° was achieved at 7.21 nm thickness of IBTMS layer. However, the coating is very thin and not mechanically strong.

Lin *et al*. prepared a UV-curable transparent superhydrophobic coating using a system containing a fluoroimide acrylate oligomer, neopentyl glycol diacrylate (NPGDA), photoinitiator, and 20–25 nm colloidal SiO_2 nanoparticles [191]. The water contact angle of the coatings increases with silica content and reached 142° at 60 wt.% SiO_2 (NPS60). Figure 1.43 clearly illustrates a rough surface enriched with nanosize aggregates. The NPS60 still exhibits good transparency (96.44% at 400 nm and 100 μm film) because its surface roughness and aggregate size are smaller than 100 nm with minor light scattering. Meanwhile, the nanocomposite coating also shows high thermal stability and mechanical durability.

Transparent antibacterial coatings are prepared by the inclusion of antibacterial nanoadditives. These nanoadditives include nanosilver [192], nanocopper [193], and nano-semiconductive oxide (i.e., ZnO [194]). To assure the transparency of the coatings, the nanometal particles were made *in situ*. For example, an aqueous $AgNO_3$/PVA solution was spin-coated on glass slides and then heated in a hot air oven at 130–190°C to create Ag nanoparticles *in situ* within transparent PVA films. The

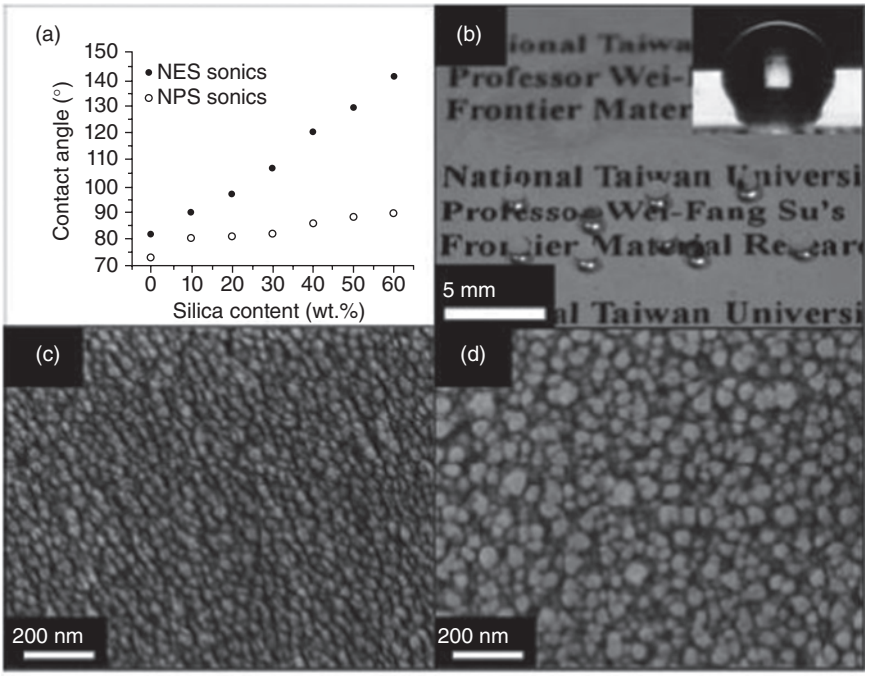

FIG. 1.43 (a) Comparison of contact angles between NES (prepared from ethoxylated bisphenol A diacrylate, NPGDA, and colloidal silica) and NPS (prepared from fluoroimide acrylate oligomer, NPGDA, and colloidal silica) series. (b) Water droplets on the surface of highly transparent NPS60 coated on glass. Inset shows the contact angle of the film is 142°. The SEM images of nanocomposites (c) NES60 and (d) NPS60. Reprinted with permission from Ref. 191. © 2010 The Royal Society of Chemistry.

composite films showed excellent antimicrobial performance toward bacteria such as *Escherichia coli* [192]. Other detailed examples of antibacterial coatings are given in Chapter 10.

1.8 CONCLUSIONS AND OUTLOOK

OINCs have been recognized as the most commonly used solution to exploit new organic coating products as well as to modify the properties of traditional organic coatings. Among the fabrication methods, addition of nanopowder is undoubtedly the simplest way. Nevertheless, the deagglomeration of nanopowder for preparation of transparent OINCs is a great challenge. To fulfill the deagglomeration well, some special deagglomeration machines, for example, grinding machine using bead with size less than 100 μm, have been manufactured. Some knowledge on surface molecular engineering of nanoparticles are also necessary to get fine nanoparticle dispersions. Due to the high-tech level of nanoparticle dispersion, some companies specializing on

nanoparticle dispersions are even established, promoting the commercialization of transparent OINCs. However, the dispersions of the nanofillers with high aspect ratio, that are useful in the preparation of transparent barrier OINCs and antistatic (or conductive) OINCs, are still lack. In addition, OINCs with extremely high nanofiller loads are difficult to attain absolute transparency. *In situ* generation of nanophase during drying step of organic coatings would be an alternative way for these cases. But it needs further efforts on exploitation of new drying process (e.g., drying in different atmospheres).

As a whole, transparent OINCs have achieved great progress in the past years. Scratch-resistant nanocomposite clearcoats for automobile and plastic lens, transparent NIR-shielding nanocomposite coatings, photocatalytic self-cleaning clearcoats, transparent antibacterial nanocomposite coatings, etc., are now available in market somehow. Of course, transparent OINCs with better performances and more functions are highly expected in the near future.

REFERENCES

1. Schmidt, H., Seiferling, B. (1986) Chemistry and Applications of Inorganic-Organic Polymers (Organically Modified Silicates). MRS Spring Meeting: Materials Research Society, Palo Alto, CA, USA.
2. Schmidt, H., Wolter, H. (1990) Organically modified ceramics and their applications. *Journal of Non-Crystalline Solids*, 121(1–3): 428–435.
3. Zhang, H., Zhang, H., Tang, L.C., Zhou, L.Y. Eger, C., Zhang, Z. (2011) Comparative study on the optical, surface mechanical and wear resistant properties of transparent coatings filled with pyrogenic and colloidal silica nanoparticles. *Composites Science and Technology*, 71: 471–479.
4. Chen, X.C., You, B., Zhou, S.X., Wu, L.M. (2003) Surface and interface characterization of polyester-based polyurethane/nano-silica composites. *Surface and Interface Analysis*, 35(4): 369–374.
5. Poovarodom, S., Hosseinpour, D., Berg, J.C. (2008) Effect of particle aggregation on the mechanical properties of a reinforced organic-inorganic hybrid sol-gel composite. *Industrial & Engineering Chemistry Research*, 47(8): 2623–2629.
6. Zhou, S.X., Wu, L.M., You, B. Gu, G.X. (2009) Preparation, structure, and properties of organic-inorganic nanocomposite coatings. in *Smart Coatings II*. ed., Theodore Provder, Jamil Baghdachi. Vol. ACS Symposium Series No. 1002 : Washington, DC: American Chemical Society, 193–219.
7. Inkyo, M., Tahara, T., Iwaki, T., Iskandar, F., Hogan, C.J., Jr, Okuyama, K. (2006) Experimental investigation of nanoparticle dispersion by beads milling with centrifugal bead separation. *Journal of Colloid and Interface Science*, 304: 535–540.
8. Joni, I.M., Purwanto, A., Iskandar, F., Okuyama, K. (2009) Dispersion stability enhancement of titania nanoparticles in organic solvent using a bead mill process. *Industrial & Engineering Chemistry Research*, 48: 6916–6922.
9. Iversen, S.B., Rasmussen, H., Christensen, C.A., Jensen, H., Reenberg, T. (2010) Production of Titania Nanoparticle Colloidal Suspensions with Maintained Crystallinity by Using a Bead Mill with Micrometer Sized Beads. Applicants: VÄLINGE INNOVATION AB and PHOTOCAT A/S, International publication number: WO2010/110726.

10. Bock, M., Engbert, T., Groth, S., Klinksiek, B., Yeske, P., Jonschker, G., Dellwo, U. (2000) Transparent coating compositions containing nanoscale particles and having improved scratch resistance. Bayer Aktiengesellschaft, USA and US Patent 6,020,419.
11. Xiong, M.N., Gu, G.X., You, B., Wu, L.M. (2003) Preparation and characterization of poly(styrene butylacrylate) latex/nano-ZnO nanocomposites. *Journal of Applied Polymer Science*, 90(7): 1923–1931.
12. Liu, Y.L., Yu, Z.F., Zhou, S.X., Wu, L.M. (2006) De-aggregation and dispersion of nanofine TiO_2 in an agitator bead mill. *Journal of Dispersion Science and Technology*, 27(7): 983–990.
13. Hazan, Y.D., Heinecke, J., Weber, A., Graule, T. (2009) High solids loading ceramic colloidal dispersions in UV curable media via comb-polyelectrolyte surfactants. *Journal of Colloid and Interface Science*, 337: 66–74.
14. Alkilany, A.M., Thompson, L.B., Murphy, C.J. (2010) Polyelectrolyte coating provides a facile route to suspend gold nanorods in polar organic solvents and hydrophobic polymers. *ACS Applied Materials & Interfaces*, 2(12): 3417–3412.
15. Vestberg, R., Piekarski, A.M., Pressly, E.D., Berkel, K.Y.V., Malkoch, M., Gerbac, J., Ueno, N., Hawker, C.J. (2009) A general strategy for highly efficient nanoparticle dispersing agents based on hybrid dendritic linear block copolymers. *Journal of Polymer Science Part A: Polymer Chemistry*, 47: 1237–1258.
16. Gao, X.Y., Zhu, Y.C., Zhao, X., Wang, Z.C., An, D.M., Ma, Y.J., Guan, S., Du, Y.Y., Zhou, B. (2011) Synthesis and characterization of polyurethane/SiO_2 nanocomposites. *Applied Surface Science*, 257: 4719–4724.
17. Amici, J., Kahveci, M.U., Allia, P., Tiberto, P., Yagci, Y., Sangermano, M. (2012) Polymer grafting onto magnetite nanoparticles by "click" reaction. *Journal of Materials Science*, 47(1): 412–419.
18. Mesnage, A., Magied, M.A., Simon, P., Herlin-Boime, N., Jegou, P., Deniau, G., Palacin, S. (2011) Grafting polymers to titania nanoparticles by radical polymerization initiated by diazonium salt. *Journal of Materials Science*, 46: 6332–6338.
19. Schmidt, H.K., Geiter, E., Mennig, M., Krug, H., Becker, C., Winkler, R.-P. (1998) The sol-gel process for nano-technologies: new nanocomposites with interesting optical and mechanical properties. *Journal of Sol-gel Science and Technology*, 13: 397–404.
20. Bauer, F., Ernst, H., Decker, U., Findeisen, M., Gläsel, H.J., Langguth, H., Hartmann, E., Mehnert, R., Peuker, C. (2000) Preparation of scratch and abrasion resistant polymeric nanocomposites by monomer grafting onto nanoparticles, 1-FTIR and multi-nuclear NMR spectroscopy to the characterization of methacryl grafting. *Macromolecular Chemistry and Physics*, 201(18): 2654–2659.
21. Chen, H., Zhou, S.X., Gu, G.X., Wu, L.M. (2004) Study on modification and dispersion of nano-silica. *Journal of Dispersion Science and Technology*, 25(6): 837–848.
22. Miller, J.D., Ishida, H. (1984) Quantitative monomolecular coverage of inorganic particulates by methacryl-functional silanes. *Surface Science*, 148(2–3): 601–622.
23. Bauer, F., Sauerland, V., Ernst, H., Glasel, H.-J., Naumov, S., Mehnert, R. (2003) Preparation of scratch- and abrasion-resistant polymeric nanocomposites by monomer grafting onto nanoparticles, 4 application of MALDI-TOF mass spectrometry to the characterization of surface modified nanoparticles. *Macromolecular Chemistry and Physics*, 204: 375–383.
24. Bauer, F., Mehnert, R. (2005) UV curable acrylate nanocomposites: properties and applications. *Journal of Polymer Research*, 12: 483–491.

25. Li, Y.L., Chen, Z.X., Li, X.X., Zeng, H.W. (2011) A new surface modification method to improve the dispersity of nano-silica in organic solvents. *Journal of Sol-Gel Science and Technology*, 58: 290–295.
26. Lu, Y.F., Zhou, S.X., Wu, L.M. (2012) De-agglomeration and dispersion behavior of TiO_2 nanoparticles in organic media using 3-methacryloxypropyltrimethoxysilane as a surface modifier. *Journal of Dispersion Science and Technology*, 33(4): 497–505.
27. Scholz, S., Kaskel, S. (2008) Surface functionalization of ZrO_2 nanocrystallites for the integration into acrylate nanocomposite films. *Journal of Colloid and Interface Science*, 323: 84–91.
28. Posthumus, W., Magusin, P.C.M.M., Brokken-Zijp, J.C.M., Tinnemans, A.H.A., van der Linde R.. (2004) Surface modification of oxidic nanoparticles using 3-methacryloxypropyltrimethoxysilane. *Journal of Colloid and Interface Science*, 269: 109–116.
29. Zhou, S.X., Garnweitner, G., Niederberger, M., Antonietti, M. (2007) Dispersion behavior of zirconia nanocrystals and their surface-functionalization with vinyl group-containing ligands. *Langmuir*, 23(18): 9178–9187.
30. Zhou, S.X., Wu, L.M. (2008) Phase separation and properties of UV-curable polyurethane/zirconia nanocomposite coatings. *Macromolecular Chemistry and Physics*, 209(11): 1170–1181.
31. Xu, K., Zhou, S.X., Wu, L.M. (2009) Effect of highly-dispersible zirconia nanoparticles on the properties of UV-curable poly(urethane-acrylate) coatings. *Journal of Materials Science*, 44(6): 1613–1621.
32. Xu, K., Zhou, S.X., Wu, L.M. (2010) Dispersion of γ-methacryloxypropyltrimethoxysilane-functionalized zirconia nanoparticles in UV-curable formulations and properties of their cured coatings. *Progress in Organic Coatings*, 67(3): 302–310.
33. Luo, K.Q., Zhou, S.X., Wu, L.M., Gu, G.X. (2008) Dispersion and functionalization of non-aqueous synthesized zirconia nanocrystals via attachment of silane coupling agents. *Langmuir*, 24(20): 11497–11505.
34. Barna, E., Rentsch, D., Bommer, B., Vital, A., von Trzebiatowski, O., Graule, T. (2007) Surface modification of nanoparticles for scratch resistant clear coatings. *KGK-Kautschuk Gummi Kunststoffe*, 60(1–2): 49–51.
35 Kang, S., Hong, S., II, Choe, C.R., Park, M., Rim, S., Kim, J. (2001) Preparation and characterization of epoxy composites filled with functionalized nanosilica particles obtained via sol-gel process. *Polymer*, 42: 879–887.
36. Luo, K.Q., Zhou, S.X., Wu, L.M. (2009) High refractive index and good mechanical property UV-cured hybrid films containing zirconia nanoparticles. *Thin Solid Films*, 517: 5974–5980.
37. Douce, J., Boilot, J.P., Biteau, J., Scodellaro, L., Jimenez, A. (2004) Effect of filler size and surface condition of nano-sized silica particles in polysiloxane coatings. *Thin Solid Films*, 466(1–2): 114–122.
38. Greenwood, P., Gevert, B. (2011) Aqueous silane modified silica sols: theory and preparation. *Pigment & Resin Technology*, 40(5): 275–284.
39. Huang, T.C., Su, Y.-A., Yeh, T.-C., Huang, H.-Y., Wu, C.-P., Huang, K.-Y., Chou, Y.-C., Yeh, J.-M., Wei, Y. (2011) Advanced anticorrosive coatings prepared from electroactive epoxy–SiO_2 hybrid nanocomposite materials. *Electrochimica Acta*, 56: 6142–6149.
40. Chen, L., Shen, H.X., Lu, Z., Feng, C., Chen, S., Wang, Y.R. (2007) Fabrication and characterization of TiO_2-SiO_2 composite nanoparticles and polyurethane (TiO_2-SiO_2) nanocomposite films. *Colloid and Polymer Science*, 285(13): 1515–1520.

41. Gomathi, A., Rao, C.N.R. (2008) Hexadecyltriethoxysilane-induced dispersions of metal oxide nanoparticles in nonpolar solvents. *Journal of Cluster Science*, 19: 247–257.
42. Luo, K.Q., Zhou, S.X., Wu, L.M., You, B. (2010) Preparation and properties of cross-linked zirconia nanoparticle films on polycarbonate. *Thin Solid Films*, 518(23): 6804–6810.
43. Iijima, M., Kobayakawa, M., Kamiya, H. (2009) Tuning the stability of TiO_2 nanoparticles in various solvents by mixed silane alkoxides. *Journal of Colloid and Interface Science*, 337: 61–65.
44. Deb, B., Kumar, V., Druffel, T.L., Sunkara, M.K. (2009) Functionalizing titania nanoparticle surfaces in a fluidized bed plasma reactor. *Nanotechnology*, 20: 465701.
45. Sayılkan, F., Asiltèurk, M., Burunkaya, E., Ertuğrul, A. (2009) Hydrothermal synthesis and characterization of nanocrystalline ZrO_2 and surface modification with 2-acetoacetoxyethyl methacrylate. *Journal of Sol-Gel Science and Technology*, 51: 182–189.
46. Hu, Y.Q., Gu, G.X., Zhou, S.X., Wu, L.M. (2011) Preparation and properties of transparent PMMA/ZrO_2 nanocomposites using 2-hydroxyethyl methacrylate as a coupling agent. *Polymer*, 52: 122–129.
47. Pandey, S., Mishra, S.B. (2011) Sol-gel derived organic–inorganic hybrid materials: synthesis, characterizations and applications. *Journal of Sol-Gel Science and Technology*, 59: 73–94.
48. Sowntharya, L., Lavanya, S., Chandra, G.R., Hebalkar, N.Y., Subasri, R. (2012) Investigations on the mechanical properties of hybrid nanocomposite hard coatings on polycarbonate. *Ceramics International*, 38: 4221–4228.
49. Sangermano, M., Amerio, E., Epicoco, P., Priola, A., Rizza, G., Malucelli, G. (2007) Preparation and characterization of hybrid nanocomposite coatings by cationic UV-curing and the sol-gel process of a vinyl ether based system. *Macromolecular Materials and Engineering*, 292: 634–640.
50. Huang, H.-C., Huang, S.-P., Hsieh, T.-E., Chen, C.-H. (2012) Characterizations of UV-curable montmorillonite/epoxy nanocomposites prepared by a hybrid of chemical dispersion and planetary mechanical milling process. *Journal of Applied Polymer Science*, 123: 3199–3203.
51. Yeh, J.M., Chen, C.L., Chen, Y.C., Ma, C.Y., Huang, H.Y., Yu, Y.H. (2004) Enhanced corrosion prevention effect of polysulfone-clay nanocomposite materials prepared by solution dispersion. *Journal of Applied Polymer Science*, 92(1): 631–637.
52. Landry, V., Riedl, B., Blanchet, P. (2008) Nanoclay dispersion effects on UV coatings curing. *Progress in Organic Coatings*, 62: 400–408.
53. Shemper, B.S., Morizur, J.-F., Alirol, M., Domenech, A., Hulin, V., Mathias, L.J. (2004) Synthetic clay nanocomposite-based coatings prepared by UV-cure photopolymerization. *Journal of Applied Polymer Science*, 93(2): 1252–1263.
54. Chen, C.G., Khobaib, M., Curliss, D. (2003) Epoxy layered-silicate nanocomposites. *Progress in Organic Coatings*, 47(3–4): 376–383.
55. Majumdar, D., Blanton, T.N., Schwark, D.W. (2003) Clay-polymer nanocomposite coatings for imaging application. *Applied Clay Science*, 23(5–6): 265–273.
56. Ranade, A., D'Souza, N.A., Gnade, B. (2002) Exfoliated and intercalated polyamide-imide nanocomposites with montmorillonite. *Polymer*, 43(13): 3759–3766.
57. Sangermano, M., Messori, M. (2010) Scratch resistance enhancement of polymer coatings. *Macromolecular Materials and Engineering*, 295(7): 603–612.
58. Zhou, S.X., Wu, L.M., Sun, J., Shen, W.D. (2002) The changes of the properties of acrylic based polyurethane via addition of nano-silica. *Progress in Organic Coatings*, 45(1): 33–42.

59. Zhou, S.X., Wu, L.M., Sun, J., Shen, W.D. (2003) Effect of nanosilica on the properties of polyester-based polyurethane. *Journal of Applied Polymer Science*, 88(1): 189–193.

60. Zhou, S.X., Wu, L.M., Shen, W.D., Gu, G.X. (2004) Study on the morphology and tribological properties of acrylic based polyurethane/fumed silica composite coatings. *Journal of Materials Science*, 39(5): 1593–1600.

61. Jalili, M.M., Moradian, S., Dastmalchian, H., Karbasi, A. (2007) Investigating the variations in properties of 2-pack polyurethane clear coat through separate incorporation of hydrophilic and hydrophobic nano-silica. *Progress in Organic Coatings*, 59: 81–87.

62. Barna, E., Bommer, B., Kürsteiner J., Vital, A., Trzebiatowski, O.v., Koch, W., Schmid, B., Graule, T. (2005) Innovative, scratch proof nanocomposites for clear coatings. *Composites: Part A*, 36: 473–480.

63. Chen, G.D., Zhou, S.X., Gu, G.X., Yang, H.H., Wu, L.M. (2005) Effects of the surface property of nanosilica particles on its redispersibility and properties of acrylic based polyurethane/silica composites. *Journal of Colloid and Interface Science*, 281(2): 339–350.

64. Chen, G.D., Zhou, S.X., Gu, G.X., Wu, L.M. (2007) Modification of colloidal silica on the mechanical properties of acrylic based polyurethane/silica composites. *Colloids and Surfaces A—Physicochemical and Engineering Aspects*, 296(1–3): 29–36.

65. Chen, G.D., Zhou, S.X., Liao, H.M., Wu, L.M. (2005) Preparation of solvent-borne acrylic-based polyurethane-modified silica nanocomposites. *Journal of Composite Materials*, 39(3): 215–231.

66. Chen, Y.C., Zhou, S.X., Yang, H.H., Gu, G.X., Wu, L.M. (2004) Preparation and characterization of nanocomposite Polyurethane. *Journal of Colloid and Interface Science*, 279(2): 370–378.

67. Chen, Y.C., Zhou, S.X., Chen, G.D., Wu, L.M. (2005) Preparation and characterization of polyester/colloidal silica nanocomposite resins. *Progress in Organic Coatings*, 54(2): 120–126.

68. Chen, Y.C., Zhou, S.X., Yang, H.H., Wu, L.M. (2005) Structure and properties of polyurethane/nanosilica compoiste. *Journal of Applied Polymer Science*, 95(5): 1032–1039.

69. Ahmadi, B., Kassiriha, M., Khodabakhshi, K., Mafi, E.R. (2007) Effect of nano layered silicates on automotive polyurethane refinish clear coat. *Progress in Organic Coatings*, 60: 99–104.

70. Sabzi, M., Mirabedini, S.M., Zohuriaan-Mehr, J., Atai, M. (2009) Surface modification of TiO_2 nano-particles with silane coupling agent and investigation of its effect on the properties of polyurethane composite coating. *Progress in Organic Coatings*, 65: 222–228.

71. Tiarks, F., Leuninger, J., Wagner, O., Jahns, E., Wiese, H. (2007) Nanocomposite dispersions for water-based coatings. *Surface Coatings International*, 90(5): 221–229.

72. Luna-Xavier, J.-L., Bourgeat-Lami, E., Guyot, A. (2001) The role of initiation in the synthesis of silica/poly(methyl methacrylate) nanocomposite latex particles through emulsion polymerization. *Colloid and Polymer Science*, 279(10): 947–958.

73. Diaconu, G., Asua J.M., Paulis, M., Leiza, J.R. (2007) High-solids content waterborne polymer-clay nanocomposites. *Macromolecular Symposia*, 259(1): 305–317.

74. Qi, D.-M., Bao, Y.-Z., Weng, Z.X., Huang, Z.-M. (2006) Preparation of acrylate polymer/silica nanocomposite particles with high silica encapsulation efficiency via miniemulsion polymerization. *Polymer*, 47(13): 4622–4629.

75. You, B. Wen, N.G., Cao, Y.C., Zhou, S.X., Wu, L.M. (2009) Preparation and properties of poly(styrene-co-butyl acrylate-acrylic acid)/silica nanocomposite latex using an acidic silica sol. *Polymer International*, 58(5): 519–529.
76. Yang, L., Zhou, S.X., Gu, G.X. Wu, L.M. (2013) Film-forming behavior and mechanical properties of colloidal silica/polymer latex blends with high silica load. *Journal of Applied Polymer Science*, 129(3): 1434–1445.
77. Xiong, M.N., Wu, L.M., Zhou, S.X., You, B. (2002) Preapration and characterization of acrylic latex /nano-SiO_2 composites. *Polymer International*, 51: 693–698.
78. Yao, L., Yang, J., Sun, J., Cai, L.F., He, L.H., Huang, H., Song, R., Hao, Y.M. (2011) Hard and transparent hybrid polyurethane coatings using in situ incorporation of calcium carbonate nanoparticles. *Materials Chemistry and Physics*, 129: 523–528.
79. Gumfekar, S.P., Kunte, K.J., Ramjee, L., Kate, K.H., Sonawane, S.H. (2011) Synthesis of $CaCO_3$–P(MMA–BA) nanocomposite and its application in water based alkyd emulsion coating. *Progress in Organic Coatings*, 72(4): 632–637.
80. Nobel, M.L., Picken, S.J., Mendes, E., Waterborne nanocomposite resins for automotive coating applications. *Progress in Organic Coatings*, 58: 96–104.
81. Kwon, J.-Y., Kim, H.-D. (2005) Preparation and properties of acid-treated multiwalled carbon nanotube/waterborne polyurethane nanocomposites. *Journal of Applied Polymer Science*, 96(2): 595–604.
82. Landry, V., Riedl, B., Blanchet, P. (2008) Alumina and zirconia acrylate nanocomposites coatings for wood flooring: photocalorimetric characterization. *Progress in Organic Coatings*, 61(1): 76–82.
83. Sow, C., Riedl, B., Blanchet, P. (2010) Kinetic studies of UV-waterborne nanocomposite formulations with nanoalumina and nanosilica. *Progress in Organic Coatings*, 67(2): 188–194.
84. Sangermano, M., Priola, A., Kortaberriac, G., Jimeno, A., Garcia, I., Mondragon, I., Rizza, G. (2007) Photopolymerization of epoxy coatings containing iron-oxide nanoparticles. *Macromolecular Materials and Engineering*, 292: 956–961.
85. Kang, D.J., Han, D.H., Kang, D.P. (2009) Fabrication and characterization of photocurable inorganic–organic hybrid materials using organically modified colloidal-silica nanoparticles and acryl resin. *Journal of Non-Crystalline Solids*, 355: 397–402.
86. Gläsel, H.-J., Bauer, F., Ernst, H., Findeisen, M., Hartmann, E., Langguth, H.,Mehnert, R., Schubert, R. (2000) Preparation of scratch and abrasion resistant polymeric nanocomposites by monomer grafting onto nanoparticles, 2 characterization of radiation-cured polymeric nanocomposites. *Macromolecular Chemistry and Physics*, 201: 2765–2770.
87. Soloukhin, V.A., Posthumus, W., Brokken-Zijp, J.C.M., Loos, J., With, G. (2002) Mechanical properties of silica-(meth)acrylate hybrid coatings on polycarbonate substrate. *Polymer*, 43: 6169–6181.
88. Kim, D., Jeon, K., Lee, Y., Seo, J., Seo, K., Han, H., Khan, S.B. (2012) Preparation and characterization of UV-cured polyurethane acrylate/ZnO nanocomposite films based on surface modified ZnO. *Progress in organic coatings*, 74(3): 435–442.
89. Bautista, Y., Gonzalez, J., Gilabert, J., Ibanez, M.J., Sanz, V. (2011) Correlation between the wear resistance, and the scratch resistance, for nanocomposite coatings. *Progress in Organic Coatings*, 70(4): 178–185.
90. Leder, G., Ladwig, T., Valter, V., Frahn, S., Meyer, J. (2002) New effects of fumed silica in modern coatings. *Progress in Organic Coatings*, 45: 139–144.

91. Zhang, H., Zhang, H., Tang, L.C., Zhang, Z., Gu, L., Xu, Y.Z., Christian, E. (2010) Wear-resistant and transparent acrylate-based coating with highly filled nanosilica particles. *Tribology International*, 43: 83–91.
92. Gianni, A.D., Amerio, E., Monticelli, O., Bongiovanni, R. (2008) Preparation of polymer/clay mineral nanocomposites via dispersion of silylated montmorillonite in a UV curable epoxy matrix. *Applied Clay Science*, 42: 116–124.
93. Mohamadpour, Sh., Pourabbas, B., Fabbri, P. (2011) Anti-scratch and adhesion properties of photo-curable polymer/clay nanocomposite coatings based on methacrylate monomers. *Scientia Iranica*, 18(3): 765–771.
94. Corcione, C.E., Frigione, M. (2012) UV-cured polymer-boehmite nanocomposite as protective coating for wood elements. *Progress in Organic Coatings*, 74: 781–787.
95. Zhang, X.H., Yang, J.W., Zeng, Z.H., Huang, L., Chen, Y.L., Wang, H.H.(2006) Stabilized dispersions of titania nanoparticles via a sol–gel process and applications in UV-curable hybrid systems. *Polymer International*, 55(4): 466–472.
96. Bauer, F., Sauerland, V., Gläsel, H.-J., Ernst, H., Findeisen, M., Hartmann, E.,Langguth, H., Marquardt, B., Mehnert, R. (2002) Preparation of scratch and abrasion resistant polymeric nanocomposites by monomer grafting onto nanoparticles, 3 effect of filler particles and grafting agents. *Macromolecular Materials and Engineering*, 287: 546–552.
97. Sangermano, M., Gaspari, E., Vescovo, L., Messori, M. (2011) Enhancement of scratch-resistance properties of methacrylated UV-cured coatings. *Progress in Organic Coatings*, 72(3): 287–291.
98. Hsiang H.-I., Chang, Y.-L., Chen, C.-Y., Yen, F.-S. (2010) Silane functional effects on the rheology and abrasion resistance of transparent SiO_2/UV-curable resin nano-composites. *Materials Chemistry and Physics*, 120: 476–479.
99. Hsiang H.-I., Chang, Y.-L., Chen, C.-Y., Yen, F.-S. (2011) Silane effects on the surface morphology and abrasion resistance of transparent SiO_2/UV-curable resin nano-composites. *Applied Surface Science*, 257: 3451–3454.
100. Schmidt, H.K., Krug, H., Sepeur-Zeitz, B., Geiter, E. (1997) Inorganic-organic nanocomposites for optical coatings. Proc. SPIE 3136. In Dunn, B.S., Mackenzie, J.D., Pope, E.J.A., Schmidt, H.K., Yamane, M., eds. *Sol-Gel Optics IV*. SPIE, San Diego, CA.
101. Daniels, M.W., Francis, L.F. (1998) Silane adsorption behavior, microstructure, and properties of glycidoxypropyltrimethoxysilane-modified colloidal silica coatings. *Journal of Colloid and Interface Science*, 205: 191–200.
102. Mosher, B.P., Wu, C.W., Sun, T., Zeng, T.F. (2006) Particle-reinforced water-based organic-inorganic nanocomposite coatings for tailored applications. *Journal of Non-Crystalline Solids*, 352: 3295–3301.
103. Chen, Q. Tan, J.G.H., Shen, S.C., Liu, Y.C., Ng, W.K., Zeng, X.T. (2007) Effect of boehmite nanorods on the properties of glycidoxypropyltrimethoxysilane (GPTS) hybrid coatings. *Journal of Sol-gel Science and Technology*, 44: 125–131.
104. Sepeur, S., Kunze, N., Werner, B., Schmidt, H. (1999) UV curable hard coatings on plastics. *Thin Solid Films*, 351: 216–219.
105. Chantarachindawong, R., Luangtip, W., Chindaudom, P.,Osotchan, T., Srikhirin, T. (2012) Development of the scratch resistance on acrylic sheet with basic colloidal silica (SiO_2)—methyltrimethoxysilane (MTMS) nanocomposite films by sol–gel technique. *The Canadian Journal of Chemical Engineering*, 90: 888–896.

106. Chau, J.L.H., Hsieh, C.-C., Lin, Y.-M., Li, A.-K. (2008) Preparation of transparent silica–PMMA nanocomposite hard coatings. *Progress in Organic Coatings*, 62: 436–439.

107. Fogelstrom, L., Malmstrom, E., Johansson, M., Hult, A. (2010) Hard and flexible nanocomposite coatings using nanoclay-filled hyperbranched polymers. *ACS Applied Materials & Interfaces*, 2(6): 1679–1684.

108. Jiratumnukul, N., Pruthipaitoon, S., Pitsaroup, T. (2006) Nanocomposite alkyd coatings. *Journal of Applied Polymer Science*, 102(3): 2639–2642.

109. Calvo, M.E., Smirnov, J.R.C., Miguez, H. (2012) Novel approaches to flexible visible transparent hybrid films for ultraviolet protection. *Journal of Polymer Science Part B: Polymer Physics*, 50: 945–956.

110. Yuwono, A.H., Xue, J.M., Wang, J., Elim, H.I., Ji, W., Li, Y., White, T.J. (2003) Transparent nanohybrids of nanocrystalline TiO_2 in PMMA with unique nonlinear optical behavior. *Journal of Materials Chemistry*, 13: 1475–1479.

111. Allen, N.S., Edge, M., Ortega, A., Liauw, C.M., Stratton, J., McIntyre, R.B. (2002) Behaviour of nanoparticle (ultrafine) titanium dioxide pigments and stabilisers on the photooxidative stability of water based acrylic and isocyanate based acrylic coatings. *Polymer Degradation and Stability*, 78(3): 467–478.

112. Zhou, S.X., Wu L.M., Xiong, M.N., He, Q.Y., Chen, G.D. (2004) Dispersion and UV-VIS property of nanoparticles in coatings. *Journal of Dispersion Science and Technology*, 25(4): 417–433.

113. Mallakpour, S., Barati, A. (2011) Efficient preparation of hybrid nanocomposite coatings based on poly(vinyl alcohol) and silane coupling agent modified TiO_2 nanoparticles. *Progress in Organic Coatings*, 71: 391–398.

114. Godnjavec, J., Znoj, B., Vince, J., Steinbucher, M., Znidarsie, A., Venturini, P. (2012) Stabilization of rutile TiO_2 nanoparticles with glymo in polyacrylic clear coating. *Materials and technology*, 46(1): 19–24.

115. Godnjavec, J., Znoj, B., Veronovski, N., Venturini, P. (2012) Polyhedral oligomeric silsesquioxanes as titanium dioxide surface modifiers for transparent acrylic UV blocking hybrid coating. *Progress in Organic Coatings*, 74: 654–659.

116. Zhang, Y.H., Yu, L., Ke, S.M., Shen, B., Meng, X.H., Huang, H.T., Lv, F.Z., Xin, J.H., Chan, H.L.W. (2011) TiO_2/SiO_2 hybrid nanomaterials: synthesis and variable UV-blocking properties. *Journal of Sol-Gel Science and Technology*, 58: 326–329.

117. Ren, Y., Chen, M., Zhang, Y., Wu L.M. (2010) Fabrication of rattle-type TiO_2@void@SiO_2 particles with both high photoactivity and UV-shielding property. *Langmuir*, 26(13): 11391–11396.

118. Sangermano, M., Borlatto, E., D'Herin Bytner, F.D., Priola, A., Rizza, G. (2007) Photostabilization of cationic UV-cured coatings in the presence of nanoTiO_2. *Progress in Organic Coatings*, 59: 122–125.

119. Hwang, D.K., Moon, J.H., Shul, Y.G., Jung, K.T., Kim, D.H., Lee, D.W. (2003) Scratch resistant and transparent UV-protective coating on polycarbonate. *Journal of Sol-Gel Science and Technology*, 26: 783–787.

120. Chen, W.-C., Lee, S.-J., Lee, L.-H., Lin, J.-L. (1999) Synthesis and characterization of trialkoxysilane-capped poly(methyl methacrylate)-titania hybrid optical thin films. *Journal of Materials Chemistry*, 9: 1999–2003.

121. Mazzocchetti, L., Cortecchia, E., Scandola, M. (2009) Organic-inorganic hybrids as transparent coatings for UV and X-ray shielding. *ACS Applied Materials & Interfaces*, 1(3): 726–734.

122. Que, W.X., Hu, X. (2003) Influence of titanium content and temperature on optical and mechanical properties of sol–gel derived TiO_2/γ-glycidoxypropyltrimethoxysilane and methyltrimethoxysilane hybrid organic–inorganic films. *Journal of Physics D: Applied Physics*, 36: 908–914.

123. Xiang, H.P., Ge, J.F., Cheng, S.H., Han, H.M., Cui, S.W. (2011) Synthesis and characterization of titania/MQ silicone resin hybrid nanocomposite via sol–gel process. *Journal of Sol-Gel Science and Technology*, 59: 635–639.

124. Osmond, M.J., McCall, M.J. (2010) Zinc oxide nanoparticles in modern sunscreens: an analysis of potential exposure and hazard. *Nanotoxicology*, 4(1): 15–41.

125. Wang, L.L., Zhang, X.T., Li, B., Sun, P.P., Yang, J.K., Xu, H.Y., Liu, Y.C. (2011) Superhydrophobic and ultraviolet-blocking cotton textiles. *ACS Applied Materials & Interfaces*, 3(4): 1277–1281.

126. Li, Y.-Q., Fu, S.-Y., Mai, Y.-W. (2006) Preparation and characterization of transparent ZnO/epoxy nanocomposites with high-UV shielding efficiency. *Polymer*, 47: 2127–2132.

127. Li, H.Y., Chen, Y.F., Ruan, C.X., Gao, W.M., and Xie Y.S. (2001) Preparation of organic–inorganic multifunctional nanocomposite coating via sol-gel routes. *Journal of Nanoparticle Research*, 3: 157–160.

128. Khrenov, V., Schwager, F., Klapper, M., Koch, M., Müllen, K. (2007) Compatibilization of inorganic particles for polymeric nanocomposites. Optimization of the size and the compatibility of ZnO particles. *Polymer Bulletin*, 58: 799–807.

129. Weichelt, F., Emmler, R., Flyunt, R., Beyer, E., Buchmeiser, M.R., Beyer, M. (2010) ZnO-Based UV nanocomposites for wood coatings in outdoor applications. *Macromolecular Materials and Engineering*, 295: 130–136.

130. Li, S.H., Toprak, M.S., Jo, Y.S., Dobson, J., Kim, D.K., Muhammed, M. (2007) Bulk synthesis of transparent and homogeneous polymeric hybrid materials with ZnO quantum dots and PMMA. *Advanced Materials*, 2007(19): 4347–4352.

131. Tu, Y., Zhou, L., Jin, Y.Z., Gao, C., Ye, Z.Z., Yang, Y.F., Wang, Q.L. (2010) Transparent and flexible thin films of ZnO-polystyrene nanocomposite for UV-shielding applications. *Journal of Materials Chemistry*, 20: 1594–1599.

132. Liu, H.T., Zeng, X.F., Zhao, H., Chen, J. F. (2012) Transparent and multifunctional polymer nanohybrid film with superhigh ZnO content synthesized by a bulk polymerization method. *Industrial & Engineering Chemistry Research*, 51: 6753–6759.

133. Jeeju, P.P., Sajimol, A.M., Sreevalsa, V.G., Varma, S.J., Jayalekshmi, S. (2011) Size-dependent optical properties of transparent, spin-coated polystyrene/ZnO nanocomposite films. *Polymer International*, 60: 1263–1268.

134. Zhang, L.Y., Yin, L.W., Wang, C.X., Lun, N., Qi, Y.X. (2010) Sol-gel growth of hexagonal faceted ZnO prism quantum dots with polar surfaces for enhanced photocatalytic activity. *ACS Applied Materials & Interfaces*, 2: 1769–1773.

135. Wang, X.L., Zhou, S.X., Wu, L.M. (2013) Facile encapsulation of SiO_2 on ZnO quantum dots and its application in waterborne UV-shielding polymer coatings. *Journal of Materials Chemistry C*, 1(45): 7547-7553.

136. Yabe, S., Yamashita, M., Momose, S., Tahira, K., Yoshida, S., Li, R.X., Yin, S., Sato, T. (2001) Synthesis and UV-shielding properties of metal oxide doped ceria via soft solution chemical processes. *International Journal of Inorganic Materials*, 3(7): 1003–1008.

137. Saadat-Monfared, A., Mohseni, M. (2014) Polyurethane nanocomposite films containing nano-cerium oxide as UV absorber; part 2: structural and mechanical studies upon UV exposure. *Colloids and Surfaces A: Physicochemical and Engineering Aspects*, 441: 752–757.

138. de Lima, J.F., Serra, O.A. (2013) Cerium phosphate nanoparticles with low photocatalytic activity for UV light absorption application in photoprotection. *Dyes and Pigments*, 97(2): 291–196.

139. Zimmennann, L., Weibel, M., Caseri, W., Suter, U.W. (1993) High refractive index films of polymer nanocomposites. *Journal of Materials Research*, 8(7): 1742–1748.

140. Antonello, A., Brusatin, G., Guglielmi, M., Martucci, A., Bello, V., Mattei, G., Mazzoldi, P., Pellegrini, G. (2010) Hybrid organic–inorganic ZnS-loaded nanocomposite films for stable optical coatings. *Thin Solid Films*, 518: 6781–6786.

141. Franc, J., Blanc, D., Zerroukhi, A., Chalamet, Y., Last, A., Destouches, N. (2006) Organo-silica–titania nanocomposite elaborated by sol–gel processing with tunable optical properties. *Materials Science and Engineering B*, 129: 180–185.

142. Chau, J.L.H., Tung, C.-T., Lin, Y.-M., Li, A.-K. (2008) Preparation and optical properties of titania/epoxy nanocomposite coatings. *Materials Letters*, 62: 3416–3418.

143. Antonello, A., Brusatin, G., Guglielmi, M., Bello, V., Mattei, G., Zacco, G., Martucci, A. (2011) Nanocomposites of titania and hybrid matrix with high refractive index. *Journal of Nanoparticle Research*, 13: 1697–1708.

144. Chang, C.-C., Cheng, L.-P., Huang, F.-H., Lin, C.-Y., Hsieh, C.-F., Wang, W.-H. (2010) Preparation and characterization of TiO_2 hybrid sol for UV-curable high-refractive-index organic–inorganic hybrid thin films. *Journal of Sol-Gel Science and Technology*, 55: 199–206.

145. Liu, B.-T., Tang, S.-J., Yub, Y.-Y., Lin, S.-H. (2011) High-refractive-index polymer/inorganic hybrid films containing high TiO_2 contents. *Colloids and Surfaces A: Physicochemical and Engineering Aspects*, 377: 138–143.

146. Takeda, M., Tanabe, E., Iwaki, T., Yabuki, A., Okuyama, K. (2008) High-concentration transparent TiO_2 nanocomposite films prepared from TiO_2 nanoslurry dispersed by using bead mill. *Polymer Journal*, 40(8): 694–699.

147. Nakayama, N., Hayashi, T. (2007) Preparation and characterization of TiO_2-ZrO_2 and thiol-acrylate resin nanocomposites with high refractive index via UV-induced cross-linking polymerization. *Composites: Part A*, 38: 1996–2004.

148. Nakayama, N., Hayashi, T. (2008) Synthesis of novel UV-curable difunctional thiourethane methacrylate and studies on organic-inorganic nanocomposite hard coatings for high refractive index plastic lenses. *Progress in Organic Coatings*, 62: 274–284.

149. Chang, C.-M., Chang, C.-L., Chang, C.-C. (2006) Synthesis and optical properties of soluble polyimide/titania hybrid thin films. *Macromolecular Materials and Engineering*, 291: 1521–1528.

150. Chang, W.-L., Su, H.-W., Chen, W.-C. (2009) Synthesis and properties of photosensitive polyimide–nanocrystalline titania optical thin films. *European Polymer Journal*, 45: 2749–2759.

151. Liou G.-S., Lin, P.-H., Yen, H.-J., Yu, Y.-Y., Tsai, T.-W., Chen, W.-C. (2010) Highly flexible and optical transparent 6F-PI/TiO_2 optical hybrid films with tunable refractive index and excellent thermal stability. *Journal of Materials Chemistry*, 20: 531–536.

152. Lee, S., Shin, H.-J., Yoon, S.-M., Yi, D.K., Choi, J.-Y., Paik, U. (2008) Refractive index engineering of transparent ZrO_2–polydimethylsiloxane nanocomposites. *Journal of Materials Chemistry*, 18: 1751–1755.

153. Tsuzuki, T. (2008) Abnormal transmittance of refractive-index-modified ZnO/organic hybrid films. *Macromolecular Materials and Engineering*, 293: 109–113.

154. Lü, C.-L., Yang, B. (2009) High refractive index organic–inorganic nanocomposites: design, synthesis and application. *Journal of Materials Chemistry*, 19: 2884–2901.

155. Tao P., Viswanath, A., Schadler, L.S., Benicewicz, B.C., Siegel, R.W. (2011) Preparation and optical properties of indium tin oxide/epoxy nanocomposites with polyglycidyl methacrylate grafted nanoparticles. *ACS Applied Materials & Interfaces*, 3: 3638–3645.

156. Liu, H.T., Zeng, X.F., Kong, X.R., Bian, S.G., Chen, J.F.. (2012) A simple two-step method to fabricate highly transparent ITO/polymer nanocomposite films. *Applied Surface Science*, 258: 8564–8569.

157. Feng, J., Huang, B.Y., Zhong, M.Q. (2009) Fabrication of superhydrophobic and heat-insulating antimony doped tin oxide/polyurethane films by cast replica micromolding. *Journal of Colloid and Interface Science*, 336: 268–272.

158. Wang, X., Hu, Y., Song, L., Xing, W.-Y., Lu, H.-D., Lv, P., Jie, G.-X. (2010) Effect of antimony doped tin oxide on behaviors of waterborne polyurethane acrylate nanocomposite coatings. *Surface & Coatings Technology*, 205(7): 1864–1869.

159. Zhang, G.-J., Chen, Z.-H., Zeng, X.-R., Yu, F., Wang, J. (2011) Preparation and characterization of poly(MMA–BA)/nano-ATO hybrid latex via miniemulsion polymerization. *Journal of Coatings Technology and Research*, 8(4): 505–511.

160. Li, Y.-Q., Kang, Y., Xiao, H.-M., Mei, S.-G., Zhang, G.-L., Fu, S.-Y. (2011) Preparation and characterization of transparent Al doped ZnO/epoxy composite as thermal-insulating coating. *Composites: Part B*, 42: 2176–2180.

161. Stefan, S., Smith, G.B. (2003) Dilute LaB6 nanoparticles in polymer as optimized clear solar control glazing. *Applied Physics Letters*, 82(24): 4346–4348.

162. Yuan, Y.-F., Zhang, L., Hu, L.-J., Wang, W., Min, G.-H. (2011) Size effect of added LaB6 particles on optical properties of LaB6/polymer composites. *Journal of Solid State Chemistry*, 184(12): 3364–3367.

163. Takeda, H., Adachi, K. (2007) Near infrared absorption of tungsten oxide nanoparticle dispersions. *Journal of American Ceramic Society*, 90(12): 4059–4061.

164. Lu, Y.F., Zhou, S.X., Gu, G.X., Wu, L.M. (2013) Preparation of transparent, hard thermochromic polysiloxane/tungsten-doped vanadium dioxide nanocomposite coatings at ambient temperature. *Thin Solid Films*, 534: 231–237.

165. Lange, J., Wyser, Y. (2003) Recent innovations in barrier technologies for plastic packaging—a review. *Packaging Technology and Science*, 16: 149–158.

166. Fredrickson, G.H., Bicerano, J. (1999) Barrier properties of oriented disk composites. *Journal of Chemical Physics*, 110(4): 2181–2188.

167. Gusev, A.A., Lusti, H.R. (2001) Rational design of nanocomposites for barrier applications. *Advanced Materials*, 13(21): 1641–1643.

168. Xiao, J., Huang, Y.L., Manke, C. W. (2010) Computational design of polymer nanocomposite coatings: a multiscale hierarchical approach for barrier property prediction. *Industrial & Engineering Chemistry Research*, 49: 7718–7727.

169. Sun, Q.H., Schork, F.J., Deng, Y.L. (2007) Water-based polymer/clay nanocomposite suspension for improving water and moisture barrier in coating. *Composites Science and Technology*, 67: 1823–1829.

170. Woo, R.S.C., Zhu, H.G., Chow, M.M.K., Leung, C.K.Y., Kim, J.K. (2008) Barrier performance of silane–clay nanocomposite coatings on concrete structure. *Composites Science and Technology*, 68(14): 2828–2836.

171. Pavlacky, E., Ravindran, N., Webster, D.C. (2012) Novel in situ synthesis in the preparation of ultraviolet-curable nanocomposite barrier coatings. *Journal of Applied Polymer Science*, 125: 3836–3848.

172. Möller, M.W., Kunz, D.A., Lunkenbein, T., Sommer, S., Nennemann, A., J, Breu (2012) UV-cured, flexible, and transparent nanocomposite coating with remarkable oxygen barrier. *Advanced Materials*, 24: 2142–2147.

173. Heidarian, M., Shishesaz, M.R., Kassiriha, S.M., Nematollahi, M. (2011) Study on the effect of ultrasonication time on transport properties of polyurethane/organoclay nanocomposite coatings. *Journal of Coatings Technology and Research*, 8(2): 265–274.

174. Priolo, M.A., Gamboa, D., Holder, K.M., Grunlan, J.C. (2010) Super gas barrier of transparent polymer-clay multilayer ultrathin films. *Nano Letters*, 10: 4970–4974.

175. Goebbert, C., Bisht, H., Al-Dahoudi, N., Nonninger, R., Aegerter, M.A., Schmidt, H. (2000) Wet chemical deposition of crystalline, redispersable ATO and ITO nanoparticles. *Journal of Sol-Gel Science and Technology*, 19: 201–204.

176. Al-Dahoudi, N., Bisht, H., Gobbert, C., Krajewski, T., Aegerter, M.A. (2001) Transparent conducting, anti-static and anti-static-anti-glare coatings on plastic substrates. *Thin Solid Films*, 392: 299–304.

177. Aegerter, M.A., Al-Dahoudi, N., Solieman, A., Kavak, H., Oliveira, P. (2004) Transparent conducting coatings made by chemical nanotechnology process. *Molecular Crystals and Liquid Crystals*, 417: 105–114.

178. Kèoniger, T., Mèunstedt, H. (2009) Influence of polyvinylpyrrolidone on properties of flexible electrically conducting indium tin oxide nanoparticle coatings. *Journal of Materials Science*, 44: 2736–2742.

179. Maksimenko, I., Gross, M., Köniğer, T., Münstedt, H., Wellmann, P.J. (2010) Conductivity and adhesion enhancement in low-temperature processed indium tin oxide/polymer nanocomposites. *Thin Solid Films*, 518(10): 2910–2915.

180. Soloukhin, V.A., Brokken-Zijp, J.C.M., Dewith, G. (2007) Conductive ATO-acrylate nanocomposite hybrid coatings: experimental results and modeling. *Journal of Polymer Science Part B: Polymer Physics*, 45: 2147–2160.

181. Sun, J.K., Gerberich, W.W., Francis, L.F. (2003) Electrical and optical properties of ceramic–polymer nanocomposite coatings. *Journal of Polymer Science Part B: Polymer Physics*, 41: 1744–1761.

182. Zhao, W.M., Li, M., Peng, H.-X. (2010) Functionalized MWNT-doped thermoplastic polyurethane nanocomposites for aerospace coating applications. *Macromolecular Materials and Engineering*, 295(9): 838–845.

183. De, S., Lyons, P.E., Sorel, S., Doherty, E.M., King, P.J., Blau, W.J., Nirmalraj, P.N., Boland, J.J., Scardaci, V., Joimel, J., Coleman, J.N. (2009) Transparent, flexible, and highly conductive thin films based on polymer-nanotube composites. *ACS Nano*, 3(3): 714–720.

184. Wang, W., Fernando, K.A.S., Lin, Y., Meziani, M.J., Veca, L.M., Cao, L., Zhang, P.Y., Kimani, M.M., Sun, Y.-P. (2008) Metallic single-walled carbon nanotubes for conductive nanocomposites. *The Journal of American Chemical Society*, 130: 1415–1419.

185. Allain, E., Besson, S., Durand, C., Moreau, M., Gacoin, T., Boilot, J.P. (2007) Transparent mesoporous nanocomposite films for self-cleaning applications. *Advanced Functional Materials*, 17: 549–554.

186. Habibi, M.H., Nasr-Esfahani, M., Egerton, T.A. (2007) Preparation, characterization and photocatalytic activity of TiO_2/methylcellulose nanocomposite films derived from nanopowder TiO_2 and modified sol–gel titania. *Journal of Materials Science*, 42: 6027–6035.

187. Ding, X.F., Zhou, S.X., Wu, L.M., Gu, G.X., Yang, J.T. (2010) Formation of supra-amphiphilic self-cleaning surfaces through sun-illumination of titania-based nanocomposite coatings. *Surface & Coatings Technology*, 205(7): 2554–2561.

188. Pinho, L., Mosquera, M.J. (2011) Titania-silica nanocomposite photocatalysts with application in stone self-cleaning. *The Journal of Physical Chemistry C*, 115: 22851–22862.

189. Dong, H.C., Ye, P.L., Zhong, M.J., Pietrasik, J., Drumright, R., Matyjaszewski, K. (2010) Superhydrophilic surfaces via polymer-SiO_2 nanocomposites. *Langmuir*, 26(19): 15567–15573.

190. Hwang J.-H., Lee, B.I., Klep, V., Luzinov, I. (2008) Transparent hydrophobic organic–inorganic nanocomposite films. *Materials Research Bulletin*, 43: 2652–2657.

191. Lin, C.-C., Hsu, S.-H., Chang, Y.-L. Su, W.-F. (2010) Transparent hydrophobic durable low moisture permeation poly(fluoroimide acrylate)/SiO_2 nanocomposite from solventless photocurable resin system. *Journal of Materials Chemistry*, 20: 3084–3091.

192. Liu, S.X., He, J.H., Xue, J.F., Ding, W.J. (2009) Efficient fabrication of transparent antimicrobial poly(vinyl alcohol) thin films. *Journal of Nanoparticle Research*, 11: 553–560.

193. Cioffi, N., Torsi, L., Ditaranto, N., Sabbatini, L., Zambonin, P.G., Tantillo, G., Ghibelli, L., D'Alessio, M.D., Bleve-Zacheo, T., Traversa, E. (2004) Antifungal activity of polymer-based copper nanocomposite coatings. *Applied Physics Letters*, 85(12): 2417–2419.

194. Xu, T., Xie, C.S. (2003) Tetrapod-like nano-particle ZnO/acrylic resin composite and its multi-function property. *Progress in Organic Coatings*, 46: 297–301.